NEUTRON FLUENCES BY NUMERICAL

SIMULATION AND ACTIVATION ANALYSIS

by

© Shlomo Kovalski

A thesis submitted to the Faculty of Graduate Studies and Research in partial fulfillment of the requirements for the degree of Master of Science.

Foster Radiation Laboratory
Department of Physics
McGill University
Montreal, Canada

אייר תשמ"ג

ABSTRACT

Spatial distributions of thermal and epithermal neutrons produced by collimated radioactive isotopic sources have been measured in assemblies suitable for elemental analysis of bulk samples by PGNCA (prompt gamma neutron capture analysis). A Monte Carlo transport code was extensively modified to predict the energy spectra of the neutron beams in a number of geometries. Very good agreement was obtained with measured distributions. The collimators were found to severely modify the neutron spectra. The modified spectrum is softer than the original and may result in a reduced uniformity of activation throughout the sample. By judicious selection of the collimator materials and dimensions one may eliminate the need for premoderation of the impinging neutron beam.

SOMMAIRE

Les distributions spatiales de neutrons thermiques et épithermiques produits par des sources d'isotopes radioactifs munies d'un collimateur ont été mesurées. Les mesures ont été faites dans des systèmes appropriés à l'analyse d'éléments dans des échantillons de volume important par PGNCA (analyse de gamma rapides suivant la capture neutronique). Un code de transport Monte Carlo a été modifié de façon extensive de façon à prédire les spectres en energie des faisceaux de neutrons pour des géométries variées. Un très bon accord a été obtenu entre les distributions mesurées et calculées. On a trouvé que les collimateurs modifiaient considérablement les spectres de neutrons. Le spectre modifié est plus doux que le spectre original et pourrait resulter d'une uniformité reduite de l'activation au travers de l'échantillon. Un choix judicieux des matériaux et des dimensions des collimateurs pourrait éliminer la nécessité d'une modération préliminaire du faisceau de neutrons incident.

TABLE OF CONTENTS

LIST OF FIGURES

LIST OF TABLES

ACKNOWLEDGEMENTS

I would like to thank Dr.J.M. Robson and Dr.J.K.P. Lee without whom this work would not have been possible. The time they spent with me and the correction of many potentially embarrassing errors are gratefully acknowledged.

Thanks are also due to the machine shop staff for their assistance when called upon and their understanding of my usually laughably inadequate instructions. The assistance of the electronics shop staff is deeply appreciated.

I would also like to thank my fellow grad students, Ali Alousi and Eric Ramsay, the former for the papers he directed my way, even if they were not of the great import he insisted in attributing to them, the latter for discussion of profound thoughts (and to obligate him to return the reference) and both for general interest and support.

Thanks are due to Henri (and Danielle) Dautet for the French version of the abstract.

I would like to acknowledge the financial support of the Carl Reinhardt and McGill Summer Scholarships.

And, finally, I would like to express my thanks to the members of my family for seeing me through some quite difficult times and making it all worthwhile.

CHAPTER I-INTRODUCTION

Non-destructive analysis of materials is a field in which varied nuclear techniques find widespread application. The wide range of situations in which an analysis of constituents is required means that no one technique is suitable in all cases. One can roughly divide the general problem into two categories: (1) analysis of very small or thin samples, often involving a search for elements at the trace level, (2) determination of constituents in bulk samples. In the following, a few of the most common methods are noted.

In almost all techniques, the general principals are similar. Targets are bombarded by a radiation which interacts with the atomic electrons or nuclei in the sample. A signal results which identifies the target. This signal may be the scattering of the incident beam or the emission of a different type of radiation. For example, in the case of nuclear magnetic resonance (NMR) experiments, which have only recently been applied to large samples (Bo82), the signal consists of a resonant absorption of the incident microwaves detected by a drop in their intensity. NMR is capable of identifying the chemical form of the target and matrix. In imaging applications to large volumes, only hydrogen is at present resolvable. NMR is inapplicable to the detection of even-even nuclei because of the zero net magnetic moment they possess.

The majority of analytical methods use either directly or indirectly ionizing radiation in contrast to the

radiofrequencies of NMR. Particle induced x-ray emission (PIXE) makes use of the large cross section for x-ray production in charged particle bombardment (Jo76). X-rays excited by protons, α particles or heavy ions and detected by high resolution silicon detectors make possible multielement analysis at high sensitivity. Incident particles in the range of 1-5 MeV/amu interact Coulombically to remove at least one inner shell electron in the target atom. As electrons from higher shells drop to fill the vacancy, x-rays are emitted. In the case of light elements, the energies are usually sufficiently low so as to require special detectors and windows as well as thin targets to avoid absorbing the radiation. Above aluminum, the matter of detection is simplified by the higher energies of the x-rays. The technique is used in surface studies, environmental analysis and on sectioned biological samples to name but a few cases. Systems similar to the above make use of electron beams or microprobes to excite x-rays. Background problems due to bremsstrahlung limit the sensitivity.

A fundamentally different approach involves measuring the energy loss of electrons traversing the target (Ot82,Ad80). This technique employs a transmission electron microscope to bombard the sample with electrons in the range of 100-1000 keV. An energy window is used to collect only those electrons which have been degraded by exciting target inner shell electrons to vacant orbitals above the Fermi level. For example, in imaging phosphorus ($L_{2,3}$ absorption edge at 138 ev), electrons which have lost 150 eV are counted. Distributions of only tens of atoms in sub-cellular

biological structures have been imaged, even for some lighter atoms. Unusually thin samples (~30nm) are, however, required to reduce energy losses due to multiple scattering and the like.

Atomic interactions are not used exclusively when charged particles are involved. At higher bombarding energies, nuclear interaction channels open yielding another avenue of analysis which has proved particularly fruitful in depth profiling of the near surface regions of targets. Both resonant and non-resonant reactions which emit neutrons, gammas or α or ^{3}He ions can be used to determine the concentration profiles of elements to a depth of several microns or more in a sample. A particularly important application in materials science has been to hydrogen profiling by ion bombardment on metals and semiconductors. Resonant reactions such as (La77)

$$^1H(^{15}N,\alpha)\,^{12}C^* \longrightarrow {}^{12}C + \gamma(4.43\text{MeV})$$

and $^1H(^7Li,\gamma)\,^8Be$ (Zi78) employ γ detection while a reaction such as $^1H(^{11}B,\alpha)\,^8Be$ uses α detection. For analysis of materials in living organisms (De81), inelastic proton scattering has even been used in a very limited fashion. Proton activation, using 160 Mev protons, has been used to measure calcium content in the spines of humans (Co81).

The advantages of charged particles rest in the ability to bend and focus them. Microprobes are now in operation in many centers. However, the limited range in matter of these probes remains the most serious limitation on their use. For analysis of large samples, only gamma rays and neutrons are suitable.

A variety of techniques employ gamma ray bombardment to obtain the elemental composition of bulk targets. Activation of a target nuclide may be achieved by a (γ, n) reaction leaving a radioactive product which can be counted by gamma or delayed neutron spectroscopy. Beta spectroscopy is impractical in bulk samples. High sensitivty can be obtained in the determination of the light elements, C, N and O (En72). Activation of the sample can be fairly uniform due to the low attenuation of the high energy gammas necessary for this technique. Obtaining sufficiently energetic gammas normally requires a linac for a bremsstrahlung source.

Gammas from long-lived radioisotopes are sufficiently energetic for use in other analysis techniques. Quantities of elements such as Hg, Cd, Fe and Pb in humans have been measured using γ rays to excite characteristic x-ray fluorescence (Sm82, La82). Attenuation of both the low energy incident radiation and the resultant fluorescence can be troublesome.

Attenuation difficulties are somewhat reduced by the use of higher energy γ rays ($\sim$1 Mev) for nuclear resonant scattering. Here, the full energy of the γ is scattered when it is in exact resonance with the target nucleus. The technique is highly specific and has been used in both medical and geophysical applications (So77, Va82).

Neutrons are perhaps the most commonly used radiation for bulk analysis. Neutron activation analysis (NAA) makes use of radioactive nuclides that result from (n,x) reactions. For slow or thermal neutron capture, the resulting nucleus is often a β^- emitter. For faster neutrons above the threshold

limits, (n,2n), (n,p), (nα) type reactions can also lead to radioactive species. Such higher energy neutrons are usually produced by accelerator based sources. The most popular method of producing a nearly monoenergetic beam is the deuteron-tritium (D-T) fusion reaction producing 14-15 Mev neutrons (Ch79). Fluxes of up 10^9 n/cm^2/s are achievable. Higher energy polyenergetic spectra are obtainable with cyclotrons via (D,Be) or (D,Li) reactions.

Nuclear reactors are the most intense source of neutrons available. Thermal neutron fluxes of up to 10^{12} n/cm^2/s are routinely accesible even with small research reactors such as the SLOWPOKE. Samples can range up to tens of grams or more in size, depending on where they are to be positioned in the reactor for irradiation. Irradiation times can vary from seconds to months following which the activated samples can be removed for counting with β spectrometers or high resolution γ detectors. Trace levels of many elements in many types of matrices can often be determined under such conditions (Ju78). However, only information relating to the whole of the sample is obtainable. The high spatial resolutions possible with charged particle beams are precluded by the inability to focus neutrons. Also, the relatively low neutron energies emitted from fission reactors are usually unsuitable for other than (n,γ) reactions.

Simplicity and portability are provided by isotopic neutron sources which will be discussed in some detail in subsequent pages. Despite the rather meager fluxes usually possible with such sources, they have truly widespread application in medical diagnosis, in situ geochemical

analysis and even laboratory mineralogical analysis (Ma82,Co81). They have even been used in nuclear structure studies (Wa64).

Activation is by no means the only channel by which neutrons can be used for analysis. Indeed, there are those nuclei for which none of the available neutron reactions result in a suitable radioactive product or for which neutrons of an energy range somewhat difficult to obtain are required. In such cases, prompt gamma neutron capture analysis (PGNCA) is often useful (Gr78).

An incident neutron (or proton) may be captured by a nucleus resulting in an excited compound nucleus. The excitation energy must equal the sum of the kinetic and binding energies of the captured neutron. Assuming that the neutron is not scattered out, the most common deexcitation mode is by γ ray emission. (The residual nucleus is often unstable against β^- decay.) The compound nucleus must exist a sufficiently long time to permit the sharing of this energy among its components. For radiative capture, the radiation width is $\Gamma_\gamma = \hbar/\tau$ where τ is the mean lifetime of the excited state. For slow neutrons, Γ_γ is of the order of 0.1 eV implying a τ of the order of 10^{-14} seconds for prompt emission. The radiation width of a given nucleus changes only slightly from resonance to resonance and radiative capture (like compound nucleus scattering) can occur at all neutron energies. Nevertheless, the (n,γ) cross section is largest below several hundred eV. In heavy nuclei (A>80) in particular, radiative capture predominates (since due to the large number of nucleons, the probability of a neutron in the

compound nucleus receiving sufficient energy to escape is small) (Be64). In this slow range below the resonance region, the cross section varies as $1/\sqrt{E}$ (or $1/v$, where E and v are the neutron energy and speed) for almost all nuclei. In the range of 1-500 keV, resonance scattering is most important while for yet higher energies, inelastic scatter and (n,2n) reactions compete.

PGNCA offers a detectable and unique signature for most elements in bulk analysis. It is instantaneous and nondestructive but suffers from a number of disadvantages. Trace elements are usually not detectable because of the limited neutron fluxes obtainable in the requisite sample-detector geometry. Background problems can be formidable because γ ray spectroscopy must be conducted in the presence of a neutron source. The neutron source requirements can be difficult to meet. For example, neutrons must be sufficiently energetic to penetrate the often large targets uniformly throughout their volume but must be slowed down for (n,γ) reactions to occur. At the same time, fast neutron damage to and slow neutron activation of the detectors must be avoided. Despite its difficulties, the method can be extremely useful, particularly if coupled to spectroscopy using γ rays from neutron inelastic scatter.

NAA and PGNCA have found widespread usage in biological and medical applications. NAA, especially with reactor based sources, can be almost unsurpassed in its ability to quantify elemental compositions of targets suitable for positioning near a reactor core. This obviously requires the removal of a sample from the organism under study. At times this may

not be a disadvantage. Thus it is often of great interest how toxic metal contamination is reflected in hair or what levels of certain trace elements are present in blood or teeth. However, in many instances, it is required that the in vivo time evolution of an element's concentration be monitored. Both NAA and PGNCA offer non-invasive techniques which have been employed by several groups to measure elemental compositions in humans. A number of elements have been studied. A non-exhaustive list includes cadmium (Kr80, Ev78), nitrogen (Va76) and mercury (Sm82) by PGNCA, calcium, phosphorus, sodium and chlorine by NAA (Ke82, Wi78), and silicon (Et82) and carbon (Ky82) by neutron inelastic scattering, i.e. (n,n'γ). Facilities for this work usually use either radioisotopic neutron sources or the D-T or D-D (deuterons on deuterons, yielding 2.5MeV neutrons) reactions.

In all the situations noted above, it is important that the neutron distributions in the target medium be known. In the case of PGNCA and NAA, thermal neutrons are most important and their spatial distribution (coupled with the attenuation of the resultant γ rays) determines the ultimate sensitivity of a system. When (n,n'γ), (n,2n), etc., type reactions are used, the change in the neutron energy spectra as a function of position must be known. Little attention has been paid in the literature to the matter of the modification by shielding and collimating materials of the energy spectra of neutron sources used in in vivo NAA and PGNCA. It is seen however that the bare source spectra commonly quoted are in fact quite different from those

impinging on a target. This matter should be addressed as it bears strongly on the feasibility of using inelastic processes for analysis. Such information can be obtained either by experimentally measuring spatial distributions and energy spectra or by calculations using numerical methods to simulate neutron transport. The work reported here deals with the measurement of thermal neutron flux distributions under a variety of conditions suitable to an in vivo elemental analysis facility as well as the modelling of such distributions by the Monte Carlo technique. No measurements of fast neutron energy spectra were carried out as we lacked a facility for this. However, numerical calculations in similar geometries were made and compared to the rather sparse literature available.

In the following, a detailed description of the Monte Carlo code used in this work is given. The experimental techniques are described in full. Results of both experiments and calculations are compared with each other and with published results. Finally, the applicability of this work to a facility for in vivo measurement of elemental composition in humans is discussed as well as possible modifications to improve such a facility.

CHAPTER II-NUMERICAL SIMULATION

SECTION II.1-GENERAL CONSIDERATIONS

The study of radiation transport is a staggeringly large field. Requirements of nuclear reactor theory and radiation shielding have led to a very great expenditure of effort in studying the transport of γ rays and neutrons in particular. At present, two methods are most commonly used: the Discrete Ordinates Transport method (DOT) and the Monte Carlo (MC) method. Both these techniques involve a numerical solution of the tranport problem. Analytic solutions are certainly more satisfying and would ideally be much more useful. However, despite the many problems which can be thus solved (Wa47), in general, most situations are not amenable to such an analysis, particularly if one does not wish to engage in very seriously limiting approximations. Also, most such calculations are not suitable for neutron transport in hydrogenous media though somewhat reasonable agreement can sometimes be reached (Ho78). (The discrepancies appear because the integro-differential equations modelling the neutron's travel are continuous in nature while the process itself consists of a number of discrete steps. The approximation suffers most severely in the case of hydrogen targets since the neutron can lose so much of its energy in a single collision with a proton of similar mass. The approach can be more successful with charged particle transport since the slowing down process really is continuous in that case.)

The neutron, being both neutral and quite massive, is

unaffected by electromagnetic interactions in a medium (assuming, for the moment, that one ignores its magnetic dipole moment) or by collisions with atomic electrons. The path it takes consists of a series of randomly oriented straight line segments whose intersection points represent target nuclei scattering a neutron in a new direction. The total path is that of a random walk. While this is certainly analogous to problems such as gaseous diffusion, it should be noted that neutrons are never present in such densities that they collide with each other. As a result, the paths followed by individual neutrons are uncorrelated with each other. Each neutron can be considered independently of the rest. It is this feature that makes possible the solution techniques discussed below. The significance of this to somewhat more analytical approaches is discussed by Weinberg and Wigner (We58,ch. VIII).

SECTION II.2-DEFINITIONS

Some definitions for terms which will appear throughout this paper are in order. These are due mostly to Beckurts and Wirtz and the MCNP transport program User Manual(MCNP79).

Consider a volume element $dV=dxdydz$ of a scattering medium at the position vector, $\bar{r}$. Let the differential density, $n(\bar{r},\bar{\Omega},E)\,dVd\Omega dE$, be the number of neutrons in dV at $\bar{r}$ with direction lying in the solid angle $d\Omega$ around the unit vector $\bar{\Omega}$ with energy between E and E+dE. $n(\bar{r},\bar{\Omega},E)$ is the density of neutrons (cm^{-3}). Integrating over E and Ω, the total number of neutrons in the region dV at r is $n(r)dV$.

The differential neutron flux is

$$F(\bar{r},\bar{\Omega},E)\,d\Omega dE dS = n(\bar{r},\bar{\Omega},E)\,v\,d\Omega dE dS \qquad (1)$$

where $v=\sqrt{2E/m}$ is the neutron velocity. This is the number of neutrons at $\bar{r}$ with energy between E and E+dE traveling in a cone of size $d\Omega$ around $\bar{\Omega}$ penetrating a surface dS each second. In Fig.II.1, for sake of clarity, $\bar{\Omega}$ has been drawn along the polar angle θ. The azimuthal angle ϕ is not shown. Note that $dS'=\cos\theta\,dS$ and that the same number of particles traveling in the direction $\bar{\Omega}$ cross dS' as do·dS, though with different weights as explained below.

The scalar flux is given by

$$\Phi(\bar{r})=n(\bar{r})\langle v\rangle=\int n(\bar{r},\bar{\Omega},E)\,v\,d\Omega dE dS=\int n(\bar{r},\bar{\Omega},E)\,v\,d\Omega dE dS'/\cos\theta \qquad (2)$$

where <v> is the average of the velocity over the energy spectrum of the neutron density. Φ has units of $(cm^{-2}s^{-1})$. In a situation where there is no time dependence in the neutron field, the fluence, which is the time integral of the flux, can be used in its stead. It has units of (cm^{-2}). In all the following, only time stationary neutron fields are considered (i.e. no pulsed sources) and the two terms will be used interchangeably. To be absolutely precise, the simulation procedure used here calculates the fluence.

Finally, the neutron current

$$J(\bar{r})=\int n(\bar{r},\bar{\Omega},E)\,v\,d\Omega dE dS' \qquad (3)$$

is the number of neutrons penetrating a 1 cm^2 surface (dS' in Fig.II.1), perpendicular to the axis of the distribution, per second. As for the flux, time dependence is assumed not to exist. Note the difference between equations (2) and (3). Each neutron which contributes dS' to the calculation of the current contributes $dS'/\cos\theta$ to the fluence. In fact, in the

Fig.II.1

Geometry for defining the neutron flux and current.

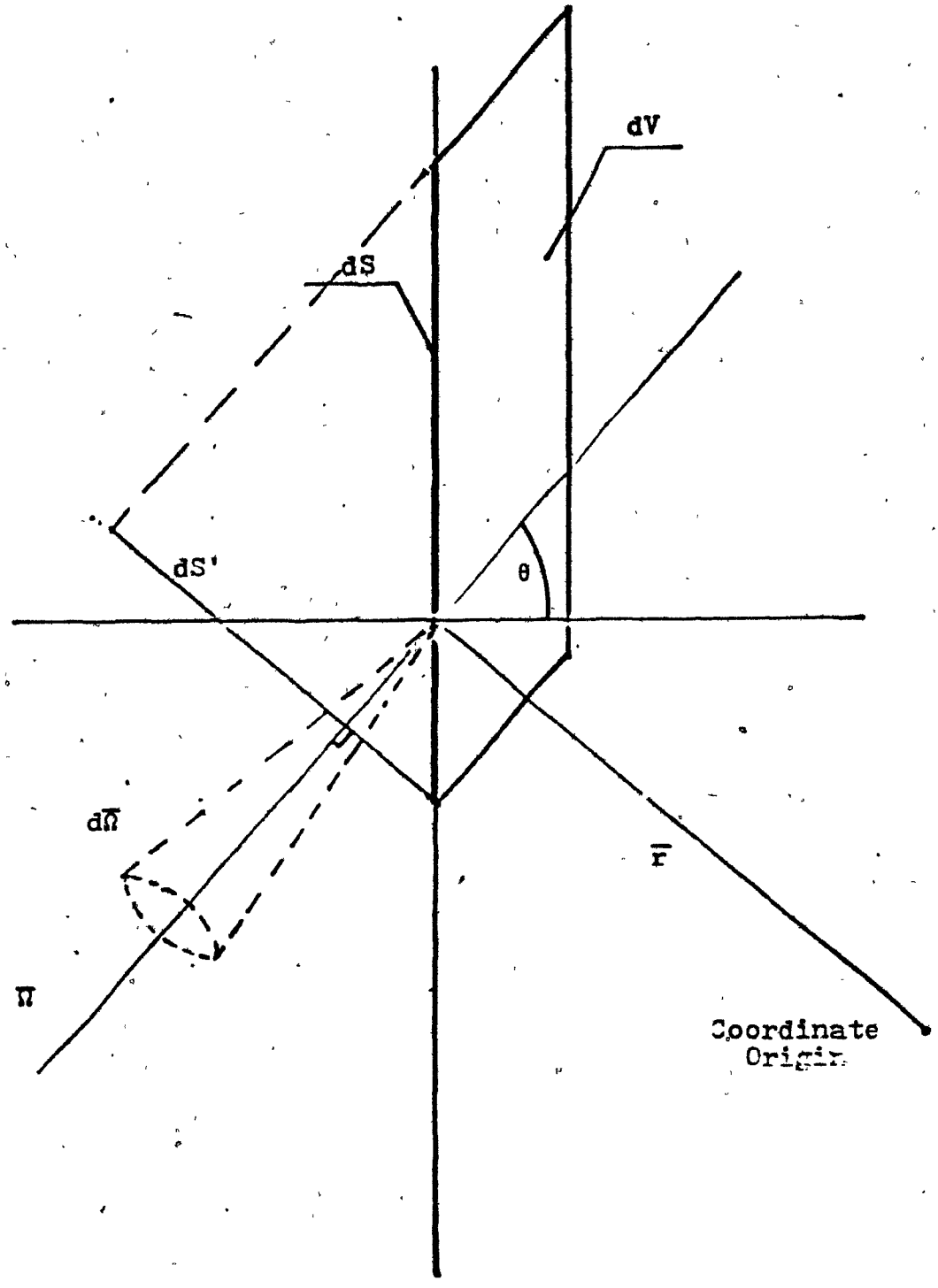
dV
dS
dS'
θ
dΩ
r
n
Coordinate
Origin

program outlined below, it is $|\cos\theta|dS$ which is tallied for the current. This definition differs from that in (Be64) in that the total rather than net number of crossings is counted here. The other definition is more meaningful in nuclear engineering where the net flow of neutrons through a region is required, i.e. the neutron balance. To calculate the probability of absorption, however, our definition is more appropriate.

It should be clear from the above that in a parallel beam normal to a counting plane the current and flux are equal. It is not difficult to show (Be64) that for an isotropic neutron field, the flux is twice the current. Between these two extremes, the ratio of flux to current varies between 1 to 2.

Section II.3-TRANSPORT EQUATION

Any consideration of the subject of neutron spectral and flux distributions must ultimately seek to obtain a solution of the Boltzmann radiation transport equation. Though no particular consideration of the equation will be made here, it is included for the sake of completeness. In its most general form, this can be written as (We58, ch.IX) (St70, app.A)

$$\frac{1}{v}\frac{\partial}{\partial t}\Phi(\bar{r},E,\bar{\Omega},t)+\Omega\cdot\nabla\Phi(\bar{r},E,\bar{\Omega},t)+\Sigma_t(\bar{r},E)\Phi(\bar{r},E,\bar{\Omega},t)=$$

$$=S(\bar{r},E,\bar{\Omega},t)+\int dE'd\bar{\Omega}'\,\Sigma_s(\bar{r},E'\to E,\bar{\Omega}'\to\bar{\Omega})\,\Phi(\bar{r},E',\bar{\Omega}',t) \qquad (4)$$

where most terms are as defined in section II.2 except for the introduction of time dependence. Also,

$(\bar{r}, E, \bar{\Omega}, t)$ is the general seven-dimensional phase space,

$1/v \frac{\partial}{\partial t} \phi(\bar{r}, E, \bar{\Omega}, t) dE d\Omega$ = net storage (gains minus losses) per unit volume and time at position $\bar{r}$ and time t' of particles of energy E to E+dE and with direction lying in $d\Omega$ about $\bar{\Omega}$,

$\bar{\Omega} \cdot \nabla \phi(\bar{r}, E, \bar{\Omega}, t) dE d\Omega$ = net convective loss per unit volume and time,

$\Sigma_t(\bar{r}, E)$ = total cross section at $\bar{r}$ for particle of energy E,

$\Sigma_t(\bar{r}, E) \phi(\bar{r}, E, \bar{\Omega}, t) dE d\Omega$ = collision loss per unit volume and time,

$\Sigma_t(\bar{r}, E' \rightarrow E, \bar{\Omega}' \rightarrow \bar{\Omega})\, dE d\Omega$ = differential scattering cross section which describes the probability per unit path that a particle of initial energy E' and direction $\bar{\Omega}'$ undergoes a scattering collision at $\bar{r}$ sending it in the direction $d\Omega$ about $\bar{\Omega}$ with a new energy in dE about E,

$\int \Sigma_s(\bar{r}, E' \rightarrow E, \bar{\Omega}' \rightarrow \bar{\Omega}) \phi(\bar{r}, E', \bar{\Omega}', t) dE d\Omega$ = inscattering gain per unit volume and time,

$S(\bar{r}, E, \bar{\Omega}, t)$ = source particles emitted per unit volume and time.

Equation (4) is a bookkeeping process that equates the net storage of particles within a differential phase space volume element ($drdEd\Omega$) to the particle gain minus particle losses in that element. In the numerical procedures most often followed, i.e. DOT and MC, the energy dependence of equation (4) is represented in terms of a finite number of energy groups. Indeed, in the DOT method, one also divides the cartesian space into a network of cells and replaces the continuous angular distribution by a set of discrete

directions with appropriate weighting factors. The Boltzmann equation is integrated over each spatial-directional cell in phase space to obtain the flux balance equation in the cell. This is combined with other equations relating the cell boundary and midpoint values. These yield a recursion formula for the fluxes throughout the system. Beginning with the values of an external source, if any, with a guess for the flux throughout the system and with boundary conditions along each of the spatial boundaries, the recursion formula is iterated for each energy group until a consistent, converged solution is reached (Jo81,DOT77). The programs readily available are either one or two dimensional in coordinate space.

The MC method is fundamentally different in its attack on the problem. Indeed, one need not explicitly consider the Boltzmann equation at all in this approach. The transport problem is solved by simulating the movement of individual particles through the system in a realistic fashion from point of origin through collisions with nuclei in the system until capture, escape, or cut-off. Particles may be run in sequence because of the independence of their paths as noted above. Mean values of the flux or of any other quantity of interest are found by analysing the histories of a large number of particles. In this situation, the value of any quantity must have an inherent statistical error of the order $\sqrt{N}$ where N is the number of contributions made to the particular quantity. In practice, it is often the case, depending on the parameter under consideration, that this error estimate provides only a lower bound. Indeed this was

found to be so in this work. Other methods of estimating the errors must be used and these will be referred to later.

Because of the statistical nature of the solutions as obtained by the MC method, various procedures are employed to reduce their variance. These no longer treat the particles as analogues of real ones but rather assign them weights depending on their past histories. These procedures then increase the number or contributions to a particular result, scoring the weights rather than detected particles. Such variance reducing techniques are included as options in many of the widely used MC programs such as MORSE (St70) and MCNP (MCNP79). However, there are instances where such procedures are less than satisfactory (Jo81). In any event, such techniques require careful consideration when used to determine which are appropriate. In this work, except for biasing of source direction in some of the calculations, as explained below, no variance reduction techniques were invoked.

In the MC method, simulation of experimental geometries can be very precise even for somewhat unusual cases. DOT calculations normally require geometries with significant symmetry. In most cases, of course, the experimental geometry also possesses some symmetry. Even in MC computer codes, this can sometimes lead to a reduction in computing costs.

Though attention has so far been focused on neutron transport, γray transport, necessary because of (n,γ) or $(n,n'\gamma)$ reactions, can also be simulated in many of the common codes though of course at higher computing cost.

At the time this work was undertaken, none of the

computer codes referred to above were available at McGill. However, a MC code developed by J.M.Robson was in use (Ro81). It was originally used in shielding studies to calculate the spatial neutron flux distributions in spherical shields of iron, concrete and wood surrounding a 14 MeV neutron generator. It also calculated the total neutron and gamma dose-rates at various distances from the source. As a test of its validity, it was used to predict the spatial distribution of the thermal neutron flux in a paraffin block around a 10 Ci AmBe neutron source. In all cases except that of the iron shield, the thermal neutron fluxes agreed very well with measured values both in terms of the shape of the distributions and absolute numbers. In the case of the iron shield, it was suggested that discrepancies were due to a lack of refinement in the modelling of the neutron spectrum following inelastic scatters. It seems possible that the lack of an (n,2n) reaction mechanism is also partly responsible. Some appreciation of the importance of the $(n,n'\gamma)$ and (n,2n) reactions can be garnered from (In75) where calculated spectra of 14 MeV neutrons passing through iron are presented with and without these processes.

For the purposes of this work, the above code was altered in a variety of ways. Three separate versions were written to model three geometries: (1) the program SPHERE, modelling a point source inside a sphere and similar to the original code, (2) COLLIM, which modelled a source of variable length or height resting beneath the bottom of a cylindrcal collimator of variable size in a cylindrical shield (Fig.II.2A) and (3) PHANT, which modelled a neutron beam of

Fig.II.2

Fig. A Geometry simulated in program COLLIM.
Source is of length L and may be oriented either vertically or horizontally at a depth d.
The parameters r_c, t_w, h_w and h_r may also be varied.

Fig. B Geometry simulated in PHANT.
A point source rests at a distance SSD along the axis of a cylindrical phantom of radius r_p and height H.
The source can illuminate a disc of radius r_b at the lower phantom face.

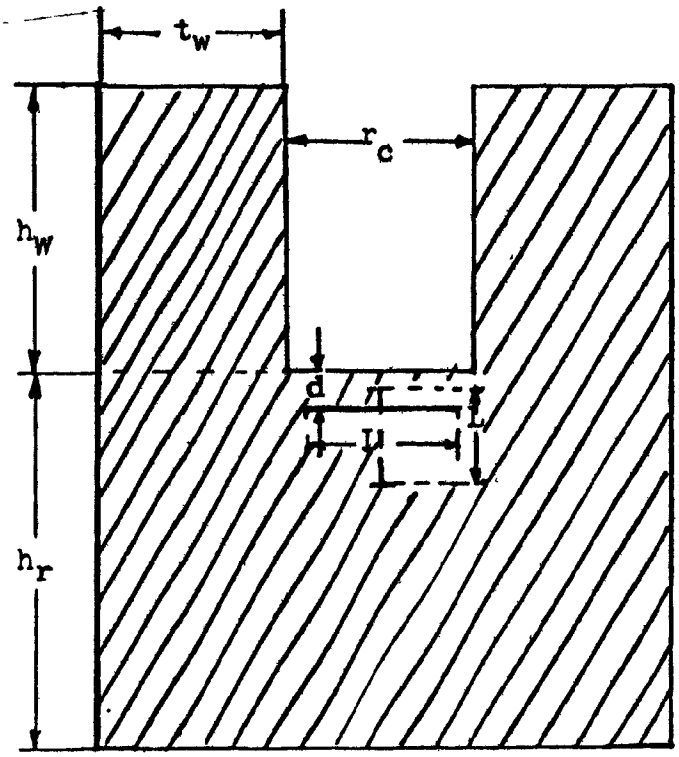

FIG. A

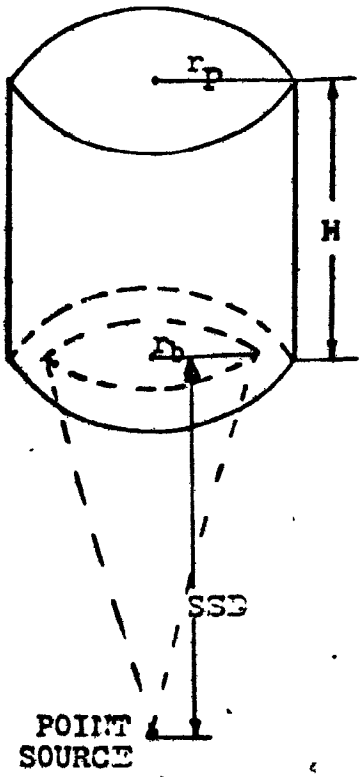

FIC. B

arbitrary diameter and divergence striking a cylindrical phantom on its bottom flat face and along its symetry axis (Fig. II.2B). The considerations discussed below are similar for all the programs. Where differences exist they will be noted. In general, "the program" will refer to all versions.

SECTION II.4-MONTE CARLO PROGRAM

Several advantages are evident in the use of the MC program discussed immediately above with respect to those commonly available. The latter are quite enormous in terms of program size and computer memory demands. Their generality, a feature of obvious great value, can also increase their running time. Implementing such a system on a particular computer installation can be quite involved. The program used here was molded to suit our very specific needs. To reduce memory requirements and speed execution, the gamma tracking of the original code was dropped. The number of homogeneous regions and elements in each region were limited. This made it possible to implement the program on a PDP-11/34 minicomputer with 32 kilobyte of memory. The program was very portable requiring no peripheral equipment. This made it possible to transfer it to the McGill University central computer with only minor modifications in the input/output statements. Given the large memory space available on this machine, the number of elements and regions could be increased. This was in fact done and a few test runs were made. The bulk of the calculations were however made on the minicomputer.

Since the MC technique is a method of statistical trials, it must have a way of simulating random events and therefore requires a random number generator. The generator (built into the computer) used in this work employs the multiplicative congruential method. It is perfectly deterministic in that if initiated at the same point it will always yield the same sequence of numbers. Nevertheless, the numbers within any one sequence appear to be randomly distributed. They are, in fact, pseudo-random.

A random number is produced from the formula

$$x_{n+1} = (2^{16}+3)\,x_n \bmod (2^{32}).$$

Integers are stored in 16 bits and two integers are used to generate each random number which then serves as the seed for the next. In practice, the algorithm consists of multiplying two numbers and retaining the least significant bits of the resultant. Such an algorithm has a finite period after which the sequence recycles. In this case the period is only several hundred million. It is quite possible to exhaust this period in some of the calculations done for this work. While a highly sophisticated generator is available at McGill (with a period of about 5×10^{18}-Ja80) and indeed is implemented on the main university computer, it was felt that this was not required since it is virtually certain that even were the generator to begin recycling, it would do so at a point in the computation different than that at which it began. Thus, for example, if the first generator call produces a value for a certain direction cosine, as long as the cycle does not restart on a call for that same direction cosine, the "randomness" of the results is preserved. The

same consideration is true with respect to the question of just how random is a sequence of pseudo-random numbers and what influence this would have on the results. The point is not trivial since some random number generators in common use are not very good (for example, the IBM supplied subroutine RANDU (Ja80)).

Any calculation of neutron transport requires as input the cross section of a reaction for a specific nuclide as a function of energy. It is the relative size of one cross section to the other which determines which interaction takes place at a collision and the total cross section which determines the occurrence of a collision. In this program, three interaction mechanisms are modelled: (1) elastic scatter, (2) inelastic scatter, and (3) capture. Their respective cross sections for a nucleus j and neutron energy k are σ_{ejk}, σ_{ijk} and σ_{cjk}. The total macroscopic cross section of a region at a neutron energy k is

$$\Sigma_{tk} = \sum_j P_j (\sigma_{ejk} + \sigma_{ijk} + \sigma_{cjk})$$

where P_j is the concentration (nuclei/cm^3) of element (isotope) j in that region. σ_{cjk} includes the processes of (n,γ), (n,p), (n,α), etc. The mean free path of a neutron is the average distance it will travel before undergoing a collision and is given by $\lambda = 1/\Sigma_{tk}$. The cross sections used in this work were all taken from BNL-325 (Ga76). They were stored in a multidimensional array which covered the range between thermal and 15 MeV energies in 26 neutron groups. The energy limits of this 26 group data library structure are given in Table II.1. Neutrons with energy greater than the upper limit of group (i) (E(i)) and less than E(i+1) were

assigned to group (i+1) and all data were drawn from the cross section array for this group. To speed calculation, no interpolation was used for neutrons whose energies did not match a group boundary. Since the lethargy interval between two groups is given by (La77,ch.3)

$$u=\ln(E(i+1)/E(i)) \quad ,$$

it can be seen that below 1 MeV the group structure represents almost equal lethargy intervals. Indeed, even for the higher energies, the lethargy intervals vary their size by less than a factor of seven for even the worst case.

The above cross section structure is by no means optimal. An evaluated cross section library with a 36 (collapsible to 21) group structure was obtained towards the end of this work (DLC31,1979). The energy structure in this library is biased at high energies owing to their importance in tissue dose delivery. Also, the groups are tailored to allow for major peaks and valleys in the total neutron cross sections for nitrogen, oxygen, silicon and iron. Since the library was prepared from evaluated point-wise cross section data by using a 1/E weighting spectrum, it is by no means obvious that it would be perfectly applicable to our case where the neutron spectra are radically different from the 1/E situation (Ce82). Nevertheless, some test runs with this library would be valuable.

The case of thermal neutron interactions (in our case, neutrons of $E < 0.1eV$) requires a note of explanation. As is well known, chemical binding effects can affect the cross section value of light nuclei for low energy neutrons when the collision energy is comparable or smaller than the

Table II.1

Energy Group Structure Used In Monte Carlo Simulation

ENERGY GROUP	UPPER ENERGY LIMIT	
1	0.1	eV
2	0.3	
3	1.0	
4	3.0	
5	10	
6	30	
7	100	
8	300	
9	1000	
10	3000	
11	10	$\times 10^3$
12	30	
13	100	
14	300	
15	1000	
16	2000	
17	3000	
18	4000	
19	5000	
20	6000	
21	7000	
22	8000	
23	9000	
24	10	$\times 10^6$
25	12	
26	15	

vibrational quantum (phonon) of the oscillatory movement of the nucleus around its equilibrium position (We58,ch.IV and Cu65,ch.I). For very low energies, the scattering cross section is increased by the order of $((A+1)/A)^2$. For hydrogen, for example, the scattering cross section is virtually constant between 1 and 1000 eV, varying between 20.3-20.4 barns. It climbs below 1 eV reaching a value of 36b at 0.025 eV for H_2 and 53b for H_2O. It monotonically increases at yet lower energies. For heavier nuclei the effect is reduced because $((A+1)/A)^2 \rightarrow 1$ and because the vibrational frequency goes down for increasing A thereby lowering the energy at which the chemical binding is manifested. The MCNP code (MCNP79) has an option which models both the chemical binding as well as crystalline effects (not discussed here) for low energy neutrons in a limited number of materials. In our program this has been dealt with simply by using the BNL-325 hydrogen cross section as measured in water targets. No other compounds are considered. This approximation was seen to work well in modelling thermal neutron scatter in one of the tests subsequently described.

Attempts were made to speed some of the calculations by employing various types of cut-offs acting on scattered neutrons and directional biasing of the source neutrons. To be specific, in the version PHANT, source neutrons were generated so that all fell within the cone defined by the angle, $\theta = \arctan(r_b/SSD)$ where $r_b \leq r_p$ always (see Fig.II.2B). This guaranteed that all neutrons struck the target. The relationship between such a source and an isotropically

emitting one is simple to derive (appendix A).

It would have been possible to introduce directional biasing in COLLIM as well since there is no need to project neutrons at the open mouth of the collimator. This was not done. However, the program did tally separately the uncollided neutron flux which exited the mouth as well as the total flux. This made it possible to evaluate the neutron gain due to the collimator, at the input energy, with a significantly reduced statistical variance than would have been present had the uncollided flux been calculated analytically or in a separate simulation.

In the original MC program (Ro81), all neutrons were followed until either capture or escape. This strategy is feasible only in the case of spherical symmetry since then only the radial coordinate of any neutron is of consequence. Since counting is done on neutrons crossing spherical shells, neutrons of all angular coordinates contribute and good statistics are not not difficult to accumulate. In our case, however, angular distributions of the neutrons are important even though cylindrical symmetry is maintained. Not all neutrons contribute to our limited counting regions and following those that do not is very time consuming indeed. It is observed that the greatest amount of time in our MC simulations of water filled geometries is consumed by the tracking of thermal neutrons since the ratio of the elastic scattering to capture cross sections is $\sigma_e(\text{water})/\sigma_c(\text{water}) \sim 160$. Put simply, thermal neutrons bounce about a great deal before being removed. Time savings in the handling of such neutrons can therefore be of great value.

Versions PHANT and COLLIM employed cut-offs acting on thermal neutrons. The mean free path (MFP) of thermals in water is short, typically much smaller than the dimensions of the system. Therefore, thermals that were more than a preset number of MFP's away from the counting region were dropped from further consideration since there was no realistic likelihood that they would ever contribute. (Typically, the distance was chosen such that the flux arriving at the counting region from a discard zone would be <1% of the flux at the scattering center- 40 MFP's were commonly used though 30 or even 20 would have been reasonable choices.)

The number of thermal collisions could also be used to discard neutrons once a preset maximum had been exceeded. In PHANT, up to 400 collisions were typically allowed. In COLLIM, no more than 200 were permitted. Tallies of all discarded neutrons were kept including the number terminated by each condition. The collision number maximum was adjusted to eliminate no more than ~5% of all thermal neutrons by this method. It was empircally determined that discarding this percentage had no statistically significant effect on results obtained with either program version.

The last type of cut-off used was based on neutron energy. In a variety of instances, we were concerned with determining energy spectra rather than thermal neutron spatial distributions. However, since the slowing down of few MeV neutrons by elastic scatter on hydrogen is a very efficient process (only 18 such collisions in pure hydrogen and 20 in water are required to slow a 2 MeV neutron to 0.025 eV) the fluxes of neutrons per energy interval between

the input energy and equilibrium thermal energy can be very low. To allow a calculation to concentrate on determining these values, neutrons could be discarded once they had dropped below an adjustable energy threshold.

A flowchart of the program (version COLLIM) is given in Fig. II.3 and further discussion will be referenced to it.

Fig. II.3A represents the input section where the parameters explained above are read into the program. The nuclear temperature noted in this section is explained below. Fig. II.3B is the flowchart of a neutron history and is for the most part self-explanatory. A few points need detailing.

When a neutron is created at the source with random direction, direction cosine v is set equal to zero. This is valid because of cylindrical symmetry. Also the direction cosines are not all independent being related by

$$u^2+v^2+w^2=1 .$$

The distance, DTC, the neutron travels before undergoing a collision is chosen as in (Ze63). The neutron is projected along its direction cosines. If it intercepts a boundary within the distance DTC, it is moved to the intersection point and a new DTC is played for. When a neutron finally does collide, the type of interaction must be selected and the appropriate subroutine called.

Fig. II.3C is a flowchart for the logic of an elastic scatter event. The neutron velocity vector is first transformed to the center of mass (CM) frame. A set of new direction cosines is then selected. The spherical polar angles are used since they are independent of each other. The angle, ϕ'_{CM}, is chosen from an equiprobable distribution

over 2π radians. The choice of θ'_{cm} is not as straightforward, except in the case of hydrogen, because the scattering is generally peaked in the forward direction. For hydrogen it is assumed isotropic over the energy range of interest (BNL400-Go62). For other elements, scattering angles are selected in many programs by calculations using tables of Legendre polynomial coefficients which have been fitted to the data. A different tack was followed in this work. The angle θ'_{cm} is given by (Ro81)

$$\theta'_{cm} = \exp(d(E^{-1})) \arccos(1-2R)$$

where $d = 0.14E^{1/2}A^{1/3}$, E is in MeV, A is the nuclear mass and R is a random number such that $0<R<1$.

The distributions given by this formula do not match the measured ones exactly. Neither do many of the more complicated procedures often used (for example, Na75). This method has the advantages of simplicity and of no memory requirement for tables. Fig. II.4 compares the approximation function to data given in BNL-400 for oxygen at two energies.

Following the selection of θ'_{cm} and ϕ'_{cm}, the neutron's original direction is rotated by the appropriate amounts and transformed back into the lab frame. Details on the derivations of the rotation formulae may be found in (Ca59).

Elastic scatter of thermal neutrons is handled differently than the above. The energy of the neutron is fixed at 0.025 eV since we use only a one-group thermal energy structure. Both θ and ϕ are selected from isotropic distributions.

If the incident neutron's energy, E, exceeds the energy

Figure II.3

Flowchart Of Monte Carlo Neutron Transport Simulation Program

Figure A: Input Section

Figure B: Main Program Logic For Tracking A Neutron

Figure C: Logic For Elastic Scatter Event

Figure D: Logic For Inelastic Scatter Event

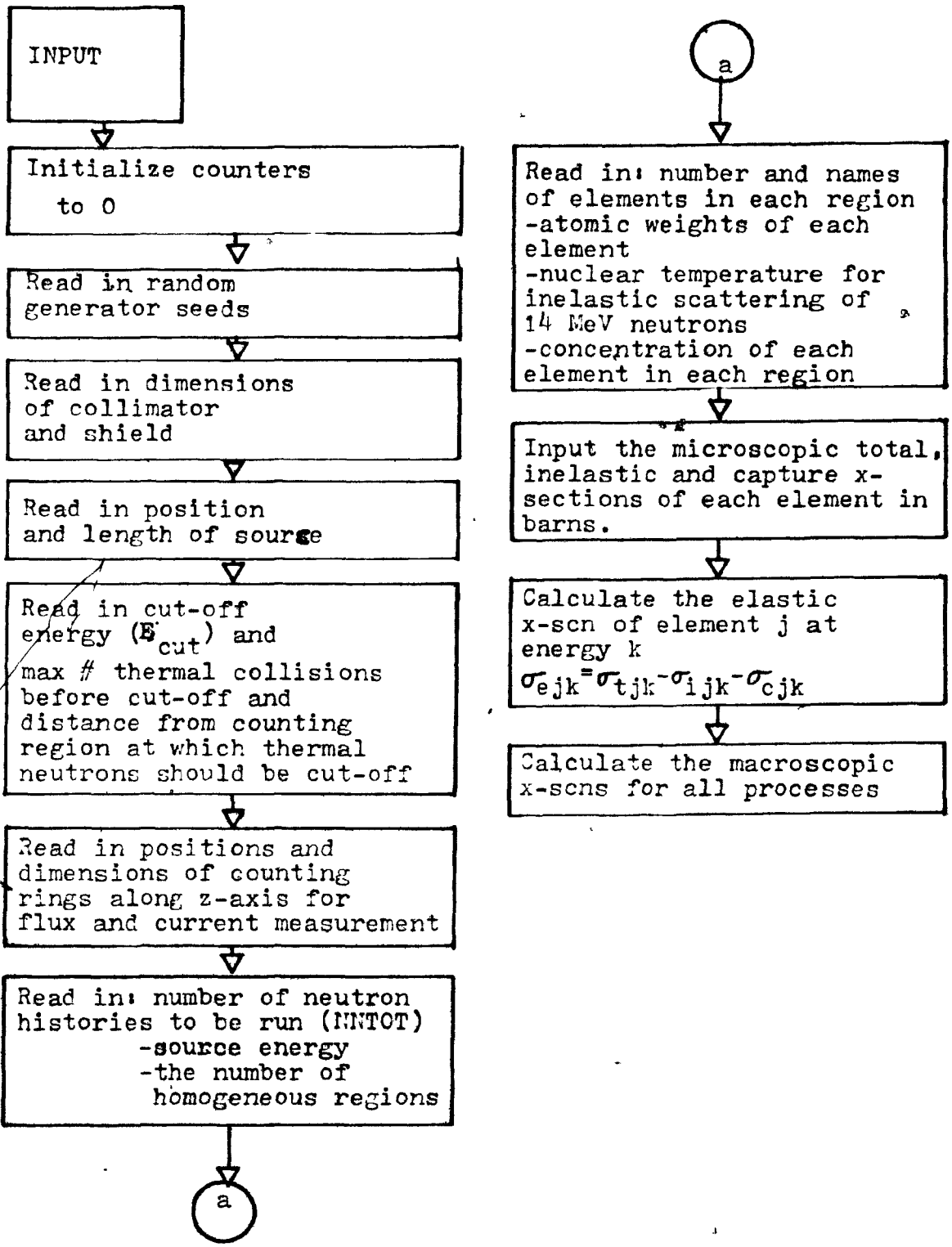
INPUT
Initialize counters to 0
Read in random generator seeds
Read in dimensions of collimator and shield
Read in position and length of source
Read in cut-off energy (E_{cut}) and max # thermal collisions before cut-off and distance from counting region at which thermal neutrons should be cut-off
Read in positions and dimensions of counting rings along z-axis for flux and current measurement
Read in: number of neutron histories to be run (NNTOT)
-source energy
-the number of homogeneous regions
a
a
Read in: number and names of elements in each region
-atomic weights of each element
-nuclear temperature for inelastic scattering of 14 MeV neutrons
-concentration of each element in each region
Input the microscopic total, inelastic and capture x-sections of each element in barns.
Calculate the elastic x-scn of element j at energy k
$\sigma_{ejk}=\sigma_{tjk}-\sigma_{ijk}-\sigma_{cjk}$
Calculate the macroscopic x-scns for all processes

Main program — neutron history

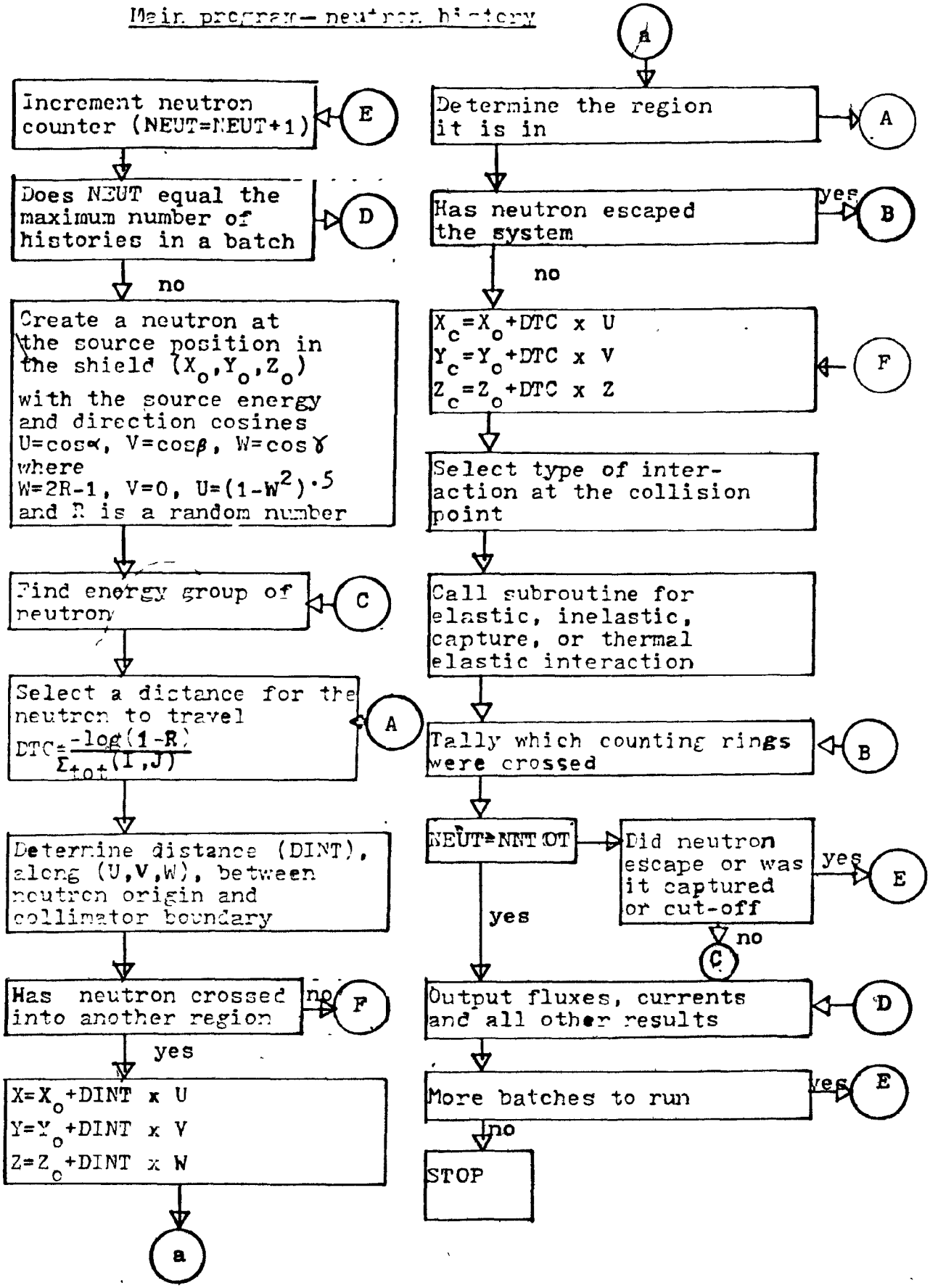

Elastic Scatter

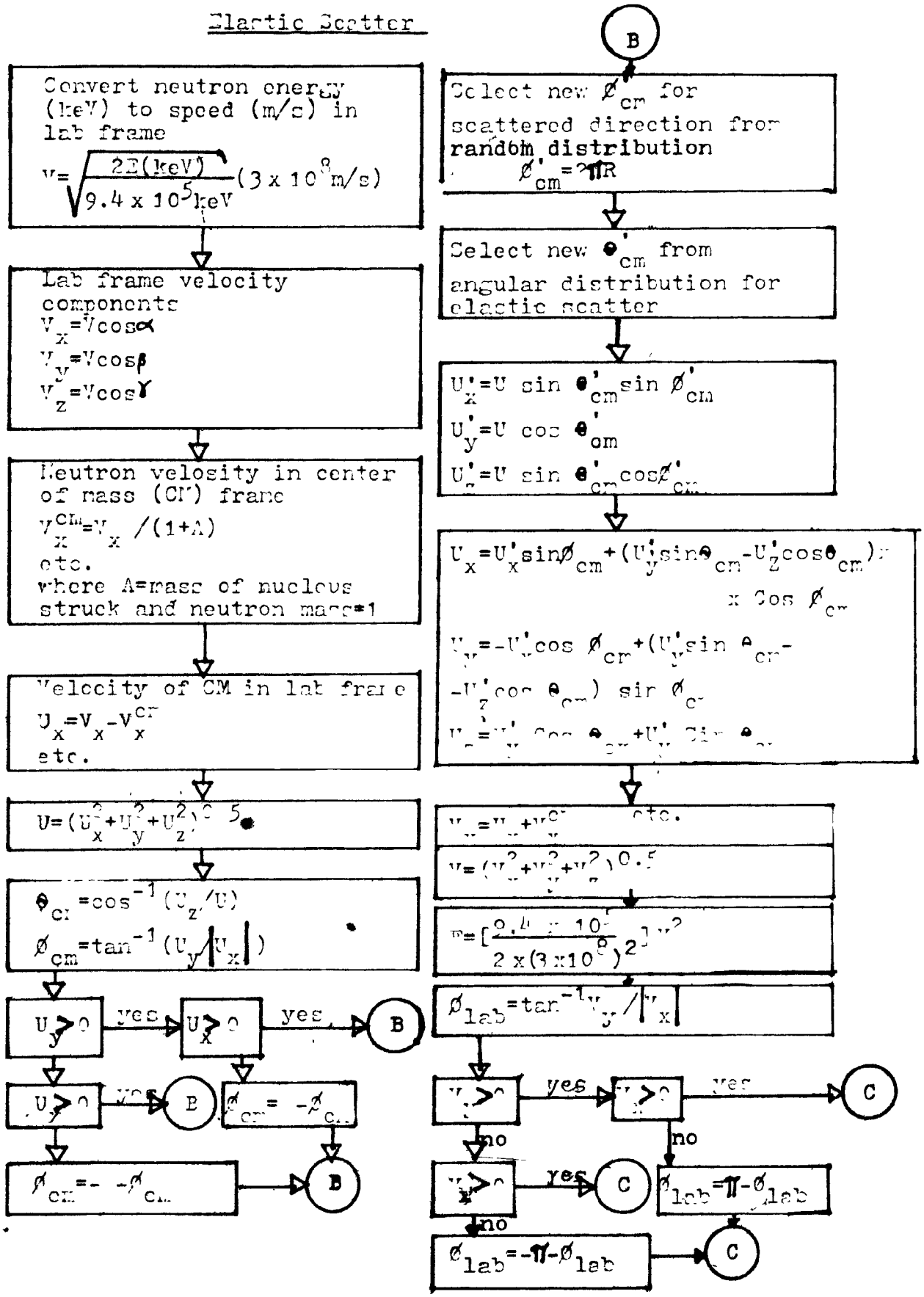

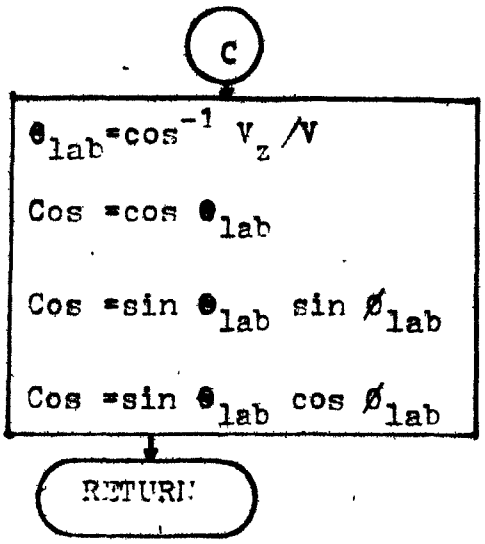
C
$\theta_{lab}=\cos^{-1} V_z/V$
Cos =cos θ_{lab}
Cos =sin θ_{lab} sin ϕ_{lab}
Cos =sin θ_{lab} cos ϕ_{lab}
RETURN

Neutron inelastic scatter

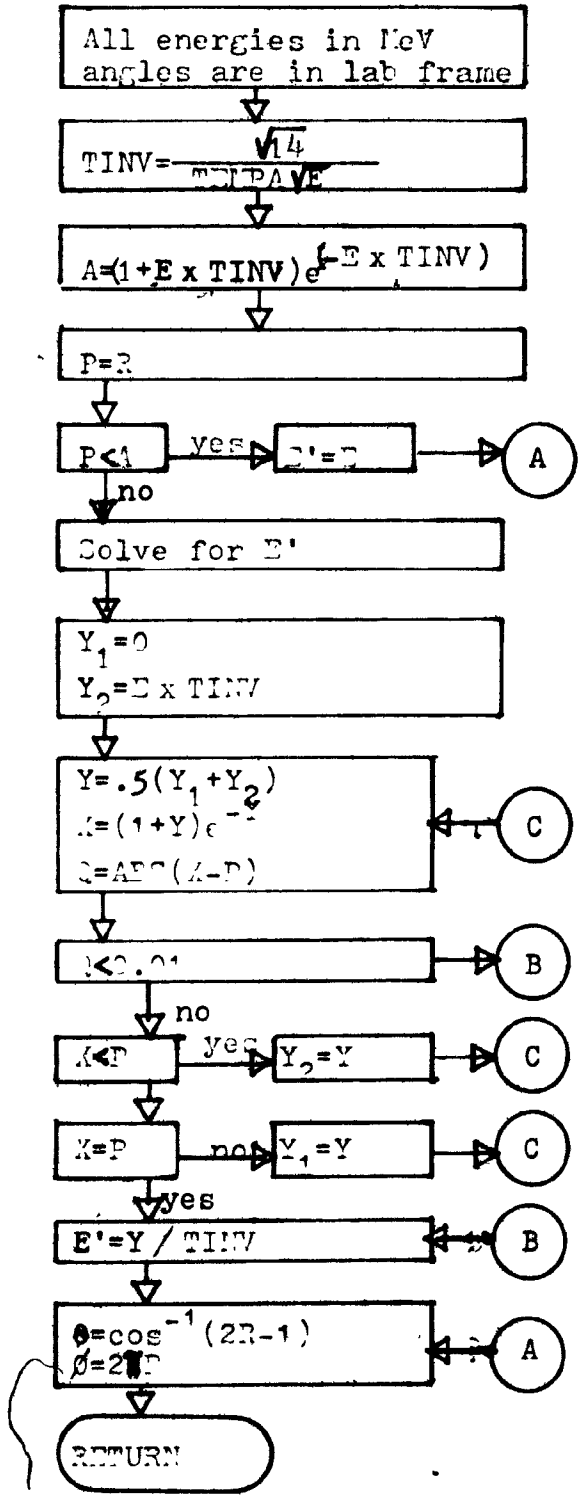

Figure II.4

Angular Distribution Of Neutrons Elastically Scattered Off ^{16}O

◇ BNL 400

□ Approximation Used In This Work

Figure A Bombarding Energy = 4 MeV

Figure B Bombarding Energy = 14 MeV

Figure A

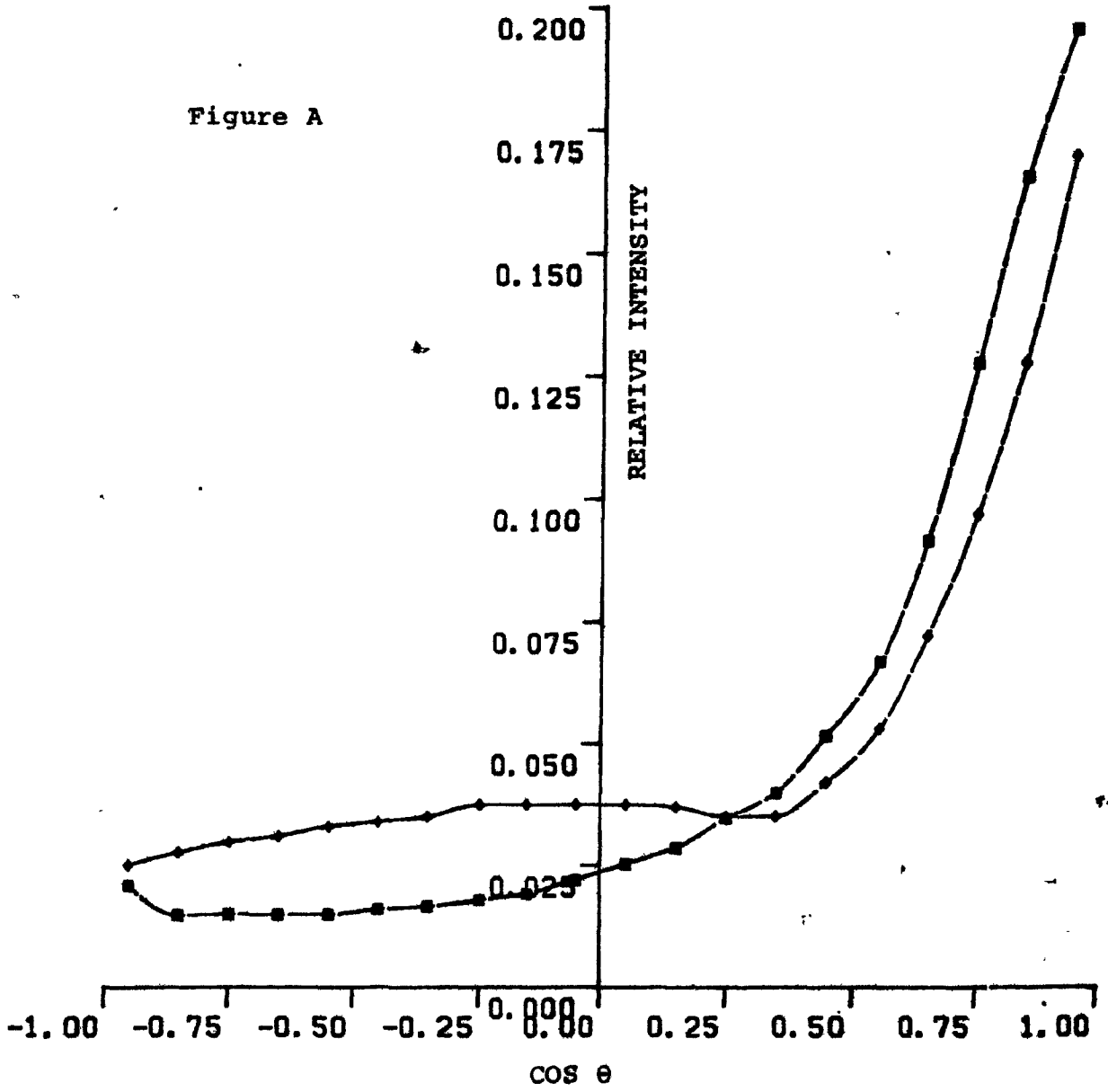
0.200
0.175
0.150
0.125
0.100
0.075
0.050
0.025
0.000
RELATIVE INTENSITY
-1.00
-0.75
-0.50
-0.25
0.00
0.25
0.50
0.75
1.00
cos θ

Figure B

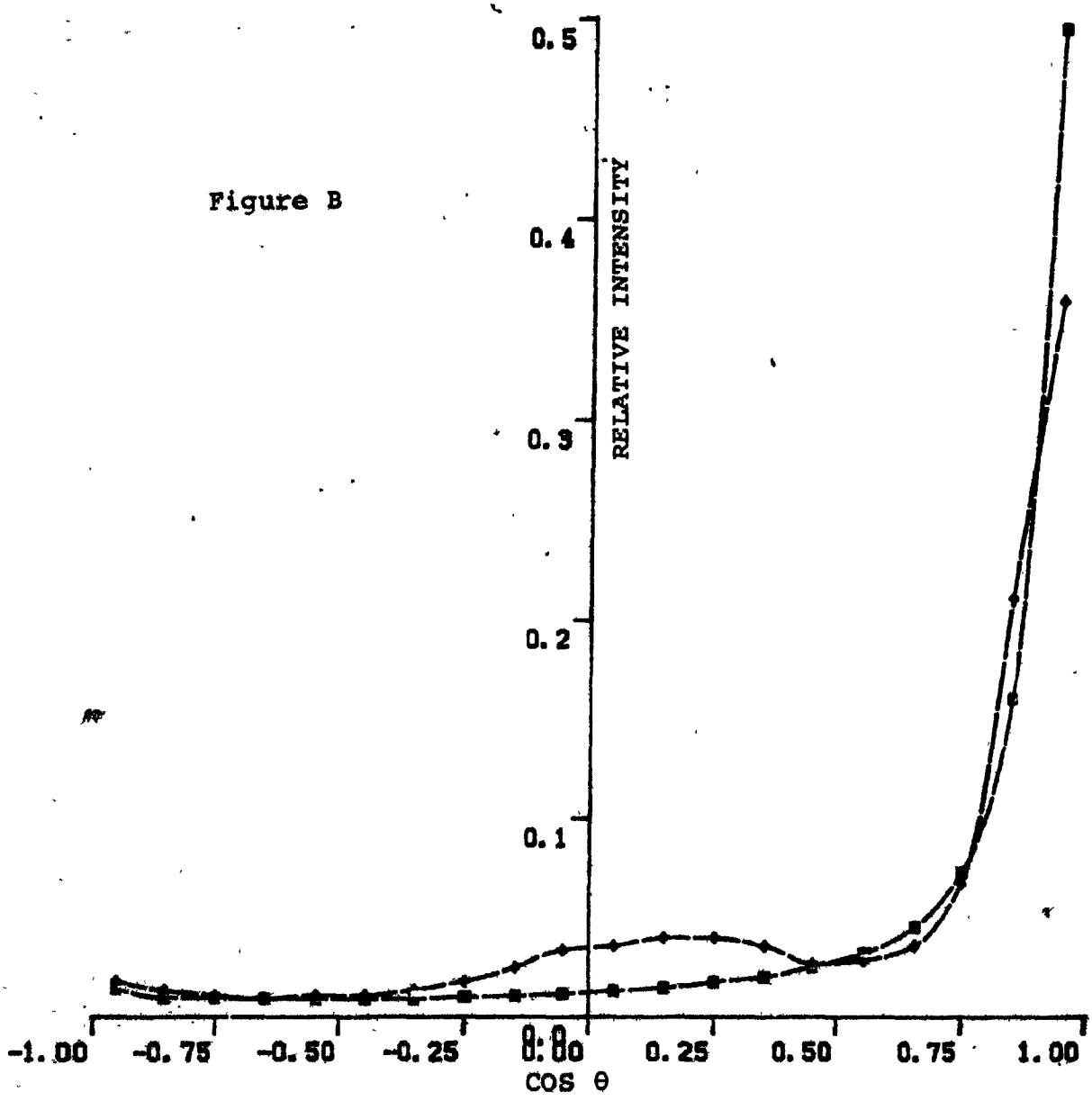
0.5
0.4
0.3
0.2
0.1
0.0
RELATIVE INTENSITY
-1.00
-0.75
-0.50
-0.25
0.00
0.25
0.50
0.75
1.00
COS θ

of the first excited state of the target nucleus, inelastic scatter begins to compete with the elastic process. It is then possible for the neutron to lose some of its energy leaving the product nucleus in an excited state which then decays to ground via γ emission. The treatment of the process in this work is open to question in that it uses a statistical analysis of the nuclear levels even for light nuclei though such an approach is strictly valid only for heavy ones. This is done for the sake of simplicity. In this approach (Sh65,ch.III), the scattered neutron's energy, E', is assumed Maxwellian. The probability density function of the distribution is proportional to $E'\exp(-E'/T)$ where $T=a\sqrt{E}$ is the nuclear temperature of the evaporation spectrum, a=constant depending on the nucleus and $0\leq E'\leq E$. T is related to the temperature T^0 for 14 MeV neutron bombardment by $T=T^0\sqrt{E(MeV)/14}$ where T^0 is taken from (Go71). Neutrons are boiled off the nucleus isotropically in the lab frame. Individual levels are ignored in this scheme and manifest themselves indirectly via their contributions to the inelastic cross section. The flowchart is presented in Fig.II.3D. The formula for selecting E' is

$$1-(1+E'/T)\exp(-E'/T)=R(1-(1+E/T)\exp(-E/T))$$

where R=random number. Solving for E' involves a transcendental equation which can be solved for by an iteration method.

SECTION II.5-SIMULATIONS

The MC programs discussed above were used in a variety of simulations. The results were compared with measurements

made by us as well as with published results of other experiments and numerical simulations covering a range of situations. Though a detailed description will be postponed until chapter IV, the scenarios studied are listed here for convenience:

1) point spread functions due to thermal neutron scatter in neutron radiography,
2) attenuation of 15 MeV neutron beams,
3) thermal and epithermal neutron distributions due to fast sources in water-filled spheres,
4) thermal neutron spatial distributions and neutron energy spectra in collimators in water shields due to internal fast sources,
5) thermal neutron spatial distributions in phantoms due to external fast sources.

The simulated phantoms noted above were assured to contain water only. Tissue equivalent (TE) liquids were used neither in the calculations nor in the measurements. This approximation significantly reduced memory requirements since water contains only two elements while TE targets contain four or more. The justification for this is discussed later.

CHAPTER III-EXPERIMENTAL METHODS

SECTION III.1-NEUTRON SOURCES

As already noted, neutrons may be produced via several mechanisms. Isotopic sources, to be discussed here, offer a number of significant advantages despite their limitations. They are small, relatively inexpensive, portable and simple to operate. Their neutron output is constant in time varying only as the radioisotope decays. Delivered doses can therefore be held fixed simply by setting exposure times. The sources are reliable and, unlike an accelerator, require no particular operator supervision or control. Physically they are rather small, simplifying shielding requirements. Also, the lower energy source neutrons result in higher thermal neutron fluxes in the target per unit dose relative to 14 MeV neutrons (Co73). This is of obvious value when using (n,γ) reactions for analysis.

Three fundamentally different isotopic sources are available: (γ,n), (α,n), and spontaneous fission (SF). Only the latter two have found significant application in elemental analysis.

(γ,n) reactions are often used to provide low energy, nearly monoenergetic neutron spectra. Photons above the neutron binding energy of a nucleus can cause neutron emission. Only deuterium and beryllium have been used as target materials because of their low (γ,n) thresholds of 2.2 MeV and 1.7 MeV, respectively. Presently, the most widely used source is ^{124}Sb-Be. It has the lowest average neutron

energy (24 keV) among all isotopic sources, a half-life of 60.3 days and is produced by irradiating the Sb filament in a reactor. In such a source, neutron production can be shut down by physically separating the γ source from the Be target. However, the intense γ radiation (1.7 MeV) and the low neutron yield are troublesome. The source is sometimes used to provide a very pure thermal neutron spectrum (Ch80).

The only SF source in general use is ^{252}Cf, which also decays by α emission. Some details are given in Table III.1. Its neutron spectrum is similar to that of ^{238}U fission and its specific neutron output is the highest of any isotopic source. Sources with emissions up to 10^{10} n/s are available and have the advantages of low γ intensity, small physical size, low heat output, low helium production and low toxicity (Amersham Industrial Radiation Products Catalogue, 1979). ^{252}Cf has been used extensively in partial body NAA and PGNCA (Mo81, Cu82). The lower energy, hence shorter penetration, of ^{252}Cf neutrons relative to the energy of (α,n) sources is usually considered to limit application to body regions near the skin surface. Studies have centered on activation of Ca in limbs and the spine and PGNCA of Hg and Cd in the liver and kidney. ^{252}Cf is also used in a variety of non-medical analysis applications (Gr78). The main impediments are its short half-life and the inability of the lower energy neutrons to excite anything other than (n,γ) reactions.

A number of different (α,n) sources are commercially available. These consist of an intimate mixture of an α emitting isotope and a target medium. Among the α emitters employed today are ^{241}Am, ^{239}Pu and ^{238}Pu. ^{226}Ra is used in

many older sources. Several light elements such as Be, B and Li can serve as the target but the highest neutron yield is obtained with Be. In this work, a single 1 Ci (37 GBq) and one 10 Ci ^{241}AmBe and two 14.3 Ci ^{239}PuBe sources were used and attention will focus on these. All were obtained from the Monsanto Corporation. Their neutron spectra are very similar and both types are commonly used in NAA and PGNCA. Some data about the sources are given in Table III.1. The average energies listed should be taken as only approximate for reasons outlined below. The PuBe sources are doubly encapsulated in stainless steel. Each is 5.5 cm high and 3.5 cm in diameter. The 10 Ci AmBe is roughly the same size. The 1 Ci AmBe is approximately 2cm x3cm.

Neutron production in the americium and plutonium sources proceeds by the $^{9}Be(\alpha,n)^{12}C$ reaction. The resulting neutron spectrum is polyenergetic. Though one would expect discrete α energies to result in discrete neutron energies, in practice this does not occur. α particles have short range and lose energy rapidly in traversing the source matrix. It is due to this that the α emitter and Be must be intimately mixed. The AmBe is packaged as a compacted mixture of americium oxide and beryllium metal powder. The PuBe is prepared as a metallic alloy. Consequently, the α spectrum striking the Be nuclei is continuous, smearing out the resultant neutron spectrum. The precise details depend on the specifics of manufacture. For example, large americium oxide grains would cause slowing down in the α emitter itself. The spectrum is further complicated by low energy neutrons from the break-up reaction

Table III.1

Properties Of Some Isotopic Neutron Sources Used In PGNCA And NAA

SOURCE	E_α (MeV)	$T_{\frac{1}{2}}$	Neutron Yield		γ exposure at 1m /Ci	Average neutron E	Principal γ energies
			n/s/g	n/s/Ci			
(α,n)							
^{238}PuBe	5.50 (72%) 5.46 (28%)	87.7y	5×10^{7}	3×10^{6}	1mRem/hr	4.4MeV	43.5keV
^{241}AmBe	5.48 (85%) 5.44 (13%)	433y	1×10^{7}	2.1×10^{6}	2.5mRem/hr	4.4MeV	59.5keV
Spontaneous Fission							
^{252}Cf	6.12 (84%) 6.08 (16%)	2.65y*	2.3×10^{12}	4.3×10^{9}	300mRem/hr	2.3MeV	42keV 100keV

*Effective $T_{\frac{1}{2}}$ - $T_{\frac{1}{2}}$ for α decay-2.73y
$T_{\frac{1}{2}}$ for SF -85.5y

Data taken from (Le78), Amersham Radiation Products catalogue, Monsanto specifications

$^{9}Be(\alpha,\alpha')^{9}Be^{*} \rightarrow {}^{8}Be + n$.

Also, the ^{12}C nucleus may be left in an excited state

$^{9}Be(\alpha,n)^{12}C^{*} \rightarrow {}^{12}C + \gamma(4.44 \text{ or } 3.21 \text{ MeV})$

thus subtracting the excitation energy from that of the neutron. For α emitters in our energy range of interest, only the 4.44 and 7.65 MeV levels of ^{12}C can be excited. Furthermore, (n,2n), (n,n'), (n,n) or even (n,f) neutron interactions in the source further modify the spectrum. Some of these factors are a function of source size and encapsulation material and thickness. Detailed discussions are given in (An72), (Vi73), (Ku77), and (Ge75). In general, the larger the source the softer the spectrum. In the case of sources containing fissile material such as ^{239}Pu, the spectrum can be further modified by fissions induced in the source by moderated neutrons reflected back into it by its radiation shielding (Ca70). Thus, even the manner in which it is stored may affect the spectrum.

Throughout this work, it was assumed that emission from the sources was isotropic. This is not strictly the case due to the scattering of neutrons in the cylindrical encapsulations. Transmission along the cylindrical axis of the source can be as much as 20% lower than normal to it. This factor is also a function of source size (Ra78). The spectrum also differs along the two axes. It is generally softer along the cylindrical one. Additionally, due to details of manufacture, the emission even in the radial direction is not necessarily uniform. This can be verified for individual sources by autoradiography. The deviation from isotropy can be marked (Bo73).

Many measurements and theoretical calculations of isotopic neutron source spectra have been published. It occurs that the general shapes of ^{239}Pu-, ^{238}Pu-, and ^{241}Am-Be spectra are similar but differences do exist between different types and even different sizes of sources. Precision measurements are difficult since spectrum deconvolution itself can introduce significant differences in independent determinations. Experimental measurements have been made with a variety of devices such as organic scintillators (Ci68, Mo81), ^{3}He spectrometers (K182) and nuclear emulsions (An62, B167). Most such measurements, as well as theoretical calculations, are somewhat unreliable below about 2 MeV. Additionally, no theoretical evaluations for ^{238}PuBe sources could be found. However, the close similarity in the α energies of ^{238}Pu and ^{241}Am would suggest comparable similarity in their neutron spectra, barring the differences in the slowing of the α's due to their different constructions. The spectra finally chosen for use in the MC calculations were those of (Ge75) for ^{241}AmBe and (B167) for ^{238}PuBe. Further details and graphs of the spectra used are given in chapter four.

SECTION III-2-SHIELDING

Shielding of sources serves two purposes. A proper shielding arrangement should protect the gamma detectors used in (n,γ) experiments from the direct neutron and gamma radiation of the sources as well as minimize gamma background due to neutron interactions in the room and construction

materials. Also, it must serve as a biological shield to reduce the radiation dose in the vicinity of the sources to tolerable levels. Neutrons of up to several MeV are strongly attenuated by hydrogen containing materials due to the large (n,p) elastic cross section. Compounds such as H_2O, CH_2 (paraffin) or polyethylene ($(CH_2)_n$) are most suitable due to ready availability and low cost. Higher energy neutrons (such as those produced by D-T reactions) are well shielded by heavy elements such as iron or lead (Cy75, St81, Ro81). For heavier elements at higher energies, inelastic scattering is most effective. In our case, sources were shielded by a combination of a 75 cm diameter water tank and additional paraffin blocks. Ordinary tap water was used in the experiments measuring neutron distributions along the collimator. For the measurements of distributions in the phantom, it was found that thermal neutrons leaking from the water shield contributed significantly to a depth of 6-7 cm. Therefore, for this part of the work, 0.5% (by weight) boron in the form of sodium borate (borax) was dissolved into the water. Additionally, the phantom rested on cadmium sheet which covered its sides as well. The boron also reduced by approximately 30-40% the 2.2 MeV gamma flux emitted by the shield due to the $^1H(n,\gamma)^2H$ reaction. The lower energy γ ray produced by

$$^{10}B(n,\alpha)^7Li^* \rightarrow {}^7Li + \gamma(478keV)$$

is more easily shielded.

A sketch of the shielding arrangement and source placement is given in Fig.II.2. Two sizes of collimators were used. They were constructed of rigid Plexiglas tubing

of length 45 cm and inner diameters of 7.5 cm and 20 cm. The distance between the bottoms of the collimators and the phantom was kept at 55 cm. Buoyancy presented considerable difficulty especially in the case of the larger tube. Indeed, lead blocks had to be placed inside of it to facilitate placement. Interchange between the two collimators could be performed by an individual in a matter of minutes. The sources themselves were kept in a watertight polyethylene bottle to prevent corrosion. They could be positioned at any depth beneath the collimator bottom. When not in use, they were lowered and covered by 60 cm of water. As they were stored in a basement, no additional shielding was required beneath them.

SECTION III.3-TARGET MEDIUM

As noted previously, the phantom measurements were conducted using water rather than a TE liquid. This was done for the sake of convenience and because of limitations imposed by the computer used for the simulation studies. Water is usually considered an adequate model of human soft tissue (Am74,Cr81). To be more accurate would require the introduction of small quantities of carbon and nitrogen principally as well as calcium, chlorine and sodium. However, formulations differ from author to author and tissue type to tissue type (Au68,Mu80). Simulating a combination of the skeletal system and soft tissue can be done (Za79) but requires care to maintain neutron transport equivalence since, usually, the TE liquid is prepared as a simple

solution while in the body some elements are considerably localized. When using water, the only suggested correction would be a density correction since soft tissue is given as 1.1 g/cm^3.

Ordinary tap water was used with no filtration or distillation. A sample of Montreal water was found equivalent to distilled in thermal neutron transport properties when tested on a thermal column at Chalk River Nuclear Laboratories (J. M. Robson, personal communication).

The phantom walls were constructed of 3 mm Plexiglas (methyl methacrylate). In terms of neutron interactions, water and Plexiglas are quite similar (Dr80). Again, only a density correction is necessary since the density of the latter is 1.18 g/cm^3. The phantom was of dimensions 30x30x40 cm^3 where the last represents the maximum depth to which it could be filled. It was supported 10 cm above the collimator mouth on an aluminium platform.

SECTION III.4-NEUTRON PROBES

As neutral particles, neutrons cannot directly produce ionization in detectors. They can however be detected and counted by a number of techniques using activation products, reactions with nuclei in proportional or ionization counters, interactions in photographic emulsions, damage tracks left in materials such as plastics, etc. In this work, neutron activation of metallic foils was used to map the spatial distributions of the thermal neutron fluxes. Foils offer a number of advantages. They are relatively cheap, insensitive

to gammas below the (γ,n) threshold, independent of external connections and rugged. They can be made sufficiently small to avoid or at least minimize flux depression. They are time integrating and as such are not suitable for time dependent fluxes. However, this is of no consequence in this work.

Any element with a large activation cross section and which yields a radioactive product with a convenient half-life, which can be shaped as desired (either in pure form or in compound or alloy) and which is chemically inert, can be used as a neutron detector. A number of elements meets these requirements in the thermal, resonance and fast energy regions (RE79) though the region of 10-500 keV remains dificult to measure. Only thermal and resonance (n,γ) activation is considered below. Characteristics of three very common thermal neutron detectors are given in Table III.2. Two other elements which have much to recommend them are vanadium and tin (G176). They have not been listed due to their short half lives.

Consider a foil of density N nuclei/cm^3 and volume V capturing neutrons at the rate of R_o per second with a resultant radioactive product of half-life $T_{1/2}$ (mean life $\tau=T_{1/2}/\ln 2$). The number of radioactive nuclei, N*, obeys

$$dN^*/dt=R_o-N^*/\tau \qquad (1).$$

The activity of a foil which has cooled for t_c seconds following an irradiation of duration t_i is given by

$$R(t_c,t_i)=R_o(1-\exp(-t_i/\tau))\exp(-t_c/\tau) \qquad (2).$$

The count rate, corrected for total detection efficiency, ϵ, including geometry effects and the like is

$$C(t_c,t_i)=\epsilon R(t_c,t_i) \qquad (3).$$

The saturated activity is that activity which would be observed immediately after an infinite irradiation (in practice, $t > 7T_{V_2}$)

$$C_o = C(t_c = 0, t_i = \infty) = \epsilon R_o \qquad (4).$$

The number of counts observed in the interval $t_2 - t_1$ is given by

$$I = \int_{t_1}^{t_2} C(t_c, t_i)\, dt_c = \tau(C(t_1, t_i) - C(t_2, t_i)) \qquad (5).$$

The count rate at saturation is

$$C_o = I/\tau / (\exp(-t_1/\tau) - \exp(-t_2/\tau)) / (1 - \exp(-t_1/\tau)) \qquad (6).$$

Assuming ϵ is known, the thermal neutron flux can be obtained from

$$\Phi = R_o / (N\sigma V) \quad \text{neutrons/cm}^2\text{/sec} \qquad (7)$$

where σ is the 0.025 eV capture cross section (see appendix B). ϵ is in fact usually difficult to ascertain from fundamental principles. Therefore, for absolute determinations, it is more usual to use a calibrated foil or source to fix this system parameter.

A number of reasons led to the selection of manganese as the detector for this work despite the availability of the other elements listed in Table III.2. An absolute calibration methodology had been previously established for Mn (J.M.Robson, personal communication). The Mn foils (actually, Mn(88%)Ni(12%), 0.005" (0.125mm or 90 mg/cm^2) nominal thickness) were rugged enough to sustain repeated handling. Both the indium and gold foils were so soft and thin that they could be torn easily and should ideally have been used with some sort of backing. The nickel content of the Mn foils presented no significant interference as can be seen from Table III.3. The only reaction of possible concern

Table III.2

Commonly Used Thermal Neutron Activation Foils

Reaction	Isotopic Abundance	$T_{\frac{1}{2}}$ of product	$\sigma(n,\gamma)$ barns*	Radiation of product	First Resonance	$\sigma(n,\gamma)$ for all resonances
$^{197}Au(n,\gamma)^{198}Au$	100%	2.695days	98.65±0.09	β^- 0.96MeV γ 0.41	4.9eV	1550±28 b
$^{115}In(n,\gamma)^{116m}In$	95.7%	54.1min	162±12	β^- 1.00MeV 0.87 0.60 γ 2.11 1.29 1.10 0.42	1.46eV	3300±100 b
$^{55}Mn(n,\gamma)^{56}Mn$	100%	2.58hrs	13.3±0.2	β^- 2.84MeV 1.03 0.65 γ 0.85	336eV	14.0±0.3 b

Only the most intense radiations have been listed.

*Measured at 2200m/s

Data taken from (Le78), (Mu81)

Table III.3

Activation Reactions Of Ni In MnNi Foils Used For Neutron Flux Measurements

Reaction	Abundance	$T_{\frac{1}{2}}$	$\sigma(n,\gamma)$ barns	Radiation
$^{58}Ni(n,\gamma)^{59}Ni$	68.3%	7.5×10^{4} y	4.6±0.3	Electron capture
$^{60}Ni(n,\gamma)^{61}Ni$	26.1%	stable	2.9±0.2	--------
$^{61}Ni(n,\gamma)^{62}Ni$	1.13%	stable	2.5±0.8	--------
$^{62}Ni(n,\gamma)^{63}Ni$	3.59%	100y	14.5±0.3	β^- 0.065 MeV
$^{64}Ni(n,\gamma)^{65}Ni$	0.91%	2.52hrs	1.52±0.03	β^- 2.14 MeV 0.65 γ 1.482 1.116

(^{64}Ni(n,)^{65}Ni) can be ignored due to the low isotopic abundance of ^{64}Ni. The relatively low $\sigma(n,\gamma)$ of ^{55}Mn means that self-shielding and flux depression are not serious and that the foils could be spaced closely together (see appendix C). The Mn β^--rays are not as strongly absorbed in the foils themselves as are those due to other elements (Fig.III.1). This is not of great significance in our case since the foils are sufficiently transparent that the activation throughout their volume is uniform. Finally, the first resonance of Mn is far removed from the thermal region (Table III.2) and causes no perturbation to the 1/v propotionality of the cross section. As a result, it was found empirically that the foils could be used to measure the thermal fluences without recourse to cadmium difference measurements as explained below.

The principal disadvantage with these probes was that their count rates were typically low necessitating longer counting intervals. Corrosion of the foils did occur when they were used in the water phantom but, as would be expected, the oxidation was found to make no difference. To eliminate possible contaminants such as sodium from human perspiration, the foils were washed in acetone before and after use. To ensure that no Mn was being dissolved off the foils by the water in the phantom, a foil was immersed in water for several days and then reweighed. No mass was lost.

Some of the perturbation effects discussed above and in appendix C were experimentally investigated for this work. Specifically, self-shielding, flux depression and absorption were considered in a set of simple tests.

Figure III.1

Absorption Of β^-'s Emitted From A Thin Foil As A Function Of Thickness Of An Absorber Of The Same Composition As The Foil. Graphs Are Normalized To 100% Transmission At Zero Absorber Thickness.

Based on Fig 11.1.8 (Be64)

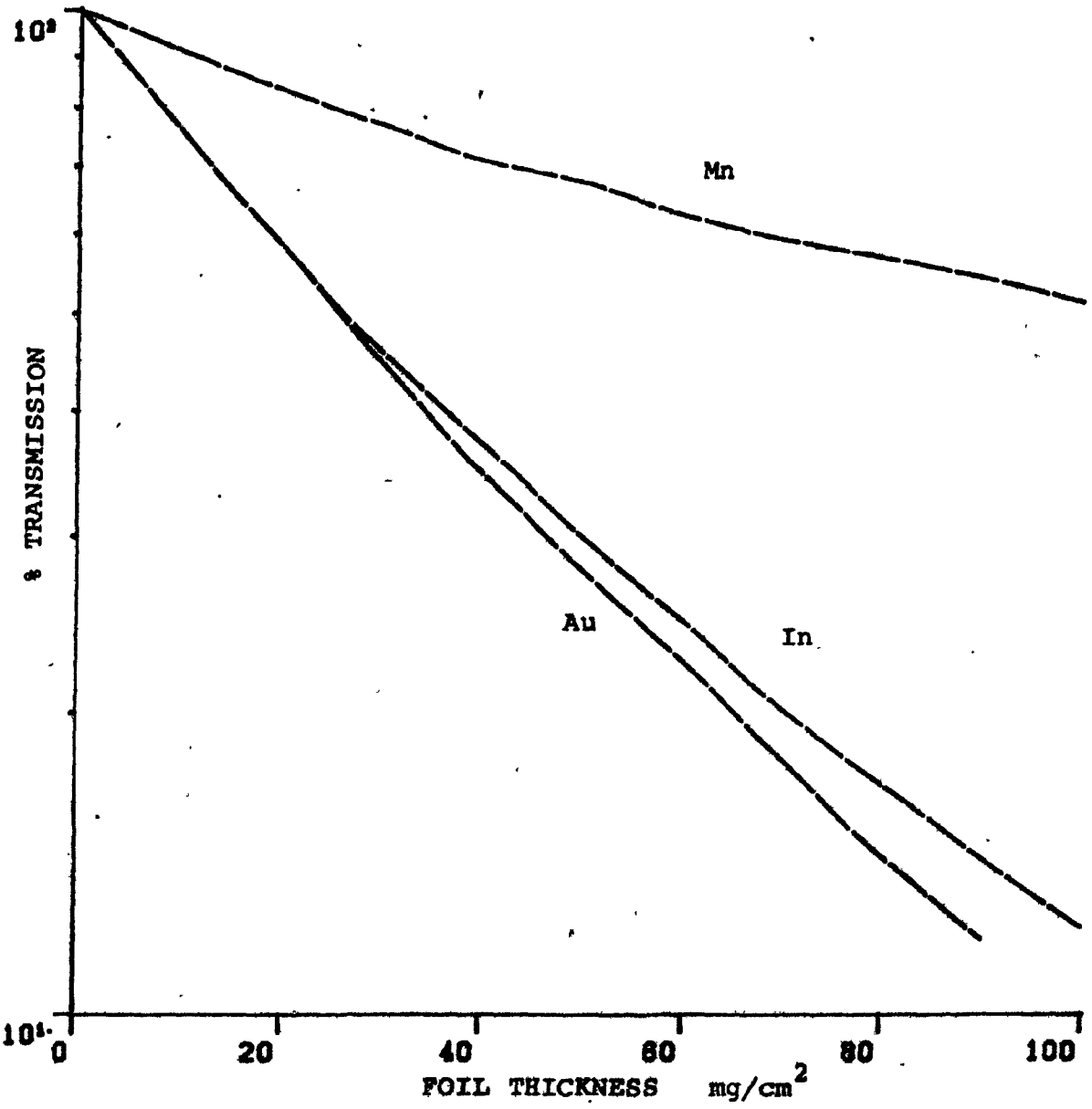
10²
10¹
% TRANSMISSION
Mn
Au
In
0
20
40
60
80
100
FOIL THICKNESS mg/cm²

Though a discussion of the foil counting system is deferred, it can be noted that the detector looked at only one side of a foil. By flipping a foil over and recounting it, one can obtain a measure of the joint effect of non-uniformity in activation throughout the probe volume as well as β^- absorption within the foil. This was done on several occasions for foils which had been irradiated in the shield's collimator. Within statistical errors, no differences were observed implying that self-shielding need not concern us. Though no serious work was done using indium, it is instructive to note that a single measurement with an In foil of thickness $\sim 110\,\mu m$ (~ 80 mg/cm^2) found a discrepancy of $\sim 4\%$ more than accounted for by statistics when counting opposite sides. Since the matter was not pursued, it is difficult to definitively state that this was due to self-shielding, but this is a matter requiring more consideration when using In.

Another test done for irradiations in the collimator involved a sandwich of three Mn foils. As discussed in the next chapter, calcuations indicate that the flux in the collimator is very close to isotropic, especially nearer the bottom. Nevertheless, some small anisotropy is not ruled out. Thus, the outer two foils of the sandwich need not necessarily yield the same activity. Activity would be lowest in the third foil. This was in fact observed but the difference between the middle and third foil was only $1.6 \pm 0.3\%$ while between the outer two it was $3.5 \pm 0.5\%$. This is in very good agreement with the value predicted for P_s in appendix C. The agreement may of course be only fortuitous

since F_s is given for the highly anistropic case of a neutron beam. It thus seems clear that not only thermal but also resonance self-shielding effects are small for these foils. As a result, however, it is also difficult to obtain an "uncontaminated" measurement of the 1/v part of the spectrum by filtering out resonance neutrons (Be64,Fig.12.1.7).

Flux density depression at a distance from a foil was considered for irradiations done in both the collimator and in the phantom since it determines the minimum spacing of foils. Though the depression is most severe in hydrogenous moderators, since the perturbed flux density extends a distance on the order of the thermal neutron diffusion length, spacings can be smaller in such moderators. In this work, Mn foils of nominal areas of 1 cm^2 and 5 cm^2 were used. The foils were roughly square in shape. To calculate perturbation effects, these were considered equivalent to circular foils of radii 0.6 cm and 1.3 cm. At a distance of 2 cm from the larger ones, the perturbation is calculated to be <1% (app.C) in water. Irradiations of foils were made in the phantom in the presence and absence of other foils 2 cm distant. No differences were discernible. In the collimator measurements (in-air scattering), the minimum spacing used was 5 cm and again no effects were observed due to neighboring foils.

Cadmium difference (CD) measurements, already referred to above, were carried out only in the collimator and only for the smaller foils since the others did not fit in the Cd boxes. These cases were nominally .037" (.095cm or 810 mg/cm^2) thick and completely enclosed the foils allowing no

leakage paths. Cd is very nearly a perfect filter with a very steep cut-off allowing only higher energy neutrons to penetrate to activate the detector. By activating a foil with and without a Cd cover, the epithermal (or epicadmium) flux can be separated from the thermal. In carrying out these measurements, the following considerations held.

The Mn cross section goes as 1/v in the range of interest. It is thus best to define an effective Cd cut-off energy, E_{Cd}, and set the cadmium correction factor (F_{Cd}) to 1 (Pr76,ch.7). (F_{Cd} =A(epi)/A(Cd) is the ratio of the epithermal component of the total activation of a bare foil to the epithermal activation of the covered foil. Without engaging in a detailed discussion concerning the determination of F_{Cd}, it may be noted that it varies as a function of the detector type and size as well as the neutron energy spectrum and angular distribution.) Selecting the proper E_{Cd} is a somewhat ambiguous procedure since it depends on the same parameters as F_{Cd} and these are not well determined in our case. For example, the neutron field in the collimator is intermediate between an isotropic one and a monodirectional beam and the degree of anisotropy varies with the height from the source. Nevertheless, it seems evident from Fig.9-11 of (ANL5800) that E_{Cd}=0.50±0.02 eV certainly brackets the correct value for our situation. The CD measurements reported in the next chapter thus represent evaluations of the neutron flux for energies of E<0.5eV and E>0.5eV. In the most extreme case, i.e. the measurements nearest the sources at a distance of 5 cm, the epicadmium flux contributed only about 2% of the activity in the Mn-

foils. Therefore, in all other work, no CD determinations were made and all contributions were assumed due to the subcadmium neutrons.

Positioning of foils presented some difficulties since one must take care that the positioning apparatus does itself not perturb the neutron field. In the case of the phantom, foils were placed on aluminum slats which slid into grooves milled into two Plexiglas sheets. These sheets formed the only two walls of an otherwise open "box" held together by thin plexi bars placed at the corners. Though the plexi is similar to water in its neutron transport properties, the sheets were spaced 20 cm apart to minimize their influence on the foils which were usually along the center line of the support (for "on-beam axis" measurements). The aluminum slats themselves could be a perturbing influence. Though $\sigma(n,\gamma)$ for Al is small (0.23 b) and would certainly not depress the flux near the foils, the slats displace water. Since their macroscopic cross sections (Σ_a=0.177 cm^{-1}, Σ_s=0.138 cm^{-1}) are very different from those of water (Σ_a=0.0222 cm^{-1}, Σ_s=3.44 cm^{-1}), they could affect the local neutron distributions. To check this, two sizes of slats were used: 2.5x20x0.17 cm^3 and 1.5x20x0.08 cm^3. Foils were always placed so as to be normal to the cylindrical axis of the collimator. Additionally, plexi slats (0.16 cm thick) were used to replace the Al in one run. These were not used in general since they were very flexible and for repositioning accuracy the more rigid Al ones were preferred. It was found that the aluminum made no difference. To further verify the innocuous nature of the plexi, one run was

made with a sheet of approximately 0.6 cm thick plexi directly beneath one of the foils at a depth of 4 cm. As can be seen from the graphs in chapter IV, at this point the thermal flux space distribution is rather flat and the density difference between Plexiglas and water should have no effect. One is therefore testing for the influence of the different elemental compositions. As expected, no effect (±2%) was observed. This does, however, disagree with results quoted by (Sm62) where a 10% reduction in the thermal neutron flux was noted due to the presence of Perspex plastic. Their result remains unexplained.

Some irradiations were also made off-axis in the phantom, i.e. foils were displaced laterally to the side of the collimator axis. Only a few such measurements were made for purposes of comparison to calculation. Typically, as a check on positioning accuracy, 2 foils were irradiated simultaneously in symmetric placement about the central axis.

As stated previously, in-phantom measurements were made with the phantom placed above the mouth of the collimator. Such a situation can however be difficult to simulate numerically because the neutron spectrum striking the target has been significantly modified (softened). The Cd sheet eliminates neutrons below 0.5 eV only. Not only the spectrum exiting the collimator need be considered but also the leakage spectrum from the vicinity of the shield near the mouth. Quite aside from energy considerations, the angular distribution of the emitted neutrons, coupled with the variations of all these factors as a function of position along the bottom face of the phantom, further complicate the

situation. Therefore, to obtain "cleaner" and more readily definable irradiation conditions, a set of runs was made with the phantom standing in the middle of a large room away from scattering surfaces and with the 1 Ci AmBe source suspended ~10 cm below it. The phantom was approximately 1.5 m above the floor and at least 2 meters from the nearest wall and the ceiling.

Two different assemblies were used to position foils along the length of the 7.5 cm collimator for flux measurements in this geometry. In one, thin Al rings, across which could be stretched adhesive tape, were affixed to a plexi "spine". In the other, 0.16 cm thick plexi slats were inserted into a wooden one. A holder was placed in the collimator such that the spine would rest upright against the collimator wall and either the tape or slat would hold the foil perpendicular to the cylindrical axis in the center, though to test for uniformity across the horizontal plane, foils were also irradiated near the collimator wall on one occasion. In this fashion, the amount of moderating and scattering material next to the foil in the collimator was minimized. To determine the perturbing influences of the different foil holders, both were irradiated separately in identical geometries. Also, an irradiation was made using the second assembly with an additional 0.16 cm plexi resting on the backs of some of the regular slats. The plexi was found to increase the measured thermal neutron flux by, evidently, scattering back into the foil thermal neutrons which had previously escaped capture. The increase, difficult to measure since it involves small differences

between somewhat large quantities, was 4(±1)% when using the second assembly. Despite this, since foil placement was both easier and more reliable, this device was normally used and a correction applied to the data.

Foils were held in place with two types of adhesive tape, one a standard "Scotch" brand tape and the other a water-proof one. Neither was found to have any effect.

As noted previously, two sizes of foils were used in this work. The selection of a particular size was determined by the intensity of the field to be measured. Fluxes in the collimator were sufficiently high that the 1 cm^2 foils yielded sufficient activity for counting. In the phantom measurements, the 5 cm^2 foils were needed to accumulate adequate statistics. Some care must be exercised in using differently sized foils since they sample different regions of the plane in which they rest. Before comparing results thus obtained, one must ensure that the field is uniform across the plane. It was found both experimentally and by calculation that the assumption of uniformity is valid in the case of the collimator but not the phantom. For the dimensions of the foils used in this work, however, no correction was deemed necessary.

SECTION III.5-COUNTING OF FOIL ACTIVITY

As seen in Table III.2, either β^- or γ detection can be used in counting the activity of the manganese foils. γ-counting is often preferred (Yo82). However, since the equipment necessary for β^- detection was immediately

available and, far more importantly, a calibration scheme had been established using β^- detection, this method was chosen.

A block diagram of the counting apparatus is sketched in Fig.III.2. Foils were placed at a fixed distance of ~1 cm from the front face of a plastic scintillator (NE102) coupled to a photomultiplier tube (PMT). Pulses were taken off the PMT dynode and sent through a preamp and amplifier to a single channel analyzer (SCA). Pulses above the lower level discriminator transmitted +5V logic signals to the scaler. Timing of the system, i.e. length of counting interval and delay between counting intervals, were controlled by timers T_1 and T_2, respectively. The length of the entire counting cycle together with the number of counts recorded were then printed out.

A plastic scintillator is a particularly suitable choice for β^- detection since it is not encapsulated. As a result, there is no window to attenuate the incident β^- rays. The scintillator and PMT were completely wrapped in black electrical tape over Al foil to shut out ambient light. Thin Al foil only was stretched across the front of the NE102. Since a 1 MeV electron has a range greater than 0.2 cm in Al (Le76,appen.VII), this cuts off only lower energy particles which are in any event discriminated against.

As stated previously, absolute flux values could be assigned to the activated Mn foils counted in the above system. To do this, a $1cm^2$ Mn foil which had previously been calibrated by irradiation in a known neutron flux was used (Ro81). Following its calibration irradiation, the count rate of this foil was compared to that of a particular

uranium foil counted in the identical geometry. This latter source has an essentially constant activity (for ^{238}U, $T_{1/2}=4.47\times10^{9}$ years). Thus, counting both the calibrating Mn and uranium foils in our system allows for an absolute determination of the flux from their ratio. Uncertainty in the original calibration, however, means that the absolute values cannot be considered more accurate than ±15%, though this is a systematic error and relative fluxes are much more accurate.

A number of potential difficulties exist with the above system. As can be seen from the decay chain in Fig.III.3 (Se56), the U foil is a considerable α emitter. Electrons are emitted at several points in the chain. However, since the range of a 6 MeV α in Al is only 0.003 cm, these should be stopped completely by the foil on the front face of the NE102. Additionally, the light output of even a 6 MeV α in NE102 is considerably less than that of a 1 MeV electron (Nuclear Enterprises catalog) and as such is effectively rejected when discriminating against low energy electrons. These effects were in fact verified by interposing various thicknesses of Al foil between the U and the scintillator. Results, plotted in Fig.III.4, are consistent with exclusive β^- production in the source. They indicate that even with no additional absorber present, no α's are counted.

Another possible source of concern is the setting of the biasing level against low energy electrons. The β^- spectra of the ^{238}U daughter nuclei are different from that of ^{56}Mn. Therefore, different discriminator settings could result in different ratios of their activities. This was checked by

counting an activated Mn foil and the U foil with different discriminator settings. It was found that their ratios were unaffected except when the lowest energy electrons (<100 keV) were included. The energy calibration is very rough (as determined with a ^{207}Bi conversion electron source) but as a general conclusion it was found that, in our range of interest, the discriminator setting had no effect.

As noted previously, two different sizes of foils were used: 1x1 cm² and 2.3x2.3 cm². Even if centered at the same point, which they were not, the solid angle subtended by the second rectangle at a disc (representing the NE102) of radius 2 cm and height of 1 cm above the source is 7(±2)% less than for the smaller. This was calculated with a very simple MC program written for this purpose. Because of slightly different positionings, in fact, the normalized count rate due to the larger foils is 20(±2)% less, in agreement with a calculation with the MC. Results were adjusted accordingly.

The counting electronics displayed good stability with time. Results of all runs were normalized by counting with the U foil before each run. In all experiments, count rates were below 100 Hz. A test made at a count rate of 200 Hz showed no dead time effects.

Figure III.2

Counting Electronics For β^- Detection

All Numbers Refer To ORTEC (EGG)
Module Numbers

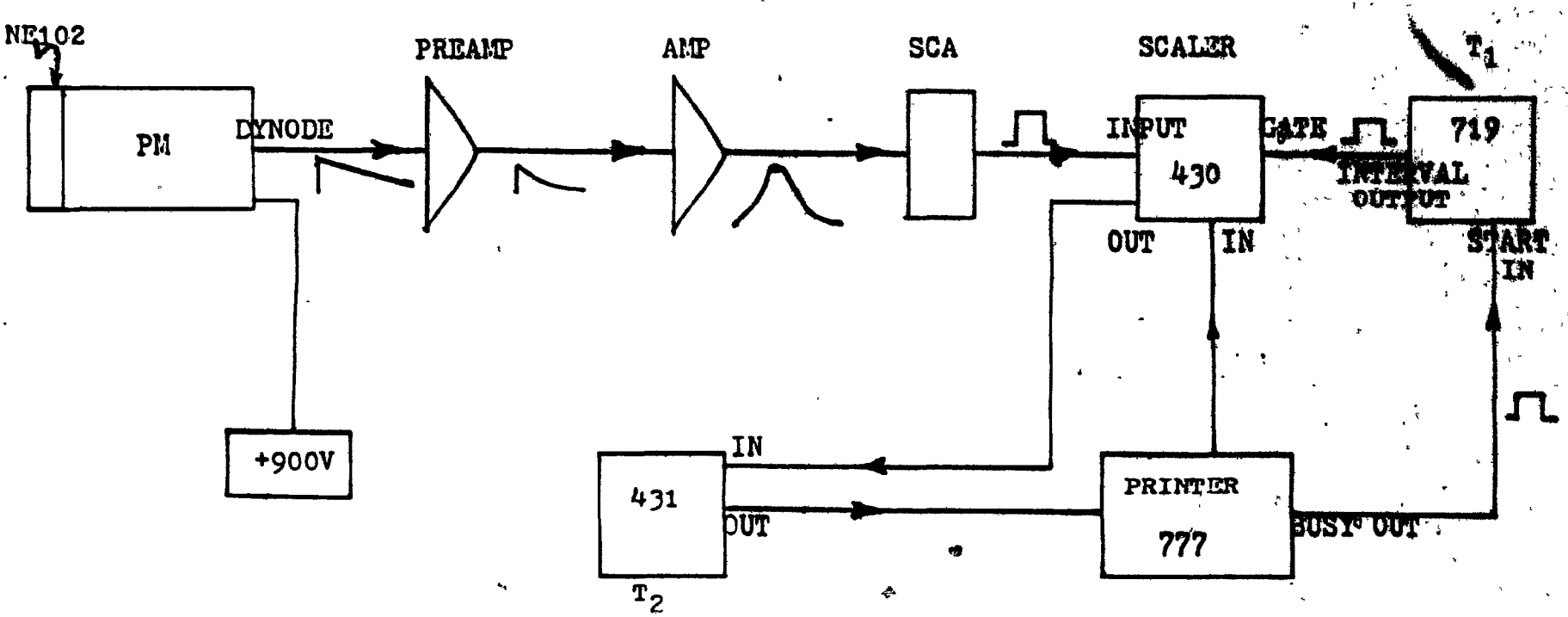
NE102
PM
DYNODE
PREAMP
AMP
SCA
SCALER
INPUT
430
GATE
INTERVAL
OUTPUT
719
T_1
START
IN
OUT
IN
+900V
IN
431
OUT
PRINTER
777
BUSY OUT
T_2

Figure III.3

Decay Chain Of ^{238}U

β^-'s And α's Are Emitted At Various Points In The Chain. Numbers Represent Energy Of Most Intense Radiation (MeV)

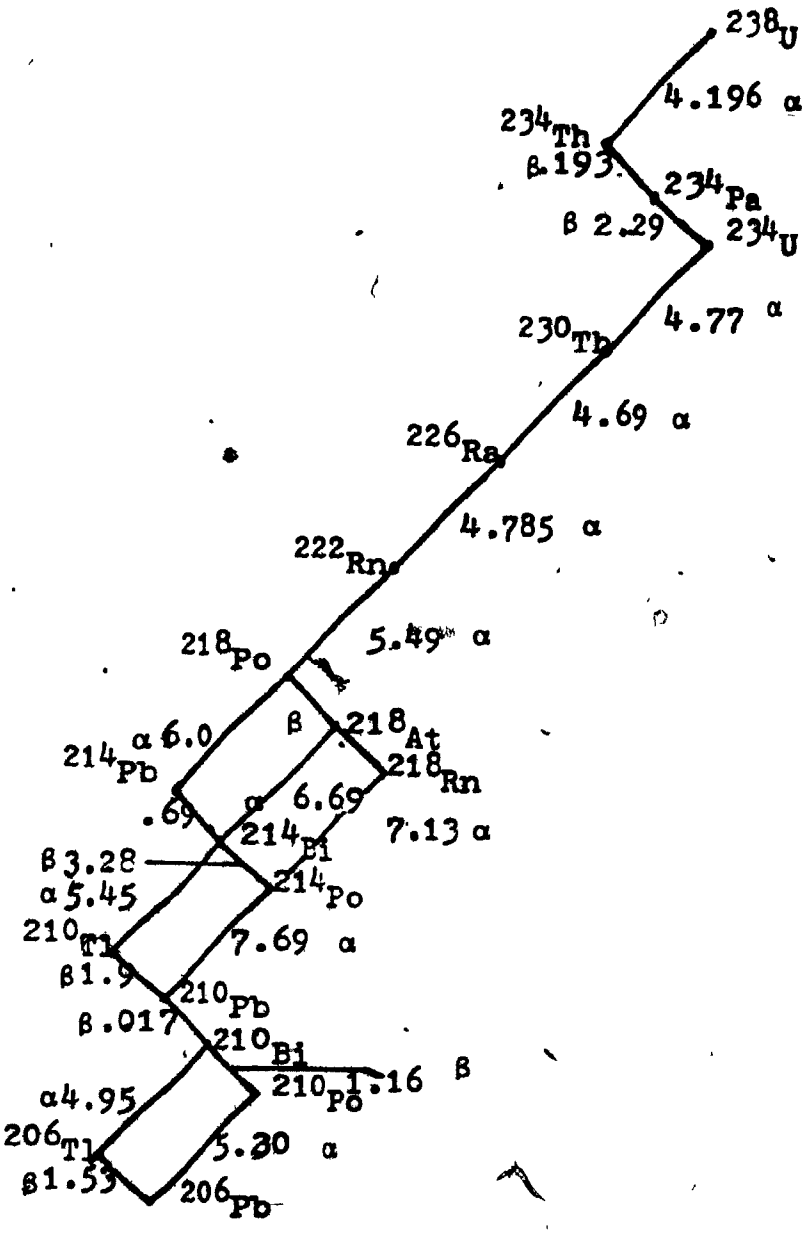
238U
4.196 α
234Th
β.193
234Pa
β 2.29
234U
230Th
4.77 α
4.69 α
226Ra
4.785 α
222Rn
5.49 α
218Po
β
218At
214Pb
α 6.0
218Rn
.69
α
6.69
214Bi
7.13 α
β 3.28
α 5.45
214Po
210Tl
7.69 α
β 1.9
210Pb
β .017
210Bi
210Po
1.16 β
α 4.95
206Tl
5.30 α
β 1.53
206Pb

Figure III.4

Count Rate Of ^{238}U Foil As A Function Of The Aluminum Absorber

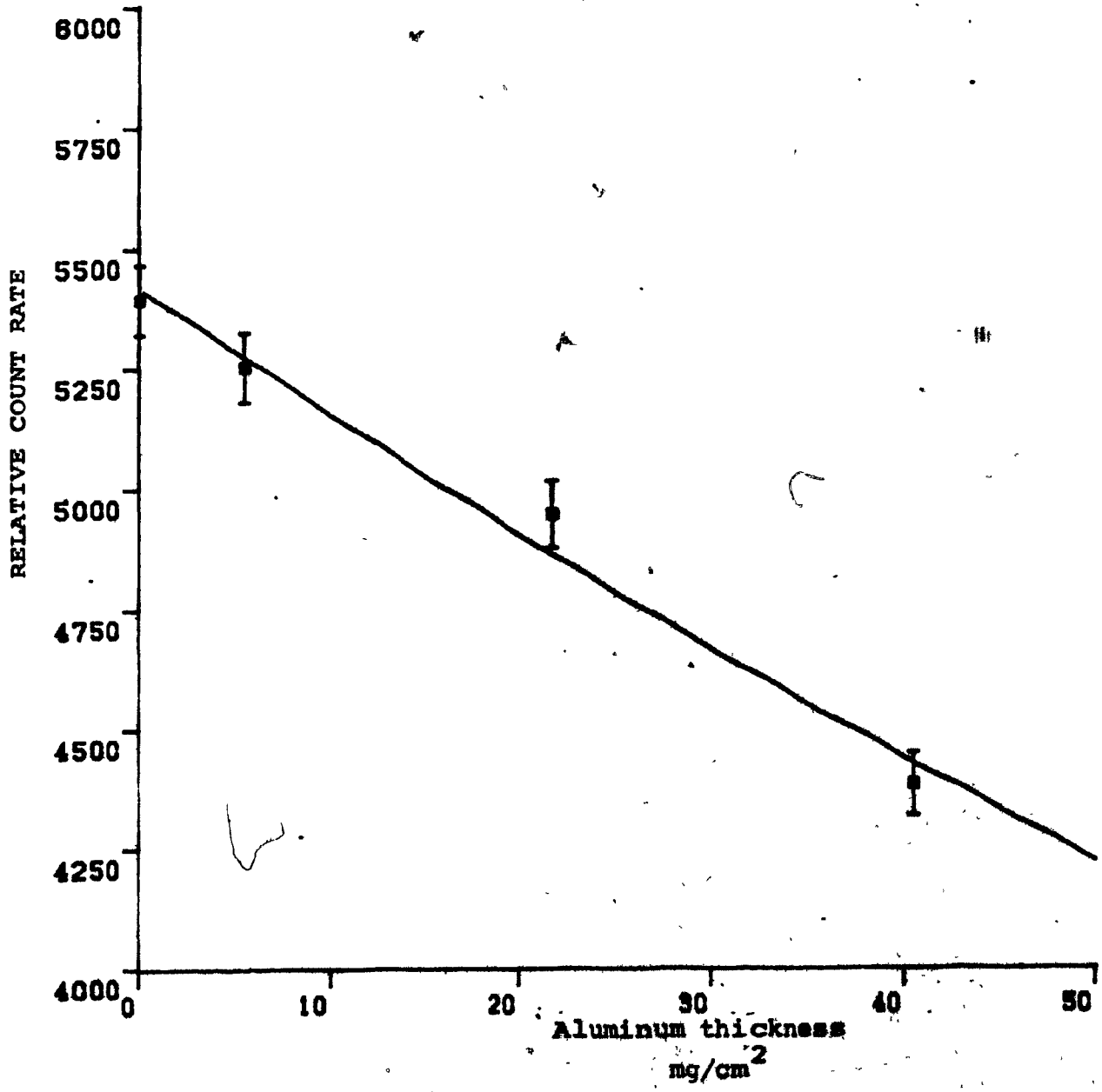
RELATIVE COUNT RATE
6000
5750
5500
5250
5000
4750
4500
4250
4000
0
10
20
30
40
50
Aluminum thickness
mg/cm^2

CHAPTER IV-RESULTS AND DISCUSSION

SECTION IV.1-TREATMENT OF DATA

Several potential sources of errors are to be found in the measurement of the thermal neutron flux spatial distributions. Perturbations caused by the activation foils themselves have already been dealt with as have solid angle effects introduced in counting foils of different sizes. Foil weights were determined to better than 0.2%, sufficiently small so as to be relatively insignificant. As earlier discussed, the same assumption was made with respect to the error arising from ignoring the epicadmium flux. The main sources of imprecision and inaccuracy in relative flux determinations were counting statistics and positioning errors. The latter were partly systematic and depended on the source-target geometry and the foil holders used. The reproducibility of results was taken to be a measure of the non-systematic component in the errors reported below. Statistical counting errors varied widely depending on the intensity of the flux being measured but, in general, were taken to be $\sqrt{N}$ where N was the number of counts collected. The error in the timing of the counting interval was taken to be negligible. Thus, from equation III.7, the standard deviation of a relative flux determination was taken to be

$$s(\phi)/\phi = \sqrt{N_c + A^2 N_b} / (N_c - AN_b)$$

where N_c is the total number of counts recorded in time Δt, N_b is the number of background counts collected over a long time to reduce the variance, A is the factor for normalizing

the background to the interval Δt and $\dot{\phi}=N_c-N_b$. For the absolute value of the flux, an additional error of ±15% is due to the uncertainty in the original calibration in addition to the statistical variance in counting the calibrating foils.

The numerical simulations present a host of potential sources of error of which some are inherent in the methodology. To begin with, the results can be no better than the available data for the cross sections. It is not always clear just what uncertainties should be assigned to such data and, indeed, there are procedures which attempt to correct cross section libraries by comparing simulations which use them to benchmark experiments (Jo81). Furthermore, as noted previously, the energy group structure may introduce systematic errors by being too coarse or weighted incorrectly (Ce82 and DLC31-section 4). The inaccuracy in modelling the elastic scatter angular distribution may also contribute. Obtaining an a priori estimate of the effect of all these factors is well nigh impossible (or at least extremely difficult) and so their individual contributions were ignored. It was simply assumed that a comparison of final results with experimental data would provide an overall assessment of their collective significance.

Quite apart from the above considerations, any results obtained with the MC program are subject to statistical fluctuations. For a large number, N, of particles of unit weight crossing a particular region, the error in N should again be $\sqrt{N}$ if one assumes a Gaussian (or Poisson) distribution. The applicability of this definition to the

simulation results is not always obvious. For example, in accumulating the flux across a particular boundary, we are counting not simply N but $\sum_{i=1}^{N} 1/\cos\theta_i$. The additional random parameter must introduce an additional uncertainty but how to appropriately account for it is not clear since it is certainly not independent of N (i.e. the value of θ decides not only the weighting of the contribution to the flux but also whether the neutron will cross at all). Then again, one must be concerned with any possible effects of the pseudo, as opposed to true, randomness of the simulation. To gauge the influence of all these considerations, several simulations were broken up into smaller batches of neutron histories so that partial results could be compared. In general, it was found that for large N ($N \sim 10^4$) the results definitely appeared to follow Poisson counting statistics. For smaller samples ($N \sim 10^2$) the results seemed to occasionally fluctuate somewhat more, i.e. it appeared that $s^2 > N$. The deviation is difficult to quantify since it is by no means overly large. Though no particular remedial action was taken, this should be borne in mind when fitting and evaluating MC results. In those instances where inter-batch fluctuations and deviations from fits are appreciable, it may be reasonable to assign lower weights to such values.

Another parameter of interest, not available in the experimental measurements, may be considered in analyzing our errors. As discussed previously, the ratio of the flux to current must vary between 1 and 2. Thus, should the simulation result in a value >2, this may give some indication of the uncertainty in, at least, the current to

flux conversion. The matter, though not pursued further here, may deserve investigation.

Both the experimental and the calculational results were fit by the linear and non-linear least squares methods (Be69) to a variety of fitting functions, both for the extraction of particular parameters of interest as well as to smooth the data. Details are given in subsequent sections.

Some simulations were made rather independently of the purposes of the main body of this work in order to validate the MC program. These are presented first.

SECTION IV.2-THERMAL NEUTRON SCATTER

In neutron radiography, neutron scattering in the radiographed object is a major contributor to the blurring of the final radiograph. To rigorously describe the quality of an imaging system, the point spread function (PSF) may be introduced. The PSF may be written as a composition of the uncollided and scattered fluxes. Details may be found in (Se82) and references therein. An evaluation of the scattered component can be most helpful in deconvoluting the final image. Segal et al (Se82) have therefore calculated, using the MORSE transport code, the degree of neutron scattering which would occur in the geometry presented in Fig.IV.1. A zero-radius beam of monoenergetic thermal neutrons impinges normally on a slab of thickness, t. The slab is uniform so that Σ_a and Σ_s (absorption and scattering macroscopic cross sections, $\Sigma_t = \Sigma_a + \Sigma_s$) are independent of position. A detection plane is situated at a distance, d,

Figure IV.1

Geometry For Evaluation Of Thermal Neutron Scatter Component To Degradation Of Radiographic Image. The Target Is Effectively Infinite Along Axes Normal To The Incident Neutron Beam. It Has A Thickness t Along The Beam Direction. Scatter Is Calculated For Various Values Of r.

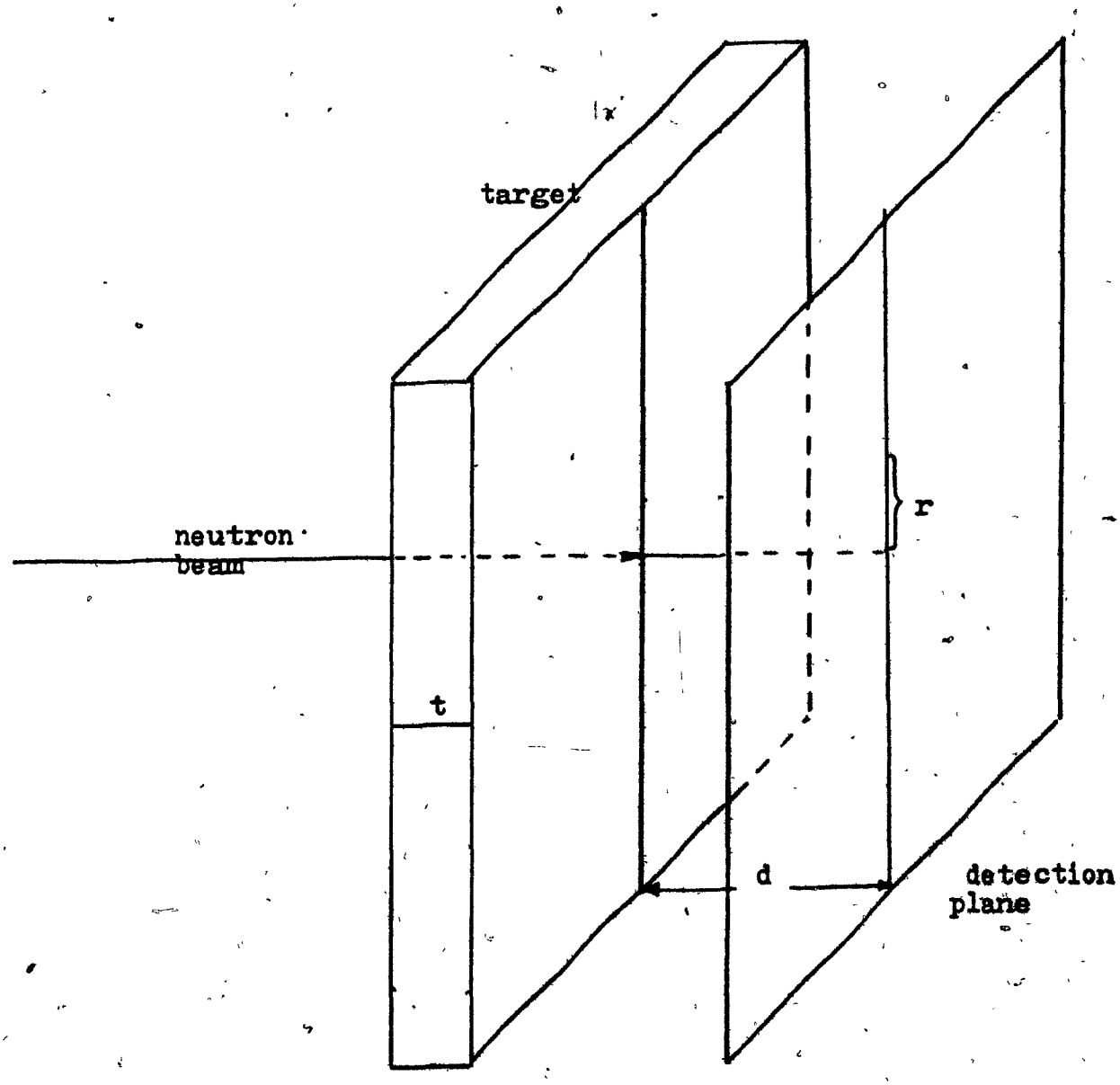
target
neutron
beam
r
t
d
detection
plane

from the rear face of the slab. The flux striking the plane is counted as a function of radius for different values of t and d as well as different slab materials.

As a first test, we have run a simulation similar to the above. However, a number of points must be noted. We have conducted the calculation for one material only - water. Water was assumed comparable to the polyethylene used by Segal et al provided that the $\Sigma_t t$ (or almost equivalently, $\Sigma_s t$) was kept the same. As can be seen from Table IV.1, this means greater thicknesses of water must be employed. Also, the polythene scattering cross section used by Segal and coworkers assumed anisotropic scattering of the thermals due to the chemical bond effect. As discussed earlier, no such factor is introduced into our calculations.

To compare our results to those of (Se82) requires plotting them as a function of r, the radial distance from the beam line. However, the program we have used counts the neutrons crossing through a certain region, i.e. a ring, bounded by $r_1 \leq r \leq r_2$. Therefore, r' was defined as that radius which would divide the ring into two smaller rings of equal area, i.e.

$$r_2^2 - r'^2 = r'^2 - r_1^2 \Rightarrow r' = \sqrt{(r_2^2 + r_1^2)/2} \quad .$$

A function of the form $a\exp(-br)$ was then least-squares fitted to the calculated values, where a and b are free parameters. In all cases, since we are fitting the scattered neutrons, the uncollided ones must be subtracted from the recorded fluxes. This is particularly simple in our case since this value is returned by the program.

Our results are presented in Fig.IV.2A for $\Sigma_s t = 3.0$ and

Table IV.1

Comparison Of Polythene And Water Cross Sections

Material	Σ_a (cm^{-1})	Σ_s (cm^{-1})	Σ_a/Σ_s	$\Sigma_t=\Sigma_s+\Sigma_n$
Polyethylene*	0.024	4.164	5.76×10^{-3}	4.188
Water**	0.022	3.443	6.39×10^{-3}	3.465

* From (Se82)
** From (La77,Appendix II)

Figure IV.2

Scattered Neutron Current (n/cm^2) Reaching The Detection Plane As A Function Of r, The Radial Distance From The Neutron Beam Axis. All Values Are Absolute And Normalized To 1 Incident Neutron.

Figure A Results for $\Sigma_s t$=3.0 and d=0.1,0.5cm

Figure B Results for $\Sigma_s t$=1.0 and d=0.1,0.5cm

Points are calculated values (this work)

Lines represent results of (Se82)

Figure A

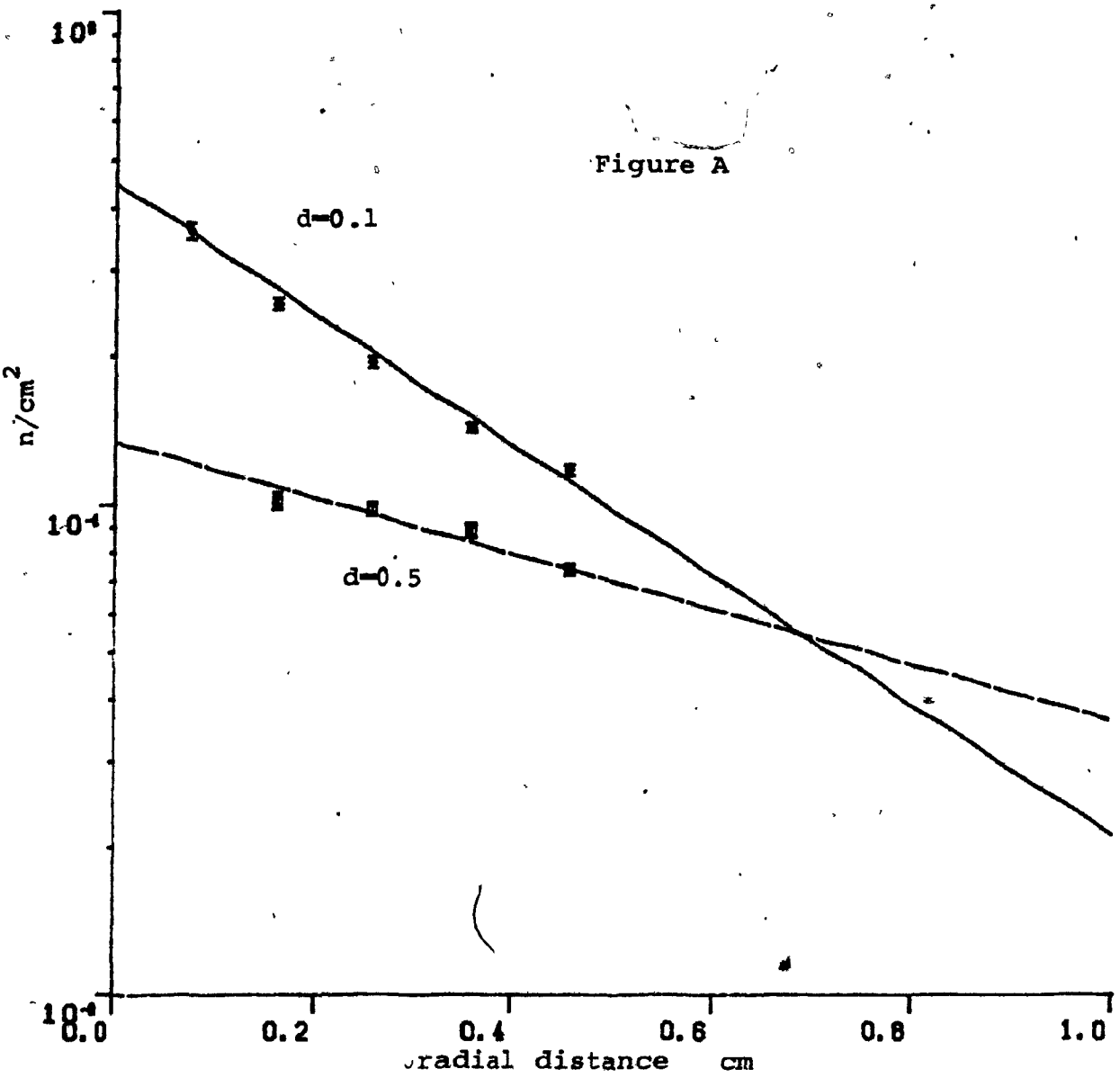

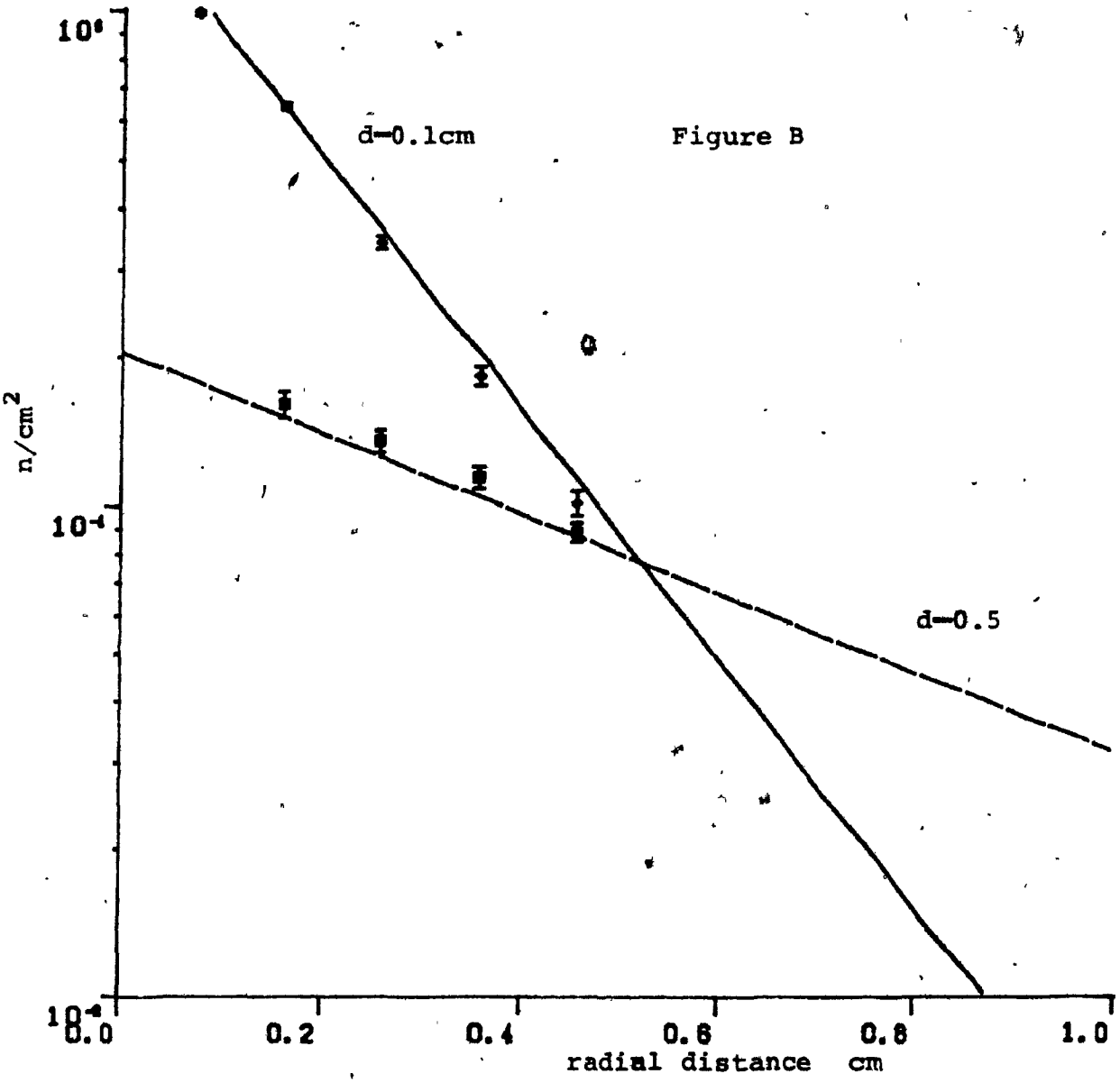

Figure B

Table IV.2

Parameters Of Fits To Data Of Fig.IV.2

Fitting Function $a \cdot \exp(-br)$

		Water		Polythene	
		a	b	a	b
	d=0.1cm	0.39(±0.01)	2.77(±0.09)	0.447	3.050
$\Sigma_s t=3.0$					
	d=0.5cm	0.125(±0.006)	1.09(±0.13)	0.134	1.304
	d=0.1cm	1.51(±0.02)	5.78(±0.09)	1.675	5.840
$\Sigma_s t=1.0$					
	d=0.5cm	0.23(±0.02)	2.01(±0.23)	0.204	1.866

d=0.1 and 0.5 cm and in Fig.IV.2B for $\Sigma_s t=1.0$. The points represent our calculated data values and the broken lines the fitted curves quoted by (Se82). Table IV.2 gives the values of the parameters. Unfortunately, Segal et al have not quoted their errors (though they seem to indicate they are on the order of 5-10%) but, gratifyingly, the agreement is seen to be good, particularly in view of the possible sources of discrepancy dicussed above. A final point: though Segal et al seem to be discussing the neutron flux in the body of their paper, their results agree with our calculated values of the neutron current and it is these which have been presented above. For example, for $\Sigma_s t=1.0$ and d=0.1cm, the flux to current ratio at r'=0.16cm is 1.3. It increases for larger r'.

SECTION IV.3-FAST NEUTRON ATTENUATION

A second simple test involved determining the attenuation of a beam of fast D-T generated neutrons in their passage through successively thicker shields of water. In this case, the calculation involved a pencil beam of 15MeV neutrons directed along the central axis of a cylinder of arbitrary height. Only neutrons of E>12MeV were counted. Scattered neutrons were counted only for very small scattering angles. Results were tabulated at different depths in the cylinder and this was considered equivalent to calculations for shields of different thicknesses and a fixed source-detector distance. The percent transmission of the incident 15MeV flux is plotted in Fig.IV.3. Because of the high energy and

Figure IV.3

Calculated Attenuation Of 15 MeV Neutron Beam Through Water Shields Of Different Thickness. The Solid Line Is A Fit To Our Data. %transmission = 1.13 x exp(-0.101t). Normalized To 1 Incident Neutron.

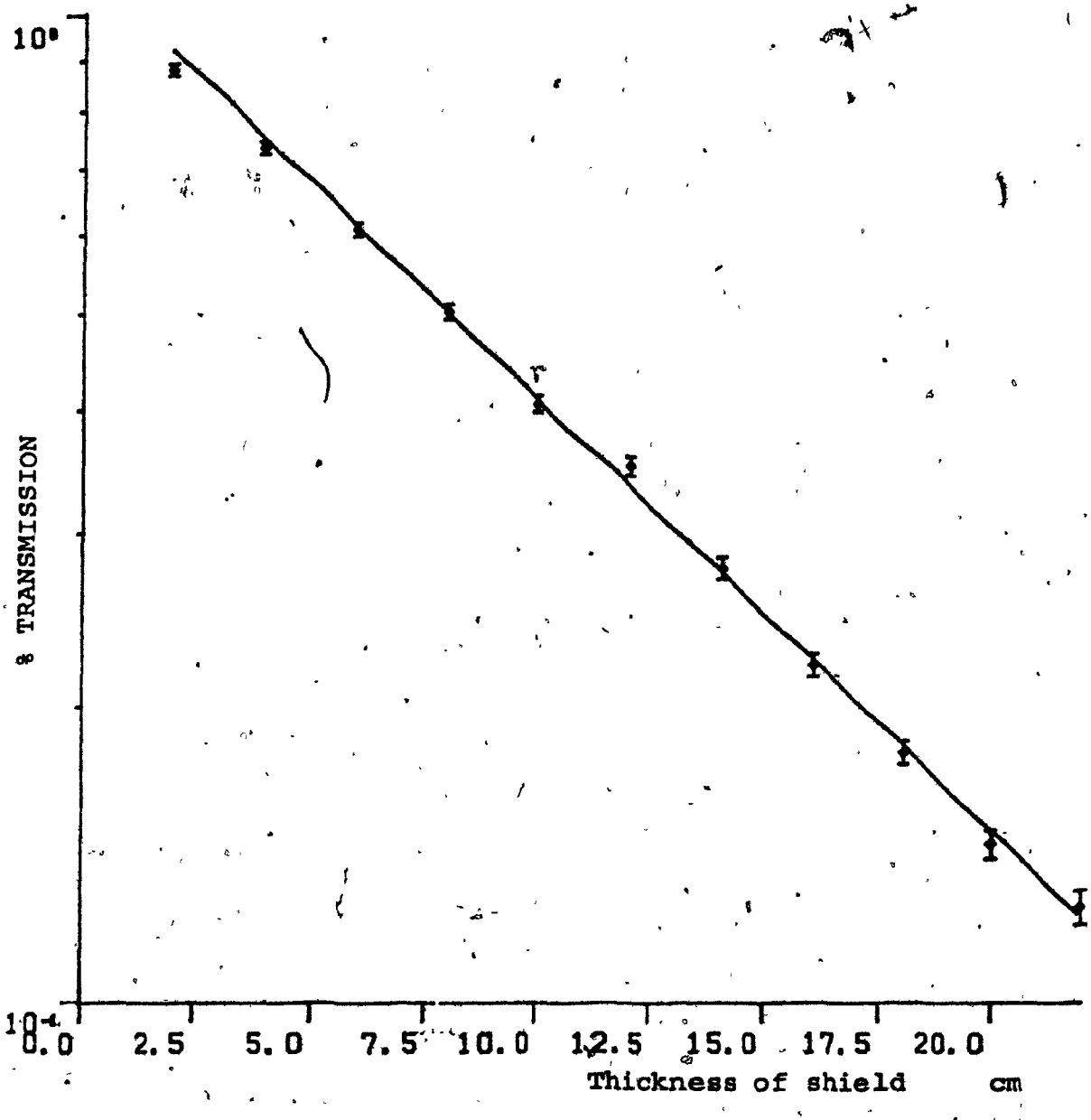
10⁰
10⁻⁴
% TRANSMISSION
0.0
2.5
5.0
7.5
10.0
12.5
15.0
17.5
20.0
Thickness of shield cm

narrow angular spread of even the collided beam, flux and current values are virtually identical, differing by ≤1% at most. Fitting the data to an exponential for thicknesses t≥6cm, we find

$$\% \text{ transmission} = 1.13(\pm 0.02)\exp(-0.101(\pm 0.002)\,t) \ .$$

Cytacki (Cy75) used an NE213 ligiud scintillator to measure the transmission of 14.7MeV neutrons through a variety of materials in different geometries. His results for a narrow beam through water yield a linear attenuation coefficient (actually, the macroscopic removal cross section) of $\Sigma = 0.103(\pm 0.002)\,cm^{-1}$ (Table 3.1 of Cy75), in excellent agreement with our calculation.

SECTION IV.4-THERMAL FLUX IN A SPHERE DUE TO FAST POINT SOURCES

The test calculations above have both been rather simple in that they test a limited number of the parameters dealt with in the most general applications of the MC program. One final, more complicated set of test calculations was carried out to validate the ability of the simulation to predict thermal and epithermal neutron distributions resulting from the slowing down of fast neutrons emitted by point sources in water spheres. It was decided to simulate ^{124}SbBe and ^{24}NaBe neutron sources since these can be sufficiently well modelled by monoenergetic source spectra.

An SbBe source was assumed to emit pure 30keV neutrons into the center of a water sphere of radius R=40cm. (The spectrum is actually more complicated than this with ~42% of

the neutrons lying in the range 4.7keV≤E≤22keV, ~52% in the range 22keV≤E≤46keV and ~5% in the range 200keV≤E≤400keV (Al81).) The resulting thermal neutron flux, Φ, times the radial distance from the source, r, is plotted in Fig.IV.4 as a function of r. The results have been normalized to one source neutron. As can be seen from the graph, $r\Phi$ for r≥6cm can be considered to lie along an exponential curve as theoretically expected (Pe53-Sec.VII-4c, Be64-Sec.17.1, Ng71). (Without entering into excessive details, the behaviour may be explained as follows: in a single collision on hydrogen, a source neutron may lose much of its energy. At lower energies, the cross section for subsequent collisions is enhanced. Thus a neutron has a high probability of being moderated and absorbed near its first collision site. The spatial distributions of the thermal and epithermal fluxes should then behave like that of the primary neutrons which itself is proportional to $\exp(-\Sigma r)/r^2$ where Σ is the total cross section at the source energy. This is true for fast neutrons of several hundred keV. For 30keV neutrons, however, thermalization occurs near the source. The flux then goes as $\Phi(r) \propto S\exp(-r/L)/(4\pi Dr)$ where D is the thermal neutron diffusion coefficient ($= \lambda_{tr}/3$), S is the source strength and λ_{tr} is the transport MFP.) Deviations appear for large r. Partial results of the run used to generate the plot were inspected and seemed to indicate larger than expected fluctuations for r>16cm. Despite this, the points were included in the fit with an assumed error of $\sqrt{N}$. The solid line is the fitting function $r\Phi = A\exp(-r/L)$ where A=0.81(±.03) and 1/L=-0.378(±.005) cm^{-1}. In analyzing

these results, we may consider the water to be an effectively infinite medium. L is then just the diffusion or relaxation length of the thermal neutrons, i.e. the distance over which the thermal neutron density falls by a factor of 1/e. For our results, L=2.64(±.04)cm compared to the measured value of 2.78(±0.01)cm given in the references quoted above. The discrepancy is introduced by the values at large r and may not be as significant as it first appears. (Since scattering on hydrogen is forward peaked in the lab frame, the once-collided flux need not be in equilibrium with the primary source neutrons. First collisions can result in only small changes in angle and energy. These collided neutrons survive out to greater distances lowering the energy of the primary componenet. The decay then does in reality become steeper at large r. However, initial expectations and inspection of the MC predictions for the energy spectra at different r due to SbBe indicate this is not the case for such low energy neutrons. It may play a role in the NaBe simulation.)

An additional comparison was made between our results and some other absolute ones (measured and calculated) reported by Holland et al (Ho78). The latter's calculated values are shown in Fig.IV.4 for several values of r. No estimate is given in the reference for the errors on these points. It should be noted, however, that their reported measurements were 10-30% lower than their own calculations. Further, their predicted fluxes are said to have fluctuated by as much as a factor of 2 depending on the details of the computational procedure. Bearing in mind these caveats,

agreement was considered satisfactory.

To further extend this test run, another was made of a 1MeV point source in a water-filled sphere of R=40cm. This was meant to represent a ^{24}NaBe source though the neutron spectrum is considerably more complex (peak energy= 957(±9)keV, average energy= 798(±71)keV) (Be81). In this case, the sphere cannot be considered infinite (MFP of a 1MeV neutron in water is 1.9cm). Both the thermal and the indium resonance spatial distributions were treated. For the latter, the neutron flux in the energy interval 1eV≤E≤3eV was taken. Our calculated values for $r^2\bar{\phi}$(thermal) and $r^2\bar{\phi}$(1.46eV), normalized to 1 source neutron, are presented in Fig.IV.5 together with some relative measured values taken from Beckurts and Wirtz (Be64,Sec.16.2) for $r^2\bar{\phi}$(1.46eV). These last have been normalized by taking the average of the ratio of our values to the measured ones as plotted on an arbitrary scale over the range of 2cm≤r≤16cm. Such a procedure is admittedly extremely simple but sufficient for our purpose. The calculated $r^2\bar{\phi}$(1.4eV) points were then fitted to an exponential, $Ae^{xp}(-\Sigma r)$, in the region of 12≤r≤24cm. The resulting function (A= 0.64(±0.11), Σ = 0.290(±0.012)) is also drawn on the graph. In this case, the relaxation length to 1.46eV for ^{24}NaBe neutrons is $1/\Sigma$=3.4(±0.1)cm, in excellent agreement with the value of 3.3 cm over the range 15≤r≤30cm quoted in (Be64). As discussed above, the value of Σ does depend on the fitting region. It should be noted that the statistics in our calculation were low, particularly for r>18cm. Also, the agreement between our predicted thermal flux and the measured (not reproduced

Figure IV.4

Absolute rΦ As A Function Of Radius Resulting From SbBe Point Source In A Water Sphere. Normalized To 1 Source Neutron.

line : fit to our data
◇ : this work
□ : calculated values from (Hɒ78)

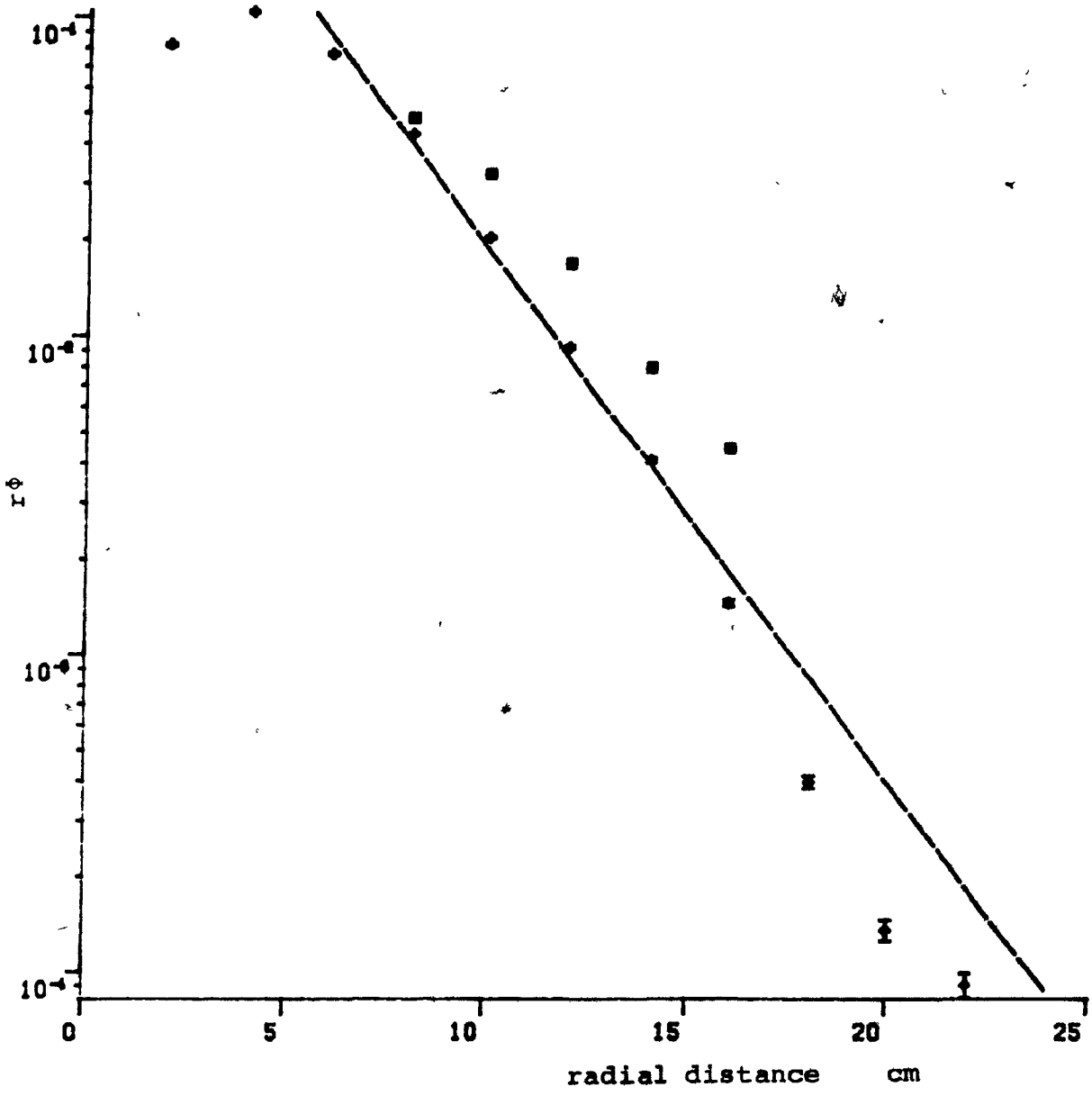
10^{-4}
10^{-5}
10^{-6}
10^{-7}
rϕ
0
5
10
15
20
25
radial distance cm

Figure IV.5

$r^2\phi$(thermal) And $r^2\phi(1<E<3eV)$ Calculated For A 1 MeV Point Source In A Water Sphere. The Values Are Absolute And Normalized To 1 Source Neutron. Solid Line Is $r^2\phi=0.64\cdot\exp(-0.290r)$. Error Bars Have Been Deleted For Clarity Of Presentation.

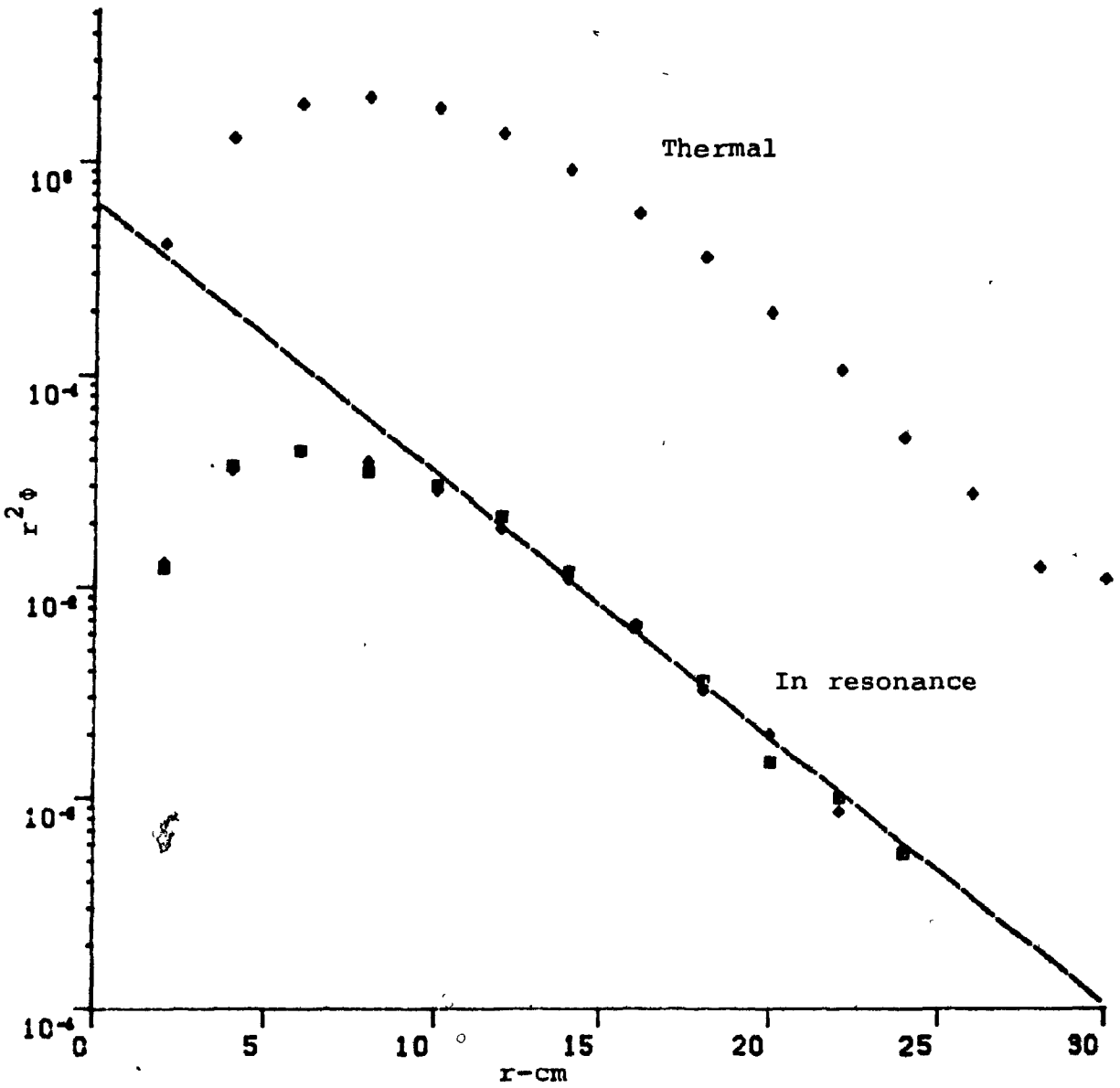
Thermal
In resonance
10^{0}
10^{-1}
10^{-2}
10^{-3}
10^{-4}
$r^2\phi$
0
5
10
15
20
25
30
r-cm

here) is not as good. The predicted seems to fall somewhat faster for large r_c.

SECTION IV.5-FLUXES IN COLLIMATORS

The above examples were considered to have shown the validity of the simulation procedure used for this work. In this section, we report results of our measurements and calculations of the neutron fluxes in a 7.5 cm collimator due to polyenergetic sources placed in the geometry of Fig.II.2- a set-up suitable for PGNCA.

The neutron flux leaving the mouth of the collimator in Fig.II.2 will consist of direct and scattered neutrons. The effect of the scattered component is to significantly alter the neutron spectrum at lower energies. In irradiating targets at the collimator exit, it was originally thought that a larger collimator would introduce less of a spectral distortion but also not permit much in the way of spatial definition of the irradiated volume. Because of this, attention was focused on smaller radii collimators. As it developed, this reasoning appears to have been faulty. A number of different source-collimator geometries were investigated but only one will be discussed in detail for reasons outlined below.

Initial experiments used the two 14.3Ci PuBe sources lying horizontally end to end beneath the bottom of the collimator. Since each source is 5.5 cm long, this means that the collimator only views a portion of them. While it is true that the principal interest in this work is the

neutron flux (fast and thermal) within the irradiated target, the geometry we are using is the same as in neutron howitzers used for neutron radiography (Co69,Pra76). It thus becomes a matter of some interest to investigate a few of the parameters often considered in optimizing these devices. In particular, we investigated the effect of source depth below the collimator on the thermal flux in it. The graph of Fig.IV.6 shows the activating neutron flux as a function of height along the collimator as measured with our Mn foils for a 5 cm source depth. The flux quite obviously falls exponentially. This is a feature to be found in all the collimator measurements. The exponential decay results from fast neutrons thermalizing in the water shield far from the source and leaking into the collimator volume. Thermal neutrons from the immediate source vicinity play a rather minor role at any significant distance from it. This was verified by inserting a Cd sleeve into the collimator and remeasuring the flux. In this case, only thermal neutrons travelling in a straight line from the bottom of the collimator are counted. The relative flux values are also shown in Fig.IV.6. This situation is at least qualitatively equivalent to that of Cox et al (Co68) who demonstrated an increase in thermal flux from a PoBe source with increasing lengths of collimator walls.

Cadmium difference measurements (chapter III) were also made at a source depth of 5 cm. The Cd ratio (R_{Cd} = activity of bare foil/activity of enclosed (Be64)) has a very large uncertainty due to the low counting rates of the Cd-covered foils. Results, given in Fig.IV.7, indicate the

Figure IV.6

Activating Neutron Flux (relative) Along Length Of A 7.6 mm Wide,50 cm Long Collimator As Measured By Mn Foil Activation. Source Is PuBe At A Depth Of 5 cm Beneath The Bottom Of The Collimator. Size Of Points Includes Errors.

◊ : Measured flux in standard collimator
□ : Measured flux in collimator with Cadmium sleeve inserted.

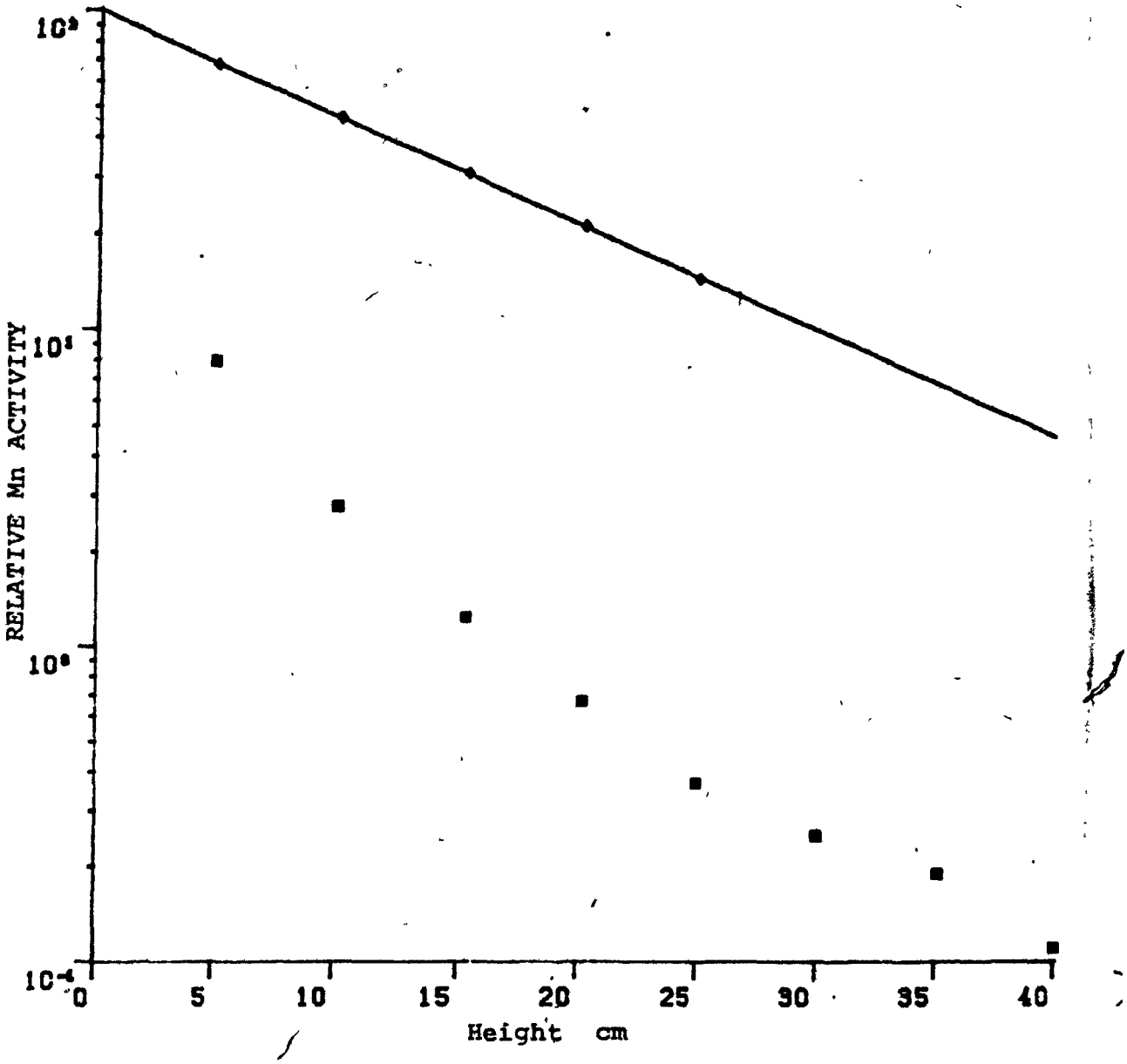
RELATIVE Mn ACTIVITY
10³
10²
10¹
10⁰
10⁻¹
0
5
10
15
20
25
30
35
40
Height cm

validity of ignoring the epicadmium contribution to the manganese activation.

As stated above, the thermal flux in the collimator was measured for a number of source depths: 0, 5, 10 and 15 cm. Exponentials were fit to all the distributions and the fitting parameters are given in Table IV.3. As can be seen, only the zero depth case's slope differed. Its shallower decay is evidently due to the absence of softening of the neutron spectrum present in the other cases because of the water above the sources. It is interesting that the other three different thicknesses of water yield the same slopes (within errors). The decrease in the total flux is in agreement with the observation by Cox et al that additional hydrogenous moderator material in front of the fast source absorbs more thermal neutrons than it produces. It might in fact be interesting to investigate the use of D_2O or graphite as the additional moderator. However, no more work was done on this topic because of two reasons. Firstly, positioning of our sources at the correct depth and symmetrically about the collimator axis proved a difficult task in our facility (from Table IV.3 it can be seen that a displacement of ≤1cm in the source depth can shift the value of the intercept, A, by >10%) and would have necessitated a different source placement design. Secondly, for greater depths, the MC calculations became prohibitively time consuming because of low statistics in the collimator and the increased number of thermals in the shield. Thus a simpler geometry was sought for subsequent analysis.

The 1Ci AmBe source was placed inside the collimator

Table IV.3

Parameters of exponential fits (ae^{-bz}) to activating neutron fluence distributions along collimator for different source depths of the PuBe capsules.

SOURCE DEPTH	a (arbitrary units)	b
0 cm	190	0.0697±0.0006 cm^{-1}
5	144	0.0776±0.0006
10	51	0.0793±0.0007
15	19	0.0779±0.0009

Figure IV.7

Cadmium Ratios Along Length Of Collimator As Measured With Cadmium Enclosed Mn Foils For PuBe Sources At Depth Of 5 cm.

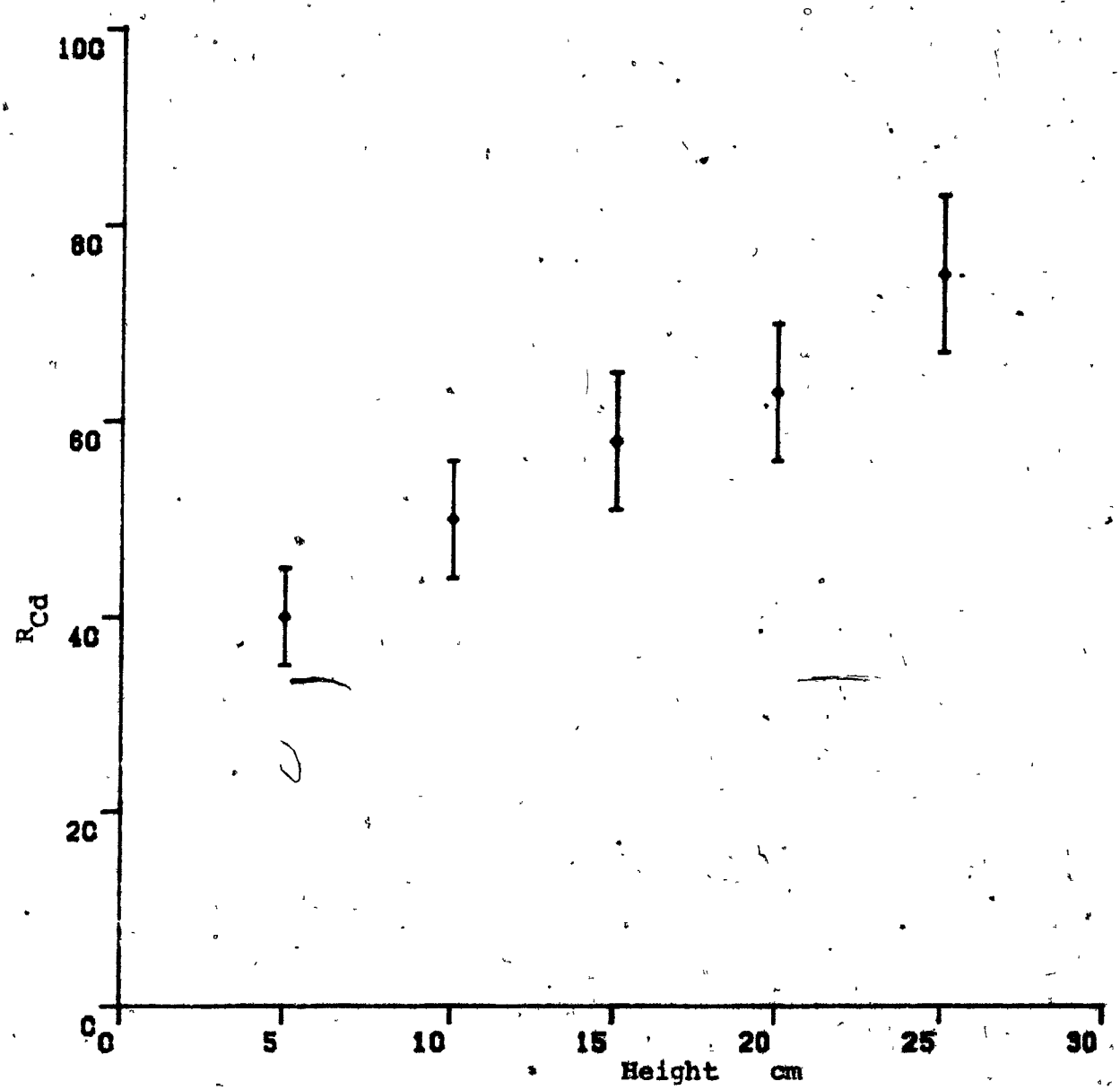
100
80
60
40
20
0
R_{Cd}
0
5
10
15
20
25
30
Height cm

resting on the bottom along its axis. Flux measurements were carried out as before. The distribution again followed an exponential except for the measured point nearest the source (Fig. IV.8). Counting statistics contributed an error of 2-3% per point. For purposes of the numerical simulation, we assumed a point source at zero depth. The neutron spectrum, taken from (Ge75), has been adapted to our coarse energy mesh and is tabulated in Table IV.4. MC simulations were run for 300keV, 1, 2,..., 8 and 9 MeV neutrons. The flux and current passing through a 7.6 cm diameter disc due to each source energy were tabulated as a function of height along the collimator. Results were normalized to a single input neutron and 1cm² area and the neutron spectrum was folded in. A final fit was then made to the resultant distribution for heights >8cm. While the slopes of the calculated and measured distributions are in excellent agreement, the absolute fluxes are not. The calculated thermal distribution (normalized to 1 AmBe neutron) is $\Phi_c(z) = (2.47\pm0.02)\times10^{-3}\exp(-0.075(\pm0.001)z)$ n/cm²/s while that of the measured is $\Phi_\epsilon(z) = (4.45\pm0.14)\times10^{-3}\exp(-0.074(\pm0.001)z)$ n/cm²/s (assuming a source strength of 2.1×10^6 n/s). Thus, at z=0, $\Phi_c/\Phi_\epsilon = 0.56\pm0.02$. Several reasons for this large discrepancy may be postulated. The actual AmBe source is an extended object whose center lay ~1.5 cm above the collimator bottom. This could in and of itself increase the measured flux by ~15% (as estimated from Fig.IV.8). Since, as noted previously, such cylindrical sources are not isotropic but radiate a reduced flux along the cylindrical axis, the number of neutrons entering into the side shielding wall to undergo

TABLE IV.4

Spectra of AmBe neutron sources as given by Geiger and van der Zwan and Kluge and Weise and adapted to our coarse energy mesh. The spectra are normalized to 1 source neutron and are given in the units of neutrons per MeV.

Energy range	Normalized intensity n/MeV	
	(Ge75)	(K182)
0-0.3 MeV	0.04	0.05
0.3-1.0	0.08	0.09
1.0-2.0	0.06	0.09
2.0-3.0	0.10	0.12
3.0-4.0	0.18	0.16
4.0-5.0	0.15	0.15
5.0-6.0	0.14	0.12
6.0-7.0	0.07	0.09
7.0-8.0	0.08	0.07
8.0-9.0	0.05	0.04
9.0-10.0	0.05	0.03

Figure IV.8

Activating Neutron Flux Distributions In Collimator For 1Ci AmBe Source. The Solid Line Is A Fit To The Calculated Distribution (using spectrum of K182) $\Phi(z)=(3.62\pm0.07)\times 10^{-3}\cdot\exp(-0.075(\pm0.001)z)\ n/cm^2/s.$ This Is Normalized To One Source Neutron per sec. Source Output Assumed To Be 2.1×10^6 n/s. The Measured Distribution Has Been Normalized To Calculation At z=0.

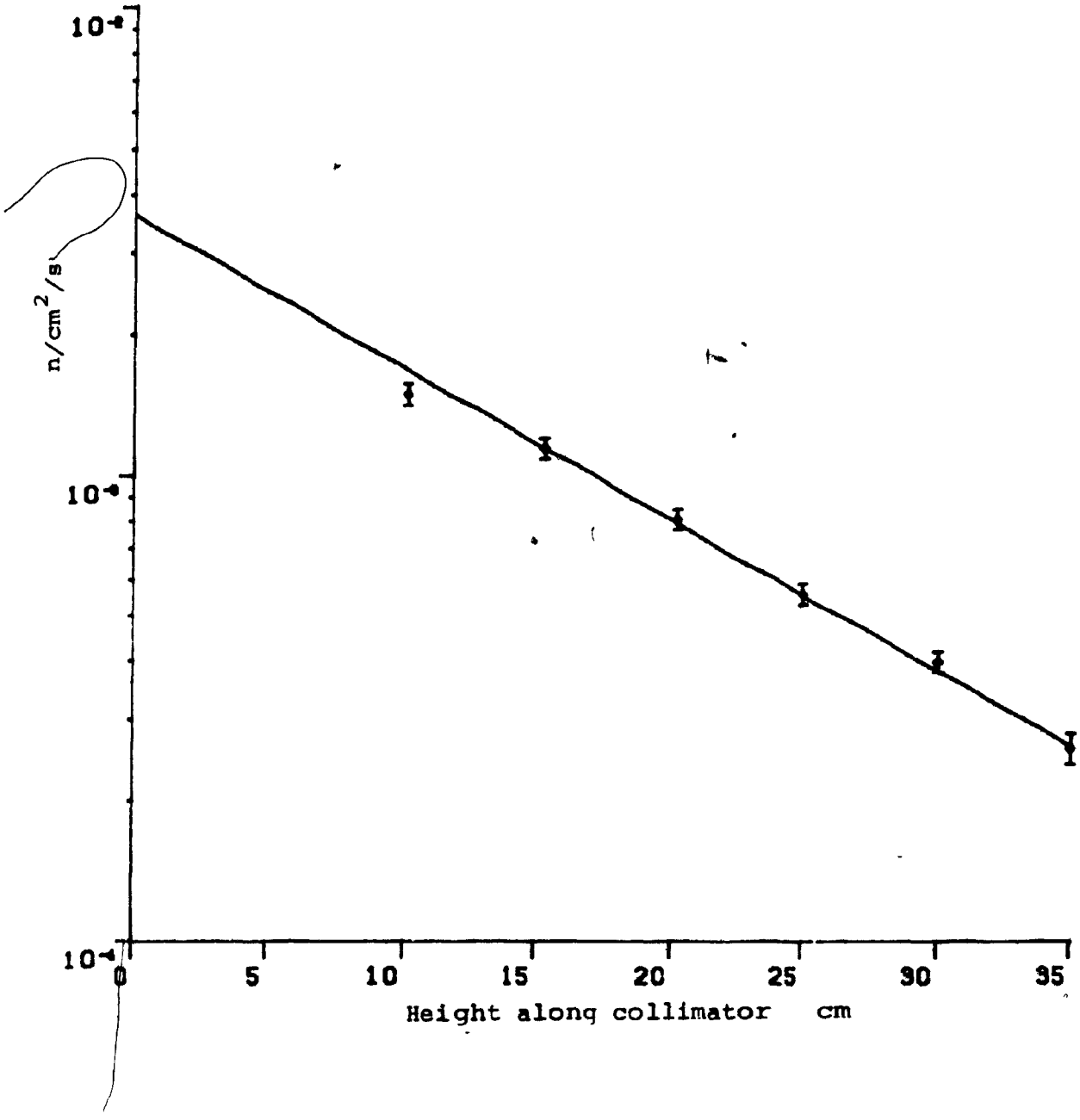
10⁻²
10⁻³
10⁻⁴
n/cm²/s
0
5
10
15
20
25
30
35
Height along collimator cm

subsequent thermalization would be enhanced and would yield an effectively more intense source. Such an effect would undoubtedly be very small, however. Far more importantly, the low energy region of the AmBe spectrum is only poorly known and is dependent on the details of source construction as well as other factors. Kluge and Weise (K182) recently reported a measurement of a 1.5Ci AmBe source in the range of 0.1-11MeV using a ^{3}He spectrometer consisting of two surface barrier detectors sandwiching ^{3}He gas. Their spectrum, adapted to our energy group structure, is also given in Table IV.4. Additional thermal neutrons are also emitted from the source and certainly contribute but their relative effect is expected to be small (Ri81). Production of neutrons of ≤100keV also occurs but the size of the component is unknown. When the spectrum of (K182) is used to calculate the spatial distribution as before, the result can be fitted ($z \geq 8$cm) by $\Phi_c(z) = (3.62 \pm 0.07) \times 10^{-3} \exp(-0.075(\pm 0.001)z)$ n/cm^2/s. At $z=0$, $\Phi_c/\Phi_e = 0.81(\pm 0.03)$. This is drawn in Fig. IV.8. Experimental points have been normalized to calculated at the intercept. The combination of positioning error and spectrum modification can thus account for the discrepancy between the calculated and measured values to well within the experimental calibration uncertainty.

Only one reference could be found for comparison to the above results. Pracy and Hague (Pr76) measured the thermal flux along a 5 cm diameter collimator in a wax howitzer assembly. Taking the region $5 \leq z \leq 20$cm as given in their Fig.3, we found a slope of -0.075 cm^{-1} in fitting their data to an exponential function, in agreement with this work.

A single measurement was made where foils were activated, not along the central axis, but near the collimator wall. In a few of the MC runs, the neutrons in the collimator were separately counted in a disc of radius 1.9 cm and a ring of inner radius 1.9 cm and outer 3.8 cm. No difference was found as a function of radius at a given height and the flux was taken to be uniform. This held true for the fast flux as well, i.e. at the collimator's exit, and along most of its length, the neutrons appeared to be travelling in a uniform beam and not along spherical radii.

The insensitivity of the distribution slope and the concomitant sensitivity of the absolute flux values on the details of the input neutron spectrum deserve particular attention. Since we lack a neutron spectroscopy facility, attention must be paid to absolute and not just relative thermal neutron measurements when trying to determine a possible spectrum for our source. Unfortunately, such a situation makes precise statements concerning the spectrum difficult since so much is dependent on poorly known parameters.

Given the quite satisfactory agreement between calculated and measured thermal distributions, an attempt was made to calculate the neutron spectra in the collimator and at its exit. Such calculations have been made for reactor thermal and cold neutron beams in guide tubes (Ch69,Ch71) but not for high energy (α,n) sources for (n,γ) and $(n,n'\gamma)$ experiments. The matter has received some experimental attention in fast neutron cross section studies using D-T sources. Khan et al (Kh81) noted an increase in the neutron fluence at a target

due to a collimator and suggested that the enhancement was due to low energy neutrons scattering off the collimator walls. They did not measure the energy of the scattered neutrons. The collimator influence on the D-T spectrum has also been addressed by investigators in radiation therapy. Hannan et al (Ha73) reported the appearance of a lower energy component in the 1-8 MeV region but found little effect due to the collimator shape or constituents (polythene or steel). The degraded neutron intensity increases with decreasing neutron energy and, surprisingly, with increasing collimator diameter. Measurements of the effect of wax collimators on the spectra of AmBe and ^{238}PuBe sources have been reported by Cox and Cleave (Co75) and, most recently, Mountford (Mo82). Both could measure the neutron spectra to a lower energy of about 1.5 MeV. The two measurements disagree throughout the spectrum. For example, Cox and Cleave report the spectrum to be dropping below 3 MeV while Mountford shows it increasing.

For the calculation of the neutron spectra, an assembly was simulated for which the depth of water below the source (the reflector) was 40 cm, the shielding wall was 32 cm thick and the collimator had a diameter of 8 cm and height of 40 cm. Neutrons were cut off below the energies of 100 keV. Counting statistics were low for individual runs. Since Mountford found no difference within his errors between PuBe and AmBe sources and the latter's spectrum has already been considered above, it was used as our input. The resultant spectrum is shown in Fig.IV.9 together with the original. For purposes of presentation, the data has been binned into 1 MeV intervals (even though calculations were made for the

Figure IV.9

Calculated neutron spectra due to AmBe source in collimator (height—40 cm, diameter—8 cm):

◇ Original bare source spectrum

□ Spectrum at mouth of collimator

Curves are eyeguides only.

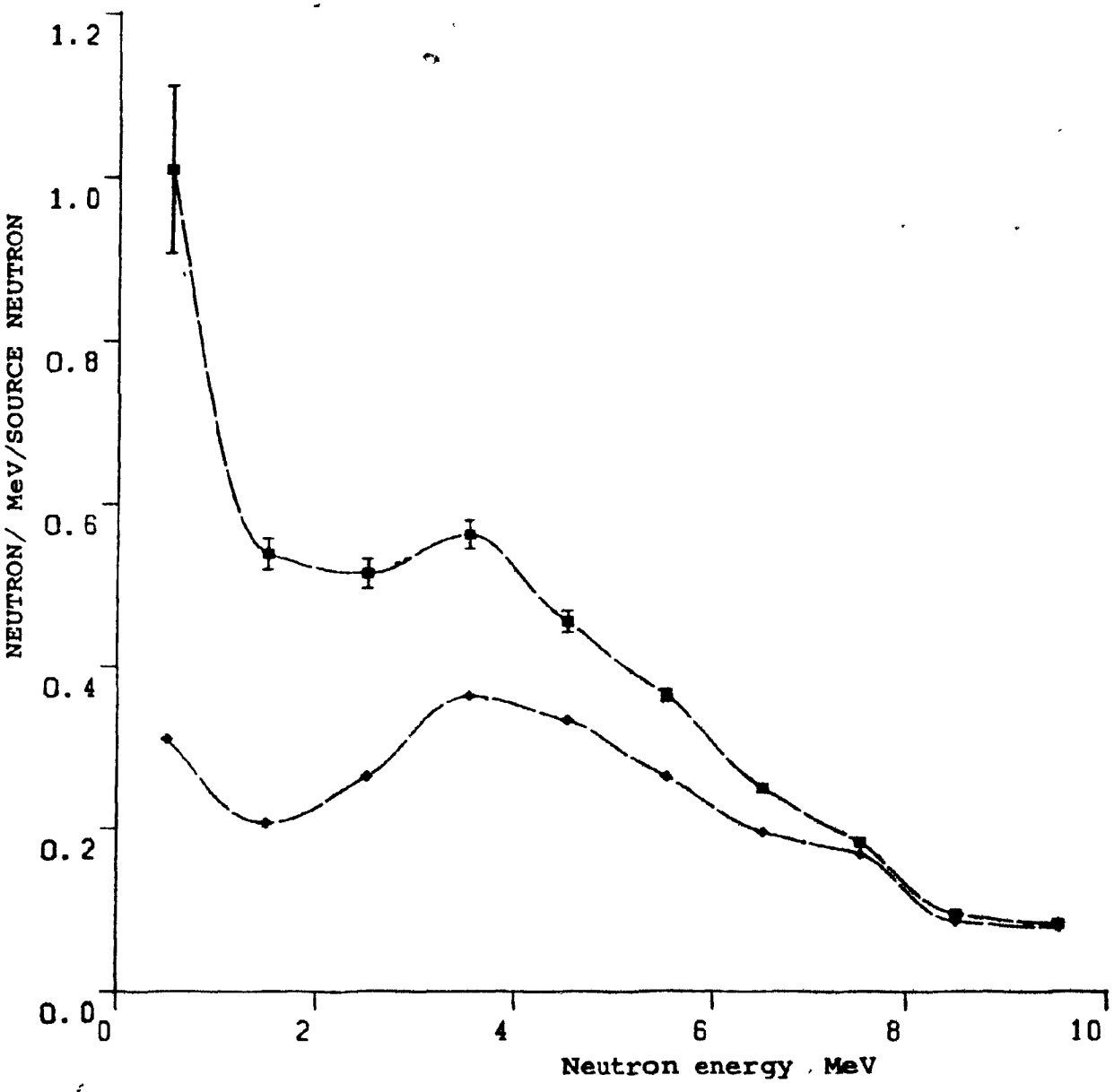
1.2
1.0
0.8
0.6
0.4
0.2
0.0
NEUTRON/ MeV/SOURCE NEUTRON
0
2
4
6
8
10
Neutron energy , MeV

Figure IV.10

Spectra at two heights in the collimator due to an AmBe source. Curve is eyeguide only.

◊ Spectrum at 20 cm height.

□ Spectrum at 40 cm height (mouth of collimator).

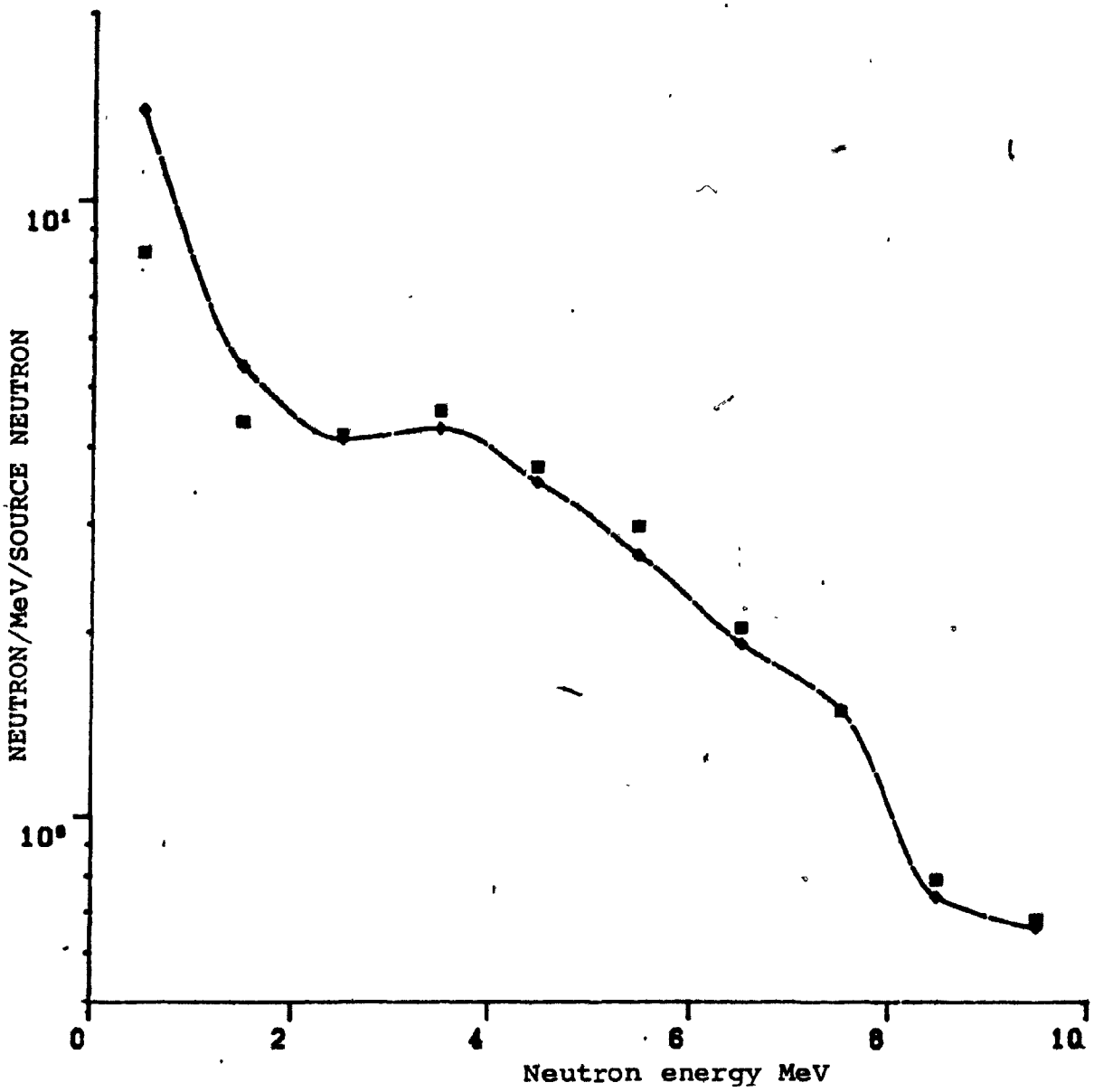
NEUTRON/MeV/SOURCE NEUTRON
10¹
10⁰
0
2
4
6
8
10
Neutron energy MeV

ranges 0.03-0.1MeV, 0.1-0.3MeV and 0.3-1.0MeV independently) and the points plotted at 0.5MeV intervals. The dashed lines are eyeguides only. The increase in the neutron flux occurs across the entire spectrum and is 5% between 9-10MeV. Though not reproduced here, the spectrum of (Mo82) (measured for a 23 cm long collimator) is in very good agreement with ours while that of (Co75) differs sharply. Slight differences in the geometries of the moderators cannot explain the discrepancies and the reasons for them remain unresolved. Because of (n,γ) discrimination difficulties in the liquid scintillator, Mountford was unable to extend his measurements below 1.5 MeV. As can be seen in Fig.IV.9, the neutron intensity continues to climb at low energies. In Fig.IV.10, we have plotted the neutron spectra at the collimator exit (height = 40cm) and within the collimator at a height of 20 cm. The latter is considerably softer. If one considers the second case equivalent to a collimator of larger radius (collimator diameter to length ratio = 8/20 compared to 8/40 at the mouth) then this agrees with the reported observations that wider collimators soften the spectrum more, in contradistinction to our initial expectations. The analogy is not perfect since in our case neutrons can be scattered back down from higher regions of the collimator. Nevertheless, there is at least qualitative agreement with the published results.

^{252}Cf has come into use in PGNCA. The lower mean energy and penetration of its neutrons have been assumed to limit its applications to probing near-surface elemental compositions in extended objects. Recently, Morgan et al

Figure IV.11

Spectra at collimator exit as calculated for ^{252}Cf and AmBe sources.

◊ Spectrum due to Cf

□ Spectrum due to AmBe

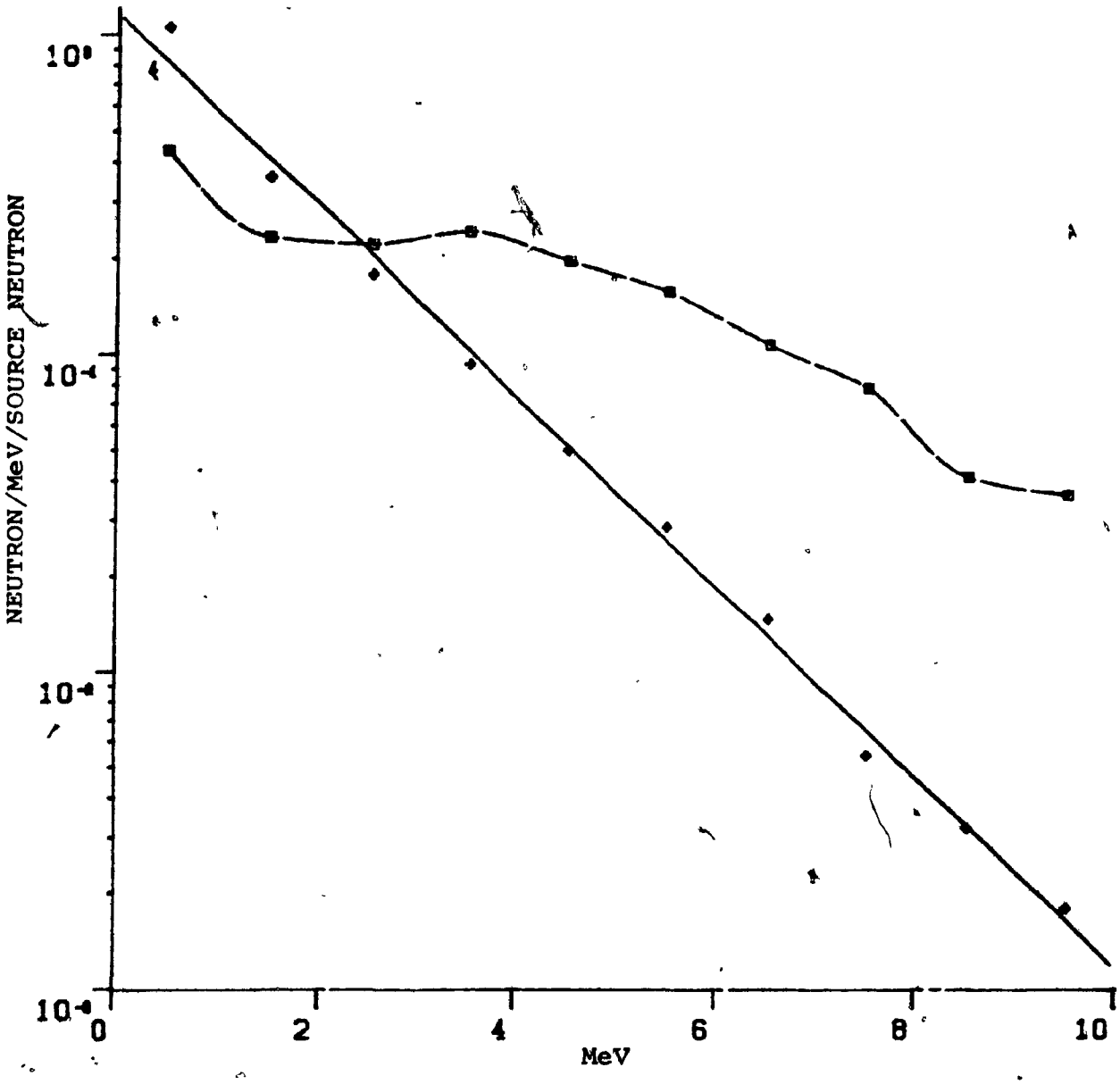
NEUTRON/MeV/SOURCE NEUTRON
10⁰
10⁻²
10⁻⁴
10⁻⁶
0
2
4
6
8
10
MeV

noted little difference in the penetration of collimated neutrons from ^{252}Cf and $^{238}PuBe$ when using steel-lined, Pb-doped polythene collimators. The presence of heavy elements will of course have a major effect on the higher energy neutrons but, as a first approximation, we have considered a ^{252}Cf source in a water shielded collimator. The spectrum was taken to be given by $N(E) \propto \sqrt{E}\exp(-E/T)$ where T=1.42 MeV (In75). The spectrum at the mouth of the collimator is given in Fig IV.11 together with that due to the AmBe calculated above. The solid line is the function $N(E) \propto \sqrt{E}\exp(-E/1.28)$. Both the ^{252}Cf and $^{241}AmBe$ spectra are softened but they are far from similar. If in fact the spectra of these types of sources are similar in the facility of (Mod1), it must be due to inelastic scattering on the heavy metals used for shielding against the gamma radiation from the sources.

SECTION IV.6-FLUXES IN TARGETS

In the initial experiments to measure the activating neutron flux in our phantom, we used the two source-collimator configurations discussed in section 5, except that we replaced the small AmBe source by the 10Ci one. The experimental method has already been discussed. The distribution one expects to find may be characterized as a Gaussian with an exponential tail. The near-surface region is a build-up region where the thermal flux increases with increasing depth due to thermalization of the incident fast beam. The far region follows the well known exponential

decay due to thermal neutron absorption as discussed above. Our first measurements displayed, not the build-up region, but rather a plateau followed by exponential decay. The plateau was caused by the large thermal neutron leakage into the phantom from the shield and was eliminated by surrounding the phantom with cadmium. Little will be said about these sets of experiments. The distribution was found to peak at a very shallow depth of 3.0 cm. (To be more precise, the AmBe source in the 7.6 cm diameter collimator gave a peak depth of 2.9±0.1 cm. The PuBe sources, resting beneath the same collimator, gave a peak depth of 3.0±0.1 cm. Resting beneath the 20cm diameter collimator, they gave 3.2±0.1 cm. The large collimator contained lead blocks for ballast.) This is significantly less than expected for our sources' energies even when assuming the softened spectrum of section 5 rather than the original. A neutron beam of as low an energy as 1 MeV (beam radius =4cm, impinging along the axis of the phantom) was found to yield a peak depth of 3.8±0.1 cm in a MC run. This value can also be estimated from two group theory (La67) from the equation $z_{max} = L_R L_D \ln(L_R/L_D)/(L_R - L_D)$ where z_{max} is the peak depth, L_R is the the fast neutron relaxation length and L_D is the thermal diffusion length. L_D=2.78 cm and for PoBe neutrons in water (similar to AmBe), $L_R = 1/\Sigma$ =10.3±0.7 cm (Be64, Sec.16.2). Therefore z_{max} = 5cm. Thus it would appear that the neutron spectrum exiting from our irradiation assembly is considerably softer than thought. Indeed, a peak depth of only 3 cm implies an incident neutron energy of only several 10's of keV's (Mo81), well below the range of our calculations or any available measurements.

This may be due to neutrons exiting the collimator or the shielding assembly. By way of comparison, Mernagh (Me77) measured a peak depth of only ~2 cm due to a PuBe source in a wax collimator. This is unusually low and a depth of 4-5 cm is more typical (La64,Mo81). Though no precise explanation is offered here, it may be noted that these last two used heavy metals in collimating the beams while both our facility (for the small collimator) and that of (Me77) did not. Conceivably, in the former case, neutrons could be scattered into the collimator mouth after having lost relatively little energy in an inelastic collision on Pb or Fe while in our case energy degradation was more severe due to elastic scatter on H.

One additional point of interest is worth mentioning here. In going from the smaller to the larger collimator, the thermal flux in the phantom increased by a factor of 4.2±0.2 at all measured depths.

The above procedure was abandoned when it appeared we could not properly characterize the neutron spectrum striking our target. A simpler geometry was chosen in which the original AmBe spectrum could be assumed. The 1Ci source was placed on a thin steel platform at a distance of 10 cm below our phantom. The resultant absolute thermal neutron flux distribution as a function of height along the axis is plotted in Fig.IV.12 in the range $0.3 \leq z \leq 14.3$ cm. An error of ±5% has been assumed for each point as estimated from the reproducibility of results in 4 independent runs. The principal sources of this error are counting statistics of the individual foils themselves as well as of the uranium

calibrating foil with some due to positioning error. The uncertainty in the absolute calibration has not been included in this estimate. The results shown in the graph were taken from one particular run and the errors on the points within this single run were ±2%. The distribution peaks at a depth of 4.6±0.1 cm.

To extract information such as the peak depths reported above, it was decide to fit the neutron distributions with analytic functions. Given the sometimes considerable statistical fluctuations in our MC results (particularly for higher energy incident neutrons or at greater depths into the phantom for lower energy ones), it was felt that the smoothing resulting from such a least-squares fit would be desirable. On theoretical grounds, one could assume the points to obey a function of the form $ae^{xp}(bz^2)$ for small z and $exp(-cz)$ for large z. It is, however, useful to be able to fit the data over the full region of interest with a single function. Fijishiro et al (Fu75) have fit $r^2\Phi$ for a point RaBe source in a water sphere using a series of weighted Laguerre polynomials. Using a modified program from (Be69), we attempted to fit our distribution for Φ with the same set of polynomials (to fourth order in z) but could not achieve satisfactory results. We found it possible to fit the data adequately with the first few Tchebeychev polynomials using

$$\Phi(z) = \{a_1 + a_2 z + a_3(2z^2-1) + a_4(4z^3-3z) + a_5(8z^4-8z^2+1)\}\exp(a_6 z)$$

where the a_i's are adjustable parameters. However, a simpler function was discovered to give not significantly worse results with fewer free parameters:

$$\Phi(z) = (a_1 z + a_2)^{a_3} \exp(a_4 z) \quad .$$

The peak depth is then given by $z_{MAX} = -(a_1 a_3/a_4 + a_2)/a_1$.

Given the adequacy of the fitting function, we were faced with two choices in evaluating our MC data. Runs were made at energies between 0.3 and 10 MeV for a point source 10 cm below the phantom and irradiating its entire surface. Thermal neutrons were tabulated when crossing discs of 2 cm radii at 1 cm depth intervals lying along the cylindrical phantom axis. One could then fit each run's results and add the points evaluated from the fits to arrive at the final distribution. Instead, it was decided to add together the raw values and fit the result. It is this which is shown in Fig.IV.12 normalized to a source strength of 2.1×10^6 n/s. As can be seen, the results agree very well with our experimental points both in shape and absolute value. At shallower depths, the experimental points are somewhat higher. This may be due to a larger than expected low energy flux as previously discussed or because of neutrons degraded and reflected back into the phantom by the steel support. Given the imprecise information available about our particular source's low energy neutron spectrum, the results in Fig.IV.12 are certainly quite satisfactory. The MC prediction peaks at 5.0±0.1 cm, a somewhat greater depth than for the measured. (The value at z=12cm has been omitted from the fit because it deviated significantly. This improved the χ^2_ν considerably but did little to the peak depth.) This further supports the likelihood of lower energy impinging neutrons. It may be noted that the thermal flux does not fall to zero at zero depth despite the presence of a Cd sheet

Figure IV.12

Absolute thermal neutron flux vs depth along the central axis of a water filled phantom due to a bare 1 Ci AmBe source (2.1×10^6 n/s) 10 cm below it.

Solid line is fit to the calculated values

$$\Phi(x) = (a_1 x + a_2)^{a_3} \cdot \exp(a_4 x)$$

$a_1 = 1.95 \times 10^{-3}$

$a_2 = 2.58 \times 10^{-5}$

$a_3 = 1.1147$

$a_4 = -.2250$

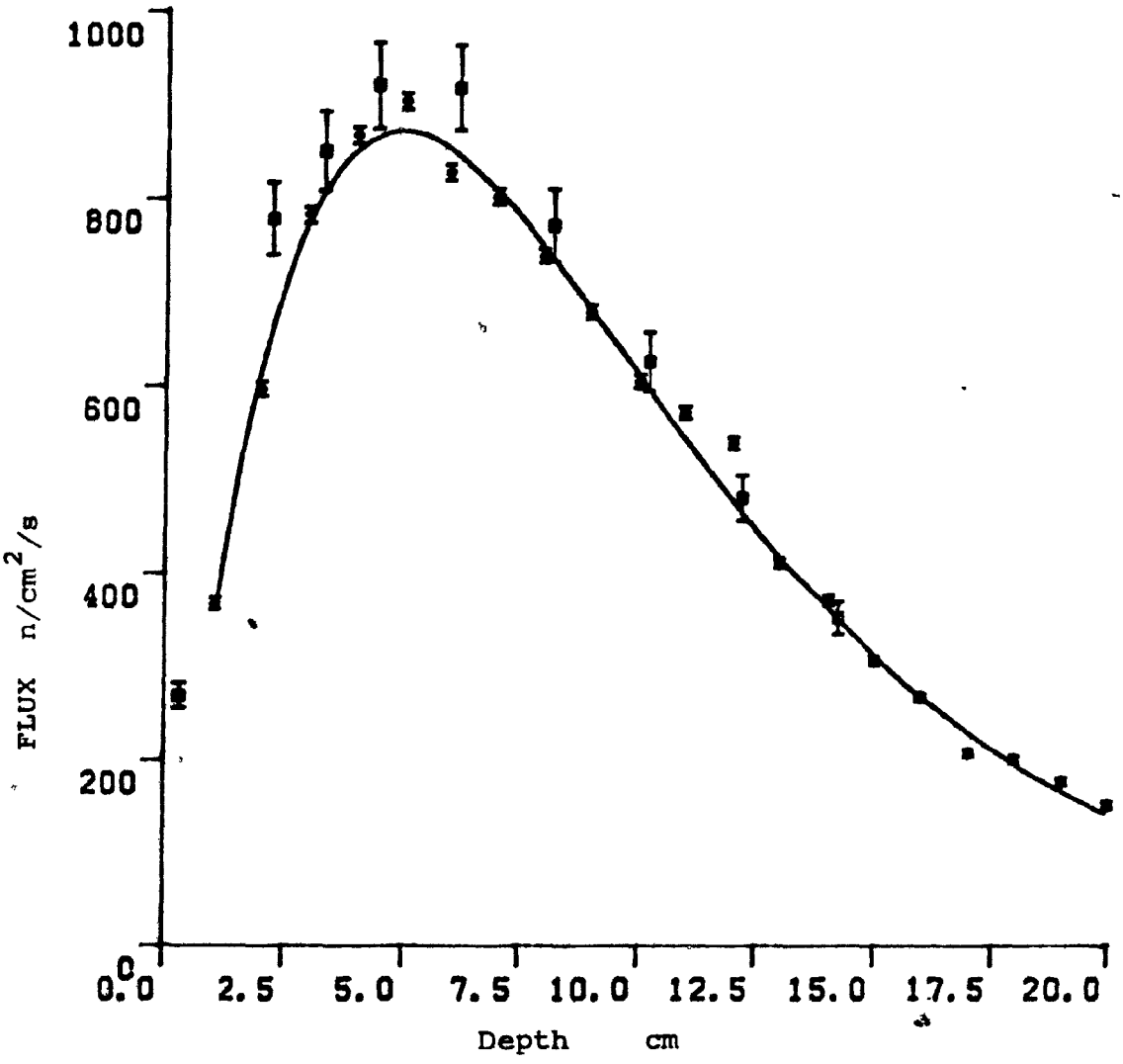
1000
800
600
400
200
0
FLUX n/cm^2/s
0.0
2.5
5.0
7.5
10.0
12.5
15.0
17.5
20.0
Depth cm

on the outside of the phantom. This is due to neutrons inside the phantom leaking out. Also, though it may appear that at larger z the experimental points are falling too quickly with respect to the calculated, a single measurement at a depth of 16.3 cm in another run did not drop below the predicted fluxes. Measurements at greater depths were difficult due to low induced activities in the foils.

SECTION IV.7-DISCUSSION AND SUMMARY

From the results presented in the previous sections, a number of conclusions may be drawn concerning the importance of the irradiation geometry and conditions on optimizing a facility for NAA or PGNCA of extended massive targets.

The neutron beams incident on a target are severely affected by the collimation in terms of both their energy and spatial distributions. Though in many published reports it has been assumed that collimation does little more than define the irradiated surface (as evidenced by their quoting the average neutron energy of the isotopic source for the average energy of the collimated beam), it is seen in this work that this is far from the reality of the situation. To begin with, an irradiator can increase the intensity of the neutron beam from a source over that expected on the basis of solid angle considerations alone. In the collimators considered in this work, this occurs due to elastic scatter off the collimator wall. For a water shield, inelastic scatter on oxygen plays a minor role even at 10 MeV. The increment can be significant. For a 40 cm long collimator of

radius 3.8 cm, the increase at the exit is 5% for source neutrons in the 9 - 10 MeV range, i.e., the highest energy of the isotopic sources considered here. At lower source energies, the enhancement is greater due to the larger (n,p) elastic scattering cross section. Additionally, neutrons scattered down into the lower energy groups from higher energies also contribute at the collimator exit. The net effect is to soften the spectrum and increase the effective source intensity, even at those low energies where the original source is a weak emitter. Large diameter collimators may increase the lower energy contribution more due to the larger solid angle subtended by the collimator wall as viewed by the neutron source. More source neutrons may scatter off it, losing energy before reaching the phantom. This effect has been claimed by Mountford. It was not specifically investigated in the course of this work but may be suggested by our calculated spectra within the collimator. Our comparison experiments using the PuBe sources and 7.6 cm and 20 cm wide collimators are not conclusive on this point since in the former collimator, part of the source was shielded from view of the phantom by water, while in the latter, some Pb was placed in the collimator. Since the collimator experiments were eventually dropped, this matter was not pursued. Nevertheless, the tentative results seemed to show little effect on the spectrum as measured by the peak depth. Additionally, the fact that the increase in the thermal fluence due to the large collimator was the same at all depths in the phantom, would suggest little difference in the neutron spectra, i.e., a softer

spectrum would have resulted in a more steeply falling thermal distribution. Thus the neutron spectrum of the partially shielded and moderated sources in the small collimator may be similar to that of the fully exposed (except for some Pb) sources in the larger one. This is in qualitative agreement with Mountford's results. Lawson et al (La64) found a marked increase in the thermal flux along the center line of a phantom due to large collimators but little change in peak depth. These authors suggested that the increase was due to thermalization of fast neutrons in the more distant parts of the beam in the phantom followed by their diffusion into the center. The consistency of the peak depth would indicate little change in the incident spectrum though they found the increase in the thermal flux to be far greater that that in the measured fast dose. The presence of large amounts of Pb in their facility may make comparison to our work difficult. The matter is certainly worth further investigation, particularly by calculation in view of the difficulty in performing measurements below 2 MeV.

When using $(n,n'\gamma)$ reactions for analysis, the matter of the precise neutron spectrum takes on great significance. While collimation increases the fast flux, it increases the low energy flux even more. Given that $\sigma(n,\gamma) > \sigma(n,n'\gamma)$ in most cases, this would increase the background γ radiation, driving down the sensitivity of such a system. In this instance, the harder the spectrum the better.

Comparisons between our numerical simulations and measurements of the thermal neutron distributions in our phantoms and collimators made it quite evident that our

irradiation assembly emitted a large flux of low energy neutrons. The peak depth obtained with our original source-shielding configuration was 3.0 cm. For apparatus using heavy metals for collimation, peak depths of ≥4 cm have been typically reported, indicating harder incident neutrons. The softening of high energy neutrons by Pb or Fe is of course well known and has been used to reduce the fast/thermal ratio in neutron howitzers (Cox 1974). However, it is possible that a correct configuration of these elements in a howitzer would result in a harder spectrum than would appear in their absence as discussed in section 5. The matter has not been directly addressed to date. The addition of an (n,2n) reaction mechanism to our MC code should allow an investigation of this effect.

Part of the original intent of this work was to study the features of an irradiation system for a PGNCA facility to measure elemental compositions in human beings. Such facilities have been constructed at a few laboratories and a number of points may be made concerning general design considerations of such apparatus.

The achievement of uniform activation and detection of elements of interest is a matter of much concern. Some researchers (Va76,He77) have employed premoderators, i.e., a thickness of moderator interposed between neutron source and target, in an attempt to eliminate the build-up region of the activating neutron distribution. It is quite evident from the work reported here that the detailed construction of such a premoderator must be considered independently for each irradiation assembly. It is even possible to eliminate the

build-up region by making use of thermal neutrons leaking out of the collimator shield. However, in most cases, borated compounds are used for shielding to reduce H capture of neutrons and the resultant γ background, thus eliminating the thermal neutron leakage. It might be possible to reintroduce a thermal neutron output from the collimator by lining it with heavy water. This would have the advantage over a premoderator of not attenuating the incident flux. The increased capture rate which might result because of this in shallow regions of the body might be of considerable importance in measuring nitrogen (for protein determination) in severely wasted subjects (Ch82).

The effect of collimation on fast neutron spectra has been shown to be highly significant. It may be reasonable to vary a PGNCA system for different types of measurements rather than making do with a fixed arrangement. For example, if heavy metal liners in a collimator do indeed yield harder spectra than simple hydrogenous shields, these could be used to advantage in an $(n,n'\gamma)$ facility, quite apart from the shielding against γ radiation which they would supply. For measuring near-surface regions the softer spectra from a wax or water howitzer might be preferred due to the higher thermal flux/unit dose they would deliver (Mo81).

In summary, a quite simple and straightforward Monte Carlo code has been developed to calculate neutron spectra and spatial distributions in geometries suitable for PGNCA or NAA of bulk targets such as human beings. We have constructed an irradiation facility, using isotopic neutron emitters, in which we have carried out a number of

measurements of the activating neutron flux in such geometries. Our measurements and calculations are in extremely good agreement if we recognize that knowledge concerning the low energy range of our neutron sources is sparse. In principal, one should measure the neutron spectrum of each particular source since output may be inhomogenous and the low energy part of the spectrum is dependent on the source construction. Such measurements can be extremely difficult and a combination of techniques involving activation foils, organic scintillators, and ^{3}He ionization chambers may be necessary to properly characterize the neutron spectrum leaving a collimator and at various points in a phantom. Calculations have shown the neutron spectra and flux to vary with collimator constructon. The addition to the program of an (n,2n) reaction mechanism and an increase in the number of homogenous regions and elements which it can handle should allow a convenient method of studying the effect of various metal inserts in collimators. This would probably necessitate transferring the program to a larger computer, but its portability would permit this with little difficulty.

APPENDIX A

It is obvious that a source emitting neutrons only into a cone is equivalent to a more intense isotropic source, as seen by a target within the cone. The relationship between the intensities of such sources is determined by how much solid angle is subtended by the cone (Fig.A1). For a point source, this is rather easy to determine.

For a point source of intensity S, the number of neutrons passing through a disc of radius r_b is the neutron current (NC)

$$NC = \int_0^{2\pi} d\phi \int_0^{\theta_{MAX}} \frac{S}{4\pi r^2} r^2 \sin\theta \, d\theta = \frac{S}{2} \int_0^{\tan^{-1} r_b/SSD} \sin\theta \, d\theta$$

$$= \frac{S}{2} \left[1 - \cos\left(\tan^{-1} \frac{r_b}{SSD} \right) \right]$$

Therefore, if S' neutrons are emitted into a cone of $\theta_{MAX} = \tan^{-1} r_b/SSD$, this is equivalent to an isotropic source of strength

$$S = 2S'/(1-\cos(\tan^{-1} r_b/SSD)) \quad .$$

The neutron flux (NF) can also be calculated in this case. Each neutron is assigned a weight of 1/cos , as seen in Fig.A2. Therefore,

$$NF = \frac{S}{2} \int_0^{\theta_{MAX}} \frac{\sin\theta}{\cos\theta} \, d\theta$$

$$= -\frac{S}{2} \ln \left[\cos\left(\tan^{-1} r_b/SSD \right) \right]$$

Figure A_1

Point source emitting neutrons into a cone.

Figure A_2

Contribution of a neutron passing through a disc of unit thickness at an angle θ to the normal.

Contribution to current $=1$

Contribution to flux $=1/\cos\theta$

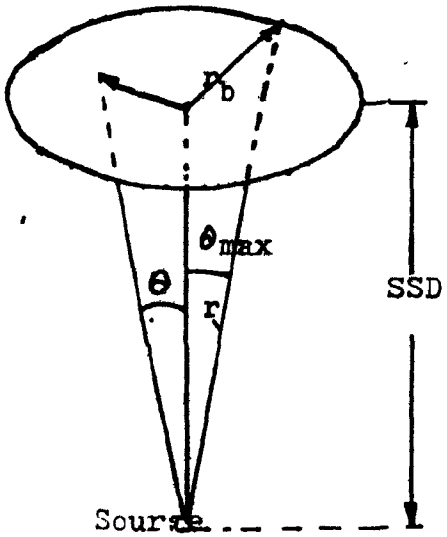

FIG.A_1

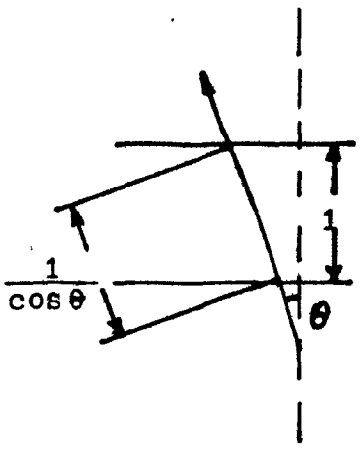

FIG.A_2

APPENDIX B

The following is adapted from (Cu65) and (Fe53).

Equation III.7 actually refers, not to the thermal flux (which is the flux of all thermal neutrons lumped together by the integral (see equation II.2)

$$\Phi_{th} = \int_0^{0.1eV} \Phi(E)dE = \int_0^{0.1eV} n(E)\,V(E)\,dE$$

but rather to the flux, Φ_0, which is calculated by assuming that all neutrons are at the energy 0.025eV, corresponding to a velocity of $v_0 = 2200 m/s$. v_0 is the most probable velocity of a Maxwellian velocity distribution at a temperature of T=293°K and is given by $v_0 = 2kT/m$. The neutron flux as a function of velocity is given by

$$\bar{\Phi}(v) = \frac{4n}{v_0^3\sqrt{\pi}}\, v^3 e^{-v^2/v_0^2}$$

where n is the neutron density. Assuming that below a resonance the cross section of the foil is proportional to 1/v so that $\sigma(v) = \sigma_0 v_0 / v$, we have

$$R_0 = Nv\int_0^\infty \bar{\Phi}(E)\sigma(E)\,dE = Nv\sigma_0 \frac{4n}{v_0^2\sqrt{\pi}} \int_0^\infty v^2 e^{-v^2/v_0^2} dv$$

$$= Nv\sigma_0 v_0 n = Nv\sigma_0 \Phi_0$$

where the integral should really only be taken to the maximum thermal velocity. Since the integrand drops off quickly, an upper bound of ∞ is valid.

The average (thermal) flux can be shown to be

$$\Phi_{th} = \frac{2}{\sqrt{\pi}}\Phi_0 = 1.128\,\Phi_0$$

Since cross sections are normally quoted for 0.025eV fluxes, Φ_0 is the appropriate distribution to be used in activation.

APPENDIX C

The following is adapted from (Pr76) and (ANL5800).

An activation foil will generally absorb enough neutrons to perturb the flux density in its environs. These perturbations are identifiable in two categories: (1) self-shielding, which is the reduction in flux density at the interior of the detector because of attenuation in the outer layers, and (2) flux depression directly outside the detector due to neutron removal- a neutron which has been captured can no longer contribute to the flux. The second is of no consequence in measurements in a neutron beam even though the flux behind the foil is lowered.

Fig.C1 is a sketch of the situation at hand. Φ_o is the unperturbed flux prior to absorber insertion. $\langle\Phi_s\rangle$ is the average surface flux at the absorber boundary. $\langle\Phi_v\rangle$ is the average volume flux inside the absorber. $\Phi(x)$ is the flux at a distance, x, from the foil in the moderator. Then the flux density depression factor at the surface is given by

$$F_d(\gamma,\tau)=\langle\Phi_s\rangle/\Phi_o$$

where $\gamma=\Sigma(\text{scatter})/\Sigma(\text{total})$ is a parameter of the medium in which the foil is imbedded and $\tau=\Sigma_a d$ where Σ_a is the macroscopic absorption cross section of the foil, including processes such as (n,p), (n,2n), etc., and d is its thickness. A number of calculations and measurements are available for evaluating $F_d(\gamma,\tau)$. These will not be detailed here. Measured values for $F_d(\gamma,\tau)$ in water as a function of τ are presented in Fig.C2.

Flux density depression at a point away from the absorber

determines how closely foils can be spaced without interfering with one another. The values of $\Phi(x)/\Phi_o$ are plotted in Fig.C3 as a function of x in water for Mn foils of radius 1.2cm. The graph has been calculated using

$$\frac{\Phi(x)}{\Phi_o} = 1 - \frac{\frac{L}{\lambda_{tr}} f(\tau)\left[e^{-x/L} - e^{-\sqrt{R^2+x^2}/L}\right]}{1+(L/\lambda_{tr})f(\tau)\left[1-e^{-R/L}\right]}$$

where for water L=2.76 cm is the thermal neutron diffusion length, λ_{tr}=0.43cm is the transport MFP, λ_s=0.14cm is the scattering MFP and $f(\tau)=(0.5-E_3(\tau))/(.33+E_4(\tau))$ where E_3 and E_4 are exponential integrals tabulated in several references (eg. ANL5800). The equation should be considered valid only for $x>\lambda_s$, i.e. away from the foil surface. Note that the equation is given incorrectly in (Pr76).

The self-shielding factor is defined by

$$F_s(\tau)=\langle\Phi_v\rangle/\langle\Phi_s\rangle \quad .$$

For thin foils ($\tau<0.05$), a valid approximation is given by $F_s(\tau)=1-\tau(1-\ln\tau)$ for a foil in an isotropic (or nearly so) field. For a foil perpendicular to a neutron beam, $F_s(\tau)=(1-\exp(-\tau))/\tau$. If the foil is at an angle, θ, to the beam, τ is replaced by $\tau/\cos\theta$ because of the increased path lengths of neutrons in the foil. The normal beam and isotropic cases are plotted in Fig.C4.

The integral flux perturbation, i.e. the combined effect of the F_s and F_d factors, in water for a disc shaped Mn foil of radius 1.2cm is given in Fig.9-4 of ANL5800 as a function of τ. For Mn, Σ_a=1.083 cm^{-1} and, in our case, the thickness is d=0.0125cm implying τ=0.01375. $\langle\Phi_v\rangle/\Phi_o$ is then approximately 0.95±0.05 so that a measured flux is at most a very few percent off the actual. For the placement of foils,

the perturbation is very small at a distance of 2cm from our foil (Fig.C3).

Figure C1

Geometric sketch of flux depression and self-shielding.

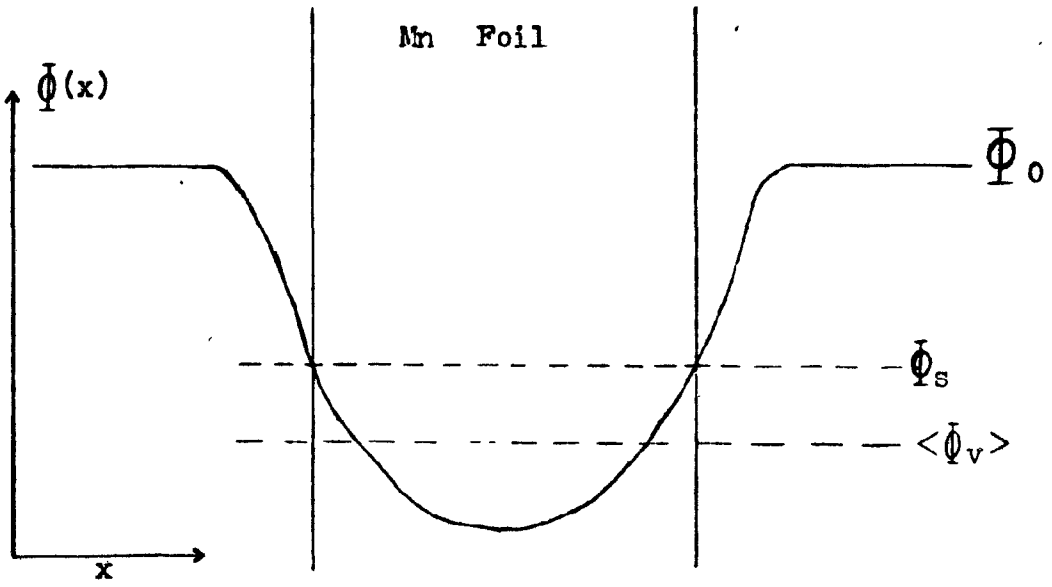
Mn Foil
Φ(x)
Φ0
Φs
<Φv>
x

Figure C2

Measured flux depression due to an In absorber disc (r =1.2 cm) in water as a function of $\tau = \Sigma_a d$.

Adapted from ANL5800, Fig. 9-2.

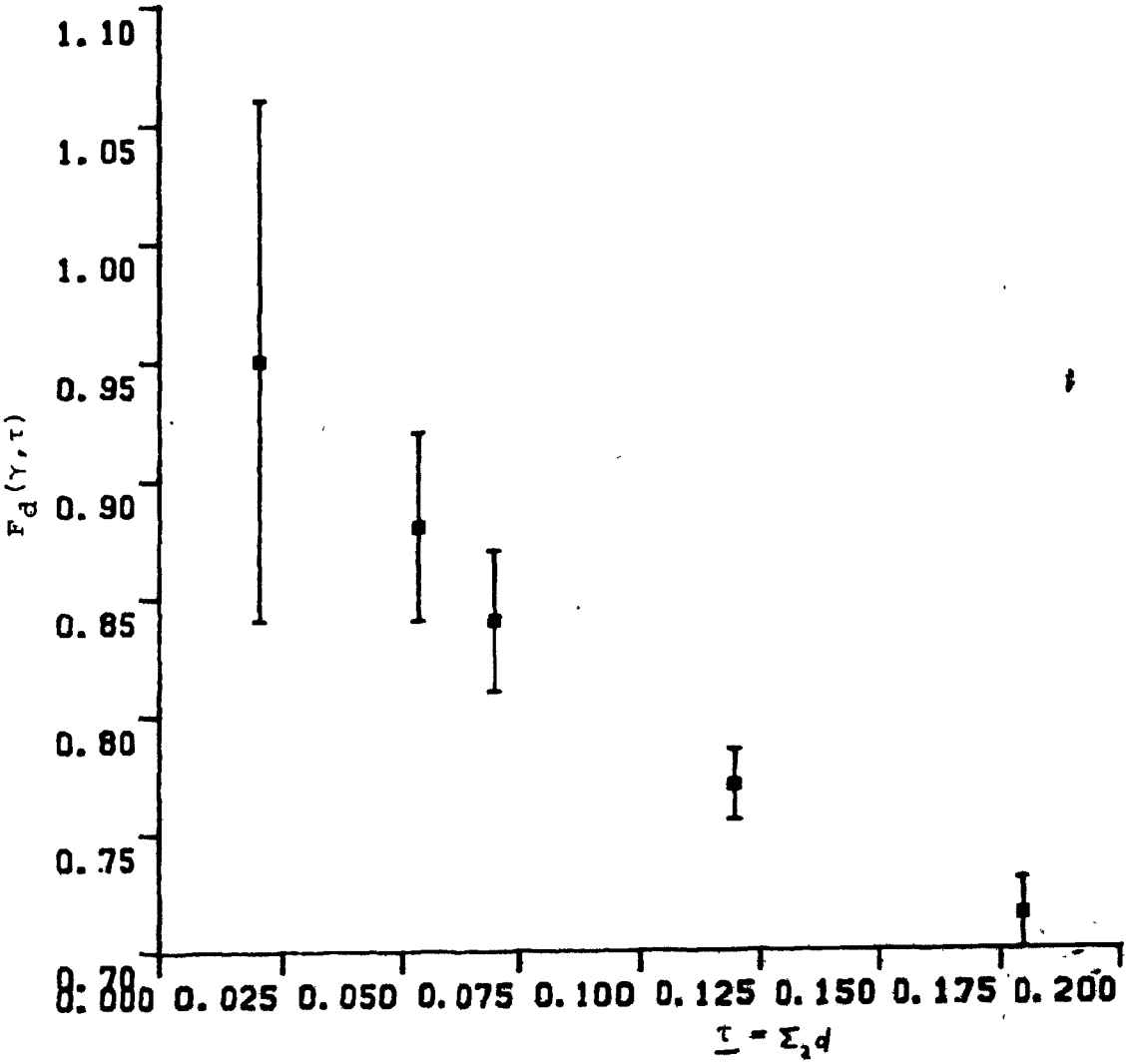
1.10
1.05
1.00
0.95
0.90
0.85
0.80
0.75
0.70
$F_d(\gamma,\tau)$
0.000
0.025
0.050
0.075
0.100
0.125
0.150
0.175
0.200
$\tau = \Sigma_2 d$

Figure C3

Calculated ratio of flux near foil to flux far from foil for a Mn disc (r =1.2 cm) vs distance from foil.

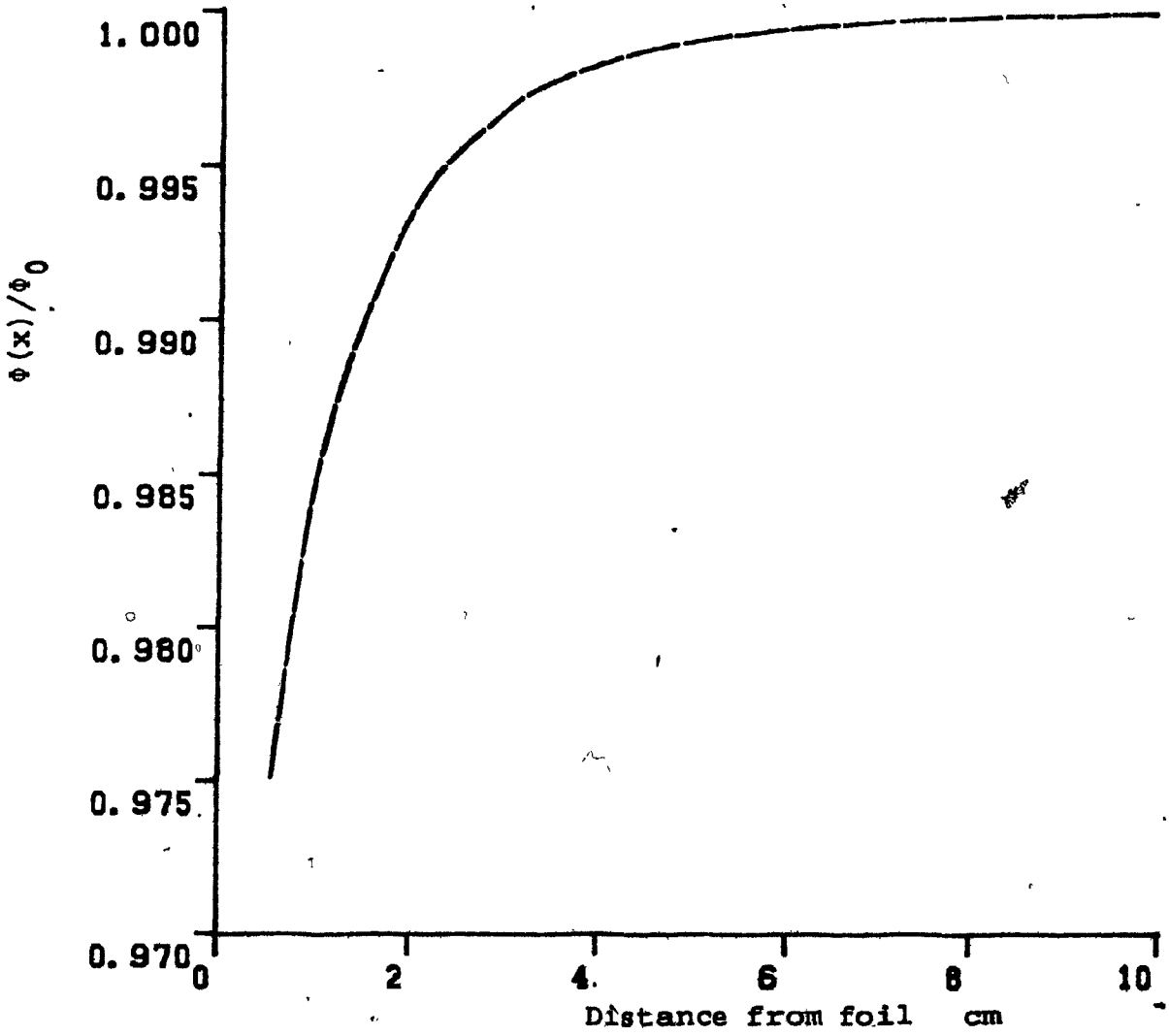
1.000
0.995
0.990
0.985
0.980
0.975
0.970
$\phi(x)/\phi_0$
0
2
4
6
8
10
Distance from foil cm

Figure C4

Self-shielding factor for normal beam and isotropic irradiation of a plane foil vs foil thickness $\tau = \Sigma_a d$.

Calculated using eq.14,15 of chapter 7 of (pr76).

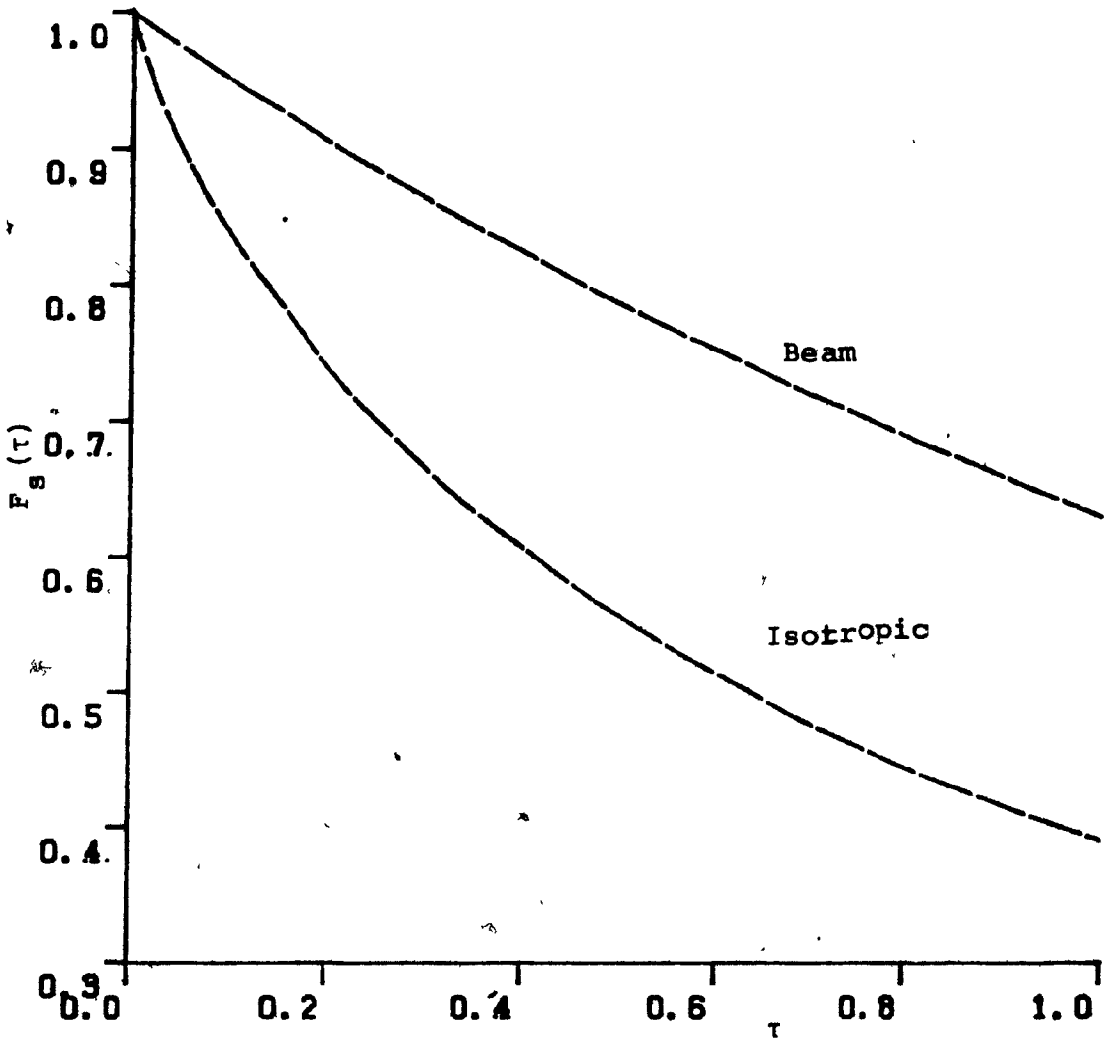
1.0
0.9
0.8
0.7
0.6
0.5
0.4
0.3
$F_s(\tau)$
Beam
Isotropic
0.0
0.2
0.4
0.6
0.8
1.0
τ

REFERENCES

(Ad80) Adamson-Sharpe K.,F.Ottensmyer,
J.of Microscopy 122(1981)309

(Al81) Albert D,K Fahrmann,E Lehmann,E Seifert
Nucl.Instr.Meth. 185(1981)387

(Am74) Amols H, Ph.D. Dissertation,Brown University,1974

(An63) Anderson M,W Bond, Nucl.Phys. 43(1963)330

(An72) Anderson M.,Neff R., Nucl.Instr.Meth. 99(1972)231

(ANL5800) REACTOR PHYSICS CONSTANTS,ANL-5800
Argonne National Lab,2nd Edition,1963

(Au68) Auxier J.,W.Snyder,T.Jones, NEUTRON INTERACTIONS AND PENETRATION IN TISSUE, in Radiation Dosimetry,Vol.1, 2nd edition,Attix,Roesch,Tochilin(eds),Academic,N.Y.,1968

(Be64) Beckurts K.H.,K.Wirtz, NEUTRON PHYSICS,
Springer-Verlag, New York,1964

(Be69) Bevington P, DATA REDUCTION FOR THE PHYSICAL SCIENCES,
McGraw Hill,N.Y.,1969

(Bl67) Block S.,J.Bryan,C.Prevo,D.Montan
Health Physics 13(1967)1025

(Bo73) Boddy K.I.Holloway,A.Elliot,D.Glaros,I.Robertson, B.East, LOW-COST FACILITIES FOR PARTIAL BODY AND TOTAL BODY IVNAA in Nuclear Activation Techniques in the Life Sciences,IAEA,Vienna,1973

(Bo82) Bottomley P, Rev.Sci.Instr. 53(1982)1319

(Ca70) Capgras A., Nucl.Instr.Meth. 82(1970)7

(Ca59) Cashwell E,C Everett, A PRACTICAL MANUAL ON THE MONTE CARLO METHOD, Pergamon,1959

(Ce82) Cesana A,V.Sanguist,M.Terrani,
Nucl.Sci.Eng. (1982) 102

(Ch80) Chatt A,S Katz, NEUTRON SOURCES FOR ACTIVATION ANALYSIS OF GEOLOGICAL MATERIALS in Short Course in NAA in the Geosciences,Mineralogical Assoc. of Canada,G.Muecke(ed) 1980

(Ch82) Chettle D.,J.Fletcher,S.Downey,M.Scott, H.James,C.Higgens, J.Radioanaly.Chem. 71(1982) 533

(Ch69) Choudry A,P Bandopadhyay, Nucl.Instr.Meth. 68(1969) 293

(Ch71) Choudry A,P Bandopadhyay, Nucl.Instr.Meth. 92(1971) 339

(Ci68) Cialella C,J Devanney, Nucl.Instr.Meth.60(1968) 269

(Co81) Cohn S., Med.Phys. 8(1981) 145

(Co73) Cohn S.,R.Fairchild,K.Shukla, NEUTRON SOURCES,ENERGY,FLUX DENSITY AND MODERATION IN TOTAL BODY NAA, in InVivo NAA, Proceedings of a Panel,Vienna-1972, IAEA,Vienna,1973

(Co69) Cox A,P Francois,R Gatrell,
Int.J.Appl.Rad.Isot. 19(1969) 541

(Co75) Cox A,C Cleave, Int.J.Appl.Rad-Isot. 26(1975) 430

(Cr81) Cross W., Health Physics 41(1981) 105

(Cu82) Cummins P,J Dutton,C Evans,W Morgan,A Sivyer,
J.Radioanaly.Chem. 71(1982) 561

(Cu65) Curtiss L., INTRODUCTION TO NEUTRON PHYSICS,
Boston Technical Publishers,Boston,1965

(Cy75) Cytacki E, Ph.D. Dissertation, U. of Wisconsin,1975

(De81) Deconnick G, Nucl.Instr.Meth. 191(1981) 543

(DLC31) DLC31,Data Library Collection,Radiation Shielding Information Center,Oak Ridge,1979

(DOT77) DOT 3.5 Transport Code,Documentation-CCC276, Radiation Shielding Information Center,Oak Ridge

(Dr80) Drozdowicz K,A.Igielski,E.Krynicka,Z.Sobczynski, U.Woznicka, Nucl.Instr.Meth. 178(1980)513

(En72) Engelmann C., PHOTON ACTIVATION ANALYSIS, in Advances in Activation Analysis,Vol.2, J.Lenihan,S.Thomson, V.Guinn(eds),Academic Press,N.Y.,1972

(Et82) Ettinger K,W Morgan,U Miola,D Vartsky,K Ellis L Wielpolski,S Cohn, Med.Phys. 9(1982)550

(Ev78) Evans C,P Cummins,J Dutton,W Morgan,A Sivyer R Ghose, Activation Analysis in the Life Sciences, IAEA,Vienna,1978

(Fe53) Feld B., THE NEUTRON, in Experimental Nuclear Physics, Vol.2, E.Segre(ed), Wiley and Sons,N.Y.,1953

(Fu75) Fujishiro M,T Tabata,J Furuta Nucl.Instr.Meth. 131(1975)259

(Ga76) Garber D.I.,R.Kinsey, NEUTRON CROSS SECTIONS,VOL.2, BNL-325,3rd Edition,1976

(Ge75) Geiger K.,L.van der Zwan, Nucl.Instr.Meth. 131(1975)315

(Gl76) Gleason G., Radiochem.Radioanal.Letts. 26(1976)39

(Go62) Goldberg M.,V.May,J.Stehn, ANGULAR DISTRIBUTIONS IN NEUTRON INDUCED REACTIONS,Vol.1,BNL-400,1962

(Go71) Goldstein H., FUNDAMENTAL ASPECTS OF REACTOR SHIELDING,Johnson Reprint Co.,N.Y.,1971

(Gr78) Greenwood R, PRACTICAL APPLICATIONS OF NEUTRON CAPTURE GAMMA RAYS in Neutron Capture Gamma Spectroscopy,Chrien(ed),1978

(Ha73) Hannan W,D Porter,R Lawson,R Railton Phys.Med.Biol. 18(1973)808

(Ho78) Holland L.,J.Walker,W.Oosterkamp,

Nucl.Instr.Meth. 151(1978)175

(In75) Ing H.,M.Cross, Nucl.Sci.Eng. 58(1975)420

(Ja80) James F, Rep.Prog.Phys. 43(1980)1145

(Jo76) Johansson S.,T.Johansson,
Nucl.Instr.Meth. 137(1976)473

(Jo81) Jones D., Annals of Nuclear Energy 8(1981)233

(Ju78) Jurney E., APPLICATION OF THE THERMAL (n,) REACTION TO ELEMENTAL ANALYSIS in Neutron Capture Gamma Spectroscopy,E.Chrien(ed),1978

(Ke82) Kennedy N,R Eastell,C Ferrington,J Simpson, M Smith,J Strong,P Tothill
Phys.Med.Biol. 27(1982)697

(Kh81) Khan N. et al, Nucl.Instr.Meth. 188(1981)309

(Kl82) Kluge H.,K.Weise, Rad.Protection Dosimetry 2(1982)85

(Kr80) Krauel J,M Speed,B Thomas,H Baddeley,B Thomas
Int.J.Appl.Rad.Isot. 31(1980)101

(Ku77) Kumar A.,P.Nagarajan, Nucl.Instr.Meth. 140(1977)175

(Ky82) Kyere K,B Oldroyd,C Oxby,L Burkinshaw,R Ellis,G Hill,
Phys.Med,Biol. 27(1982)805

(La82) Laird P, Nucl.Instr.Meth. 193(1982)377

(La75) Lamarsh J., INTRODUCTION TO NUCLEAR ENGINEERING,
Addison-Wesley,N.Y.,1975

(La77) Lanford W.,R.Golub, Phys.Rev.Letts. 39(1977)1509

(La64) Lawson R.,D.Watt, Phys.Med.Biol. 9(1964)487

(La67) Lawson R.,D.Clarke,D.Watt,
Phys.Med.Biol. 12(1967)201

(Le78) Lederer C.,V.Shirley(eds), TABLE OF THE ISOTOPES, 7th edition,Wiley,1978

(Ma82) Matthews I,Spyrou N, Int.J.Appl.Rad.Isot. 33(1982)61

(MCNP79) MCNP-A GENERAL MONTE CARLO CODE FOR NEUTRON AND CHARGED PARTICLE TRANSPORT-USER'S MANUAL, LA-7396-M,Los Alamos Lab,1979

(Me77) Mernagh J, Ph.D. Dissertation, University of Toronto,1976

(Mo81) Morgan W.,D.Vartsky,K.Ellis,S.Cohn Phys.Med.Biol. 26(1981)413

(Mo82) Mountford P., Phys.Med.Biol. 27(1982)1245

(Mu81) Mughabghab S.,M.Divadeenam,N.Holden, NEUTRON CROSS SECTIONS,Vol.1,Part A,Academic,1981

(Na75) Nagarajan P.,P Setulakshmi, A RANDOM SAMPLING PROCEDURE FOR ANISOTROPIC DISTRIBUTIONS Bhabha Atomic Research Center,BARC-789,1975

(Ng71) Nguyen D.,M.Slayton,J.Frew, Nucl.Sci.Eng. 46(1971)416

(Nu80) Nutton D,S Harris, Phys.Med.Biol. 25(1980)1173

(Ot82) Ottensmeyer P., Quantitative Spectroscopic Mapping of Atomic Elements in Micro-anatomical Surveys, Talk delivered at 1982 CAP Congress, Abstracted in Physics in Canada,Vol.38,No.3,1982

(Pra76) Pracy M.,A.Haque, Nucl.Instr.Meth. 135(1976)217

(Pr76) Profio A., EXPERIMENTAL REACTOR PHYSICS, Wiley and Sons,N.Y.,1976

(Ra78) Rao U.,A.Kumar,S.Misra,P.Nagarajan,U.Gupta Nucl.Instr.Meth.155(1978)249

(RE79) COMPILATION OF NEUTRON DETECTOR MATERIALS, Reactor Experiments Inc., Bulletin B-44M,1979

(Re81) Reeder P.,R.Warner, Nucl.Instr.Meth. 180(1981)523

(Ri80) Rieppo R., Int.J.Appl.Rad.Isot. 32(1981)219

(Ro81) Robson J.M.,J.Kroon,
Nuclear Technology/Fusion 1(1981)160

(Se82) Segal Y,A Gutman,A Fishman,A Notea,
Nucl.Instr.Meth. 197(1982)557

(Se65) Segre E., NUCLEI AND PARTICLES, Benjamin Co.,N.Y.,1965

(Sm62) Smith J,S.Boot, Phys.Med.Biol. 7(1962)45

(Sh65) Shreider Y, THE MONTE CARLO METHOD, Pergamon,1965

(Sm82) Smith J,S Athwal,D Chettle,M Scott
Int.J.Appl.Rad.Isot. 33(1982)557

(So77) Soverby B.,W.Ellis,R.Greenwood-Smith, BULK ANALYSIS FOR Cu AND Ni IN ORES USING GAMMA RAY RESONANCE SCATTERING, Nuclear Techniques and Mineral Resources Vienna Symp.,1977, IAEA,Vienna,1977

(St81) Stelts M,S Donaldson,J Povelites,
Nucl.Instr.Meth. 187(1981)483

(St70) Straker E.,P.Stevens,D.Irving,V.Cain,The MORSE Code,ORNL-4585,1970,Oak Ridge Report

(Va76) Vartsky D, Ph.D. Dissertation,U. of Birmingham,1976

(Va82) Vartsky D, et al, Nucl.Instr.Meth. 193(1982)359

(Vi73) Vijaya A.,A.Kumar, Nucl.Instr.Meth. 111(1973)435

(Wa47) Wallace P.,J.LeCaine,Chalk River Report,1947

(Wa64) Wasson O.,K.Wetzel,C.Bockelman
Phys.Rev. 136B(1964)B1640

(We58) Weinberg A.,E.Wigner, THE PHISICAL THEORY OF NEUTRON CHAIN REACTORS,U.Chicago Press,1958

(Wi78) Williams E,K Boddy,I Harvey
Phys.Med.Biol. 23(1978)405

(Yo82) Young F.,J.Pronko, Rev.Sci.Instrum. 53(1982)1228

(Za79) Zamenhof R.,O.Deutsch,B.Murray,
Med.Phys. 6(1979)179

(Ze63) Zerby C, A MONTE CARLO CALCULATION OF THE RESPONSE OF GAMMA RAY SCINTILLATION COUNTERS in Methods in Computational Physics,Vol.1,B Alder,S Fernbach, M Rotenberg (eds), Academic,1963

(Zi78) Ziegler J. et al, Nucl.Instr.Meth. 149(1978)19